ABSTRACT

Title of Document: MOLECULAR STRUCTURE AND ORGANIZATION IN ORGANIC MONOLAYERS AT AQUEOUS/VAPOR INTERFACES

Suleyman Zuhtu Can, Ph.D., 2008

Directed By: Professor Robert A. Walker
Department of Chemistry and Biochemistry

The goal of this thesis is to understand how the asymmetry of interfaces affects the structure of adsorbed surfactants and organization within the monolayer. These studies employ a variety of experimental techniques including surface tensiometry and vibrational sum frequency spectroscopy, a nonlinear optical method having surface specificity. The first studies in this thesis examine the ability of different neutral organic surfactants to form films at the aqueous/vapor interface. Specifically, structure and organization within monolayers formed by insoluble and soluble alcohols at aqueous/vapor interfaces were investigated. Relatively simple organic molecules were used to isolate both intermolecular interactions within adsorbed films and the competition between attractive and repulsive forces experienced between monolayer monomers and the aqueous subphase. Results of the experiments allowed us predict that linear alcohols form tightly packed monolayers at

the aqueous/vapor interface. This organization allows the alcohol OH group to make strong H-bonds with the water subphase while the hydrocarbon chains interact with each other through attractive van der Waals forces. Our studies showed that the interplay between the van der Waals attraction and the hydrophobic repulsion is the primary factor in determining the equilibrium interfacial structures of 2- and 3-position alcohols. The primary conformer structures predicted for 2-position alcohols include all-trans conformations for insoluble monolayers and a model containing two gauche defects for soluble monolayers. In an effort to model these results we initiated a series of classical molecular dynamics simulations designed to develop molecular insights into the equilibrium structures inferred from experiments. Computer simulations were also used to separate and compare the individual forces contributing to film organization.

Our studies in the last part of the thesis focus on the effect of charged soluble surfactants on the structure and organization of phospholipid monolayers adsorbed to aqueous/air interfaces. The self driven spreading of 1,2-dipalmitoyl-*sn*-glycero-3-phosphocholine (DPPC) on aqueous surfaces to form monolayers was a matter interest in these experiments. The effect of surfactants as a potentially competing surface active species was explored with a function of surfactant bulk phase concentration. The results showed significantly different effects depending on whether the surfactant was anionic or cationic.

MOLECULAR STRUCTURE AND ORGANIZATION IN ORGANIC MONOLAYERS AT AQUEOUS/VAPOR INTERFACES

By

Suleyman Zuhtu Can

Dissertation submitted to the Faculty of the Graduate School of the
University of Maryland, College Park, in partial fulfillment
of the requirements for the degree of
Doctor of Philosophy
2008

Advisory Committee:
Professor Robert A. Walker, Chair
Professor Neil Blough
Professor Jeffrey Davis
Professor Douglas English
Professor Sergei Sukharev

Dedication

To my family

Acknowledgements

I gratefully acknowledge support and guidance from Professor Robert A. Walker. Without his support and encouragement, this study could not have been conducted.

I thank Professor Ilan Benjamin from University of California Santa Cruz for his help and guidance throughout the molecular dynamics simulations study.

I also thank all past and current Walker Research Group members Dr. Okan Esentürk, Dr. William Steel, Dr. Carmen Huffman, Dr. Michael Pomfret, Wendy Heiserman, Michael Brindza, Antony Dylla, Renee Siler, Bryan Eigenbrodt and Debjani Roy for their contributions through exemplary scientific work and discussions as well as a friendly group ambiance. I am especially grateful Dr. Okan Esentürk for his guidance and training on the experimental setup during the early stages of this work.

Undergraduate members of the group have also played important roles in these research activities. Deesha D. Mago and Chia Fang Chang contributed directly to this work with their careful and valuable surface tensiometry experiments. I appreciate their help.

I thank my friends and colleagues Oktay Demircan and Selim Alayoğlu for academic discussions as well as sharing the time we spent during our PhD studies in the United States.

Table of Contents

List of Tables

List of Figures

Chapter 1: Introduction

1.1. Liquid Interfaces

1.1.1. Importance of Aqueous Interfaces

To motivate the study of water surfaces, many researchers will cite that 70 % of the earth is covered with water.[1] Technically this statement is true, but left unsaid is that the water itself is often covered with a thin, monomolecular film of biologically derived, organic surfactants. These surfactants will preferentially adsorb to the aqueous/air interface from bulk solution and organize themselves to maximize a system's overall free energy. The way in which these molecules arrange themselves is not always easy to predict. At aqueous interfaces asymmetric forces will help one end of the surfactant remain solvated in water and force the other end of the molecule out of the aqueous phase. Furthermore, space limitations at the interface and competition among different surface active species will force molecules to adopt unique conformations to balance the forces acting on them. Thus, we expect properties of an interface to be quite different from the properties of bulk solutions.

Structure and organization of molecules at interfaces is very important for many areas in the environmental and biological sciences as well as for technological applications. Formation of aerosols from ocean spray requires the formation of organic monolayers to stabilize small liquid droplets. Organic films on water surfaces will also impact the uptake of organic and inorganic volatile compounds and surface specific reactions. A third effect of organic films on water is to change the surface

roughness and the optical scattering properties of the water surface. The most familiar example of this last effect is the spreading of oil on the surface of a lake and seeing the waves dampen. From a technological perspective, the effect of films on water surfaces will influence remote sensing capabilities of satellites and airplanes. The first studies in this thesis examine the ability of different neutral organic surfactants to form films at the aqueous/vapor interface. Specifically, structure and organization within monolayers formed by insoluble and soluble alcohols at aqueous/vapor interfaces were investigated. Computer simulations were also used to develop a molecular level understanding of the forces contributing to film organization.

One of the most common classes of surface active, biological molecules are phospholipids. Phospholipids along with other biological molecules construct the membranes of cell organelles as well as the plasma membrane. Given their pervasive presence throughout the plant and animal kingdoms, these molecules represent the primary building blocks of biofilms formed on surfaces. Hydrophobic tail(s) and a hydrophilic headgroup are the two major parts of a phospholipid. Varying headgroup and tail composition of phospholipid molecules imparts specific organizational tendencies to these molecules adsorbed at the aqueous/vapor interface. Thus, the molecular shape of a phospholipid monomer will play a large role in determining the long range structure in monolayers. Specific details about the structure within phospholipid monolayers are explored in Chapter 5. Our studies in this thesis focus on the effect of charged soluble surfactants on the structure and organization of phospholipid monolayers adsorbed to aqueous/air interfaces.

1.1.2. Adsorption at Interfaces

The goal of this thesis is to understand how the asymmetry of interfaces affects the structure of adsorbed surfactants. Answers to questions about how molecular shape and intermolecular forces control interfacial structure have far reaching consequences. Molecules at liquids surfaces have higher free energies than in bulk. This result is easy to understand because at surfaces, molecules have lost roughly half of the neighbors they would have in bulk solution. A liquid's surface tension represents a quantitative measure of this excess free energy possessed by liquids at the interface having strong intermolecular interactions have high surface tensions and vice versa. For instance, water, a strongly associating liquid, has a liquid/vapor surface tension of 72.0 mN/m at 25 °C due to large excess of high energy, dangling OH bonds at the interface. In contrast n-octane has a surface tension of 21.1 mN/m at 25 ˚C due to weak van der Waals interactions of a hydrophobic region between the liquid and the vapor. The excess free energy attributed to the to surfaces means that any solute in solution that is capable of reducing a system's surface free energy will preferentially partition to interfaces. One example of this effect is the adsorption of simple surfactants to the air/water interface. Surfactants such as sodium dodecyl sulfate (SDS) and dodecyl trimethylammonium bromide (DTAB) are common ingredients in soaps and other personal care products. With charged headgroups and long hydrophobic tails, SDS and DTAB spontaneously adsorb to surfaces to reduce the number of free OH groups of water at the interface. The charged headgroups of these surfactants however limit the effective organization of monomers due to the layer of similar charge created at the interface. On the other

hand, if a surfactant has a neutral headgroup such as 1-dodecanol, monomers pack together more efficiently due to the fact that there are no charge constraints keeping the monomers separated.

Studying the properties of molecules at interfaces present considerable challenges. First, unlike the bulk of the material, the interface has more limited space meaning that the number of molecules at surfaces is always very, very small relative to the number of molecules in bulk solution. Another difficulty with liquid surfaces – water surfaces in particular – is their sensitivity to contamination. Any molecule with a hydrophobic moiety is a potential adsorbate on the aqueous surface. Thus, experiments require extreme analytical care when preparing samples for study.

To study structure and organization of monolayers adsorbed to aqueous surfaces, experiments must overcome these difficulties. The way we accomplish these goals are discussed in detail below. The remainder of this chapter is organized as follows: Section 1.2 describes the tools used to study structure and organization of molecules at liquid surfaces. These tools include surface tension measurements, surface-specific vibrational spectroscopy, and classical molecular dynamics simulations. Next, the specific systems examined are described. Specifically, this section includes subsections describing similarities and differences between insoluble and soluble alcohols, and phospholipids. The phospholipid systems consist of mixed monolayers containing lipid and varying surface coverages of soluble charged surfactants.

1.2. Tools for Probing Interfaces

Different analytical techniques can be used to measure specific properties of monolayers at interfaces. Surface tension methods give valuable thermodynamic information about the surfaces. With surface tension techniques, one can determine the surface area of a molecule or measure the level of interaction between the adsorbed species and resulting interfacial properties. Conventional surface tension techniques are specific to liquid surfaces and can not be used for interfaces formed with solid surfaces.

Although surface tension measurements are useful for studying the liquid surfaces, they provide limited information about the surface species and structures. Additional methods are necessary to probe specific properties relating to molecular structure and organization. Nonlinear spectroscopic techniques are excellent tools with their inherent surface and molecular specificity. The following sections outline the techniques used throughout the study.

1.2.1. Surface Tensiometry

Surface tension measurements studying the adsorption properties of target molecules generally mark the first steps in characterizing surface activity and interfacial molecular organization. The surface tension of a liquid can be measured by recording the force of a liquid pulling a wetted plate, known as Wilhelmy plate method (Figure 1.1).

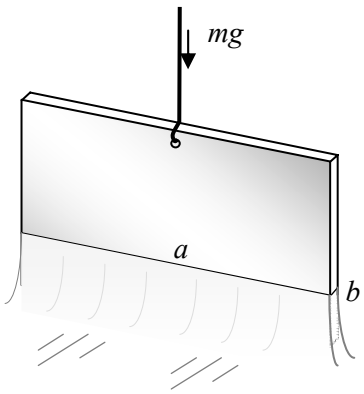

Figure 1.1. A typical Wilhelmy plate with a perimeter of l ($l=2(a+b)$) used in surface tension measurements.

The surface tension of a liquid relates to the force is given by

$$\gamma = F / l \tag{1.1}$$

where F stands for the force and given as $F = mg$ and l is the perimeter of the plate.

Molecules such as surfactants can lower a liquids surface tension by spontaneously adsorbing to the liquid surface and reducing the number of energetically unfavorable interactions between the solvent and the vapor. The surface tension of a pure liquid decreases according to how many molecules adsorbed at the interface. The difference between surface tension of a neat and surface tension of a multi-component interface is called surface pressure, π.

$$\pi = \gamma_0 - \gamma_{\text{soln}} \tag{1.2}$$

Surface pressure is directly proportional to the excess surface coverage of adsorbed molecules at the interface. The surface tension of water at 25 °C, for example, is decreased from 72.0 mN/m to ~18 mN/m for a surface completely covered by a monolayer of 1-nonanol molecules. Such a change in surface pressure of

a liquid is used to calculate the surface coverage of the interfacial molecules in units of the number of molecules per unit area using a Gibbs isotherm analysis:

$$d\pi / d \ln C = (n / A)kT \tag{1.3}$$

where C, k and T correspond to the bulk phase concentration of the molecules, Boltzmann's constant and temperature of the medium, respectively.[2] Plotting π versus $\ln C$ and finding the slope of the steepest ascent allows the surface excess to be determined. Figure 1.2 shows a representative isotherm for 1-heptanol. The number of molecules per unit area (n / A) at terminal monolayer coverage is calculated to be 5.08×10^{18} particles/m^2 and the area per single molecule is 19.7 Å^2/molecule. These values are typical for isotherms having slopes of 25 in π versus $\ln C$ and Chapter 3 examines in great detail how this behavior depends on monomer structure.

The methods for measuring the surface tension of a system depend on the type of system being studied. For example, if surfactant species are soluble in the subphase (e.g. 1-heptanol in water), solutions are prepared with known bulk phase concentrations of surfactants and allowed to establish an equilibrium between 1-octanol monomers adsorbed to the aqueous surface and 1-octanol monomers solvated in bulk solution. Here one important point to note is that the amount of material adsorbed to the surface depends on the bulk phase concentration given the fixed total surface area set by experimental conditions. Bulk concentration can be changed by serially diluting a solution saturated with the soluble surfactant. A representative surface pressure isotherm obtained for 1-heptanol is show in Figure 1.2.

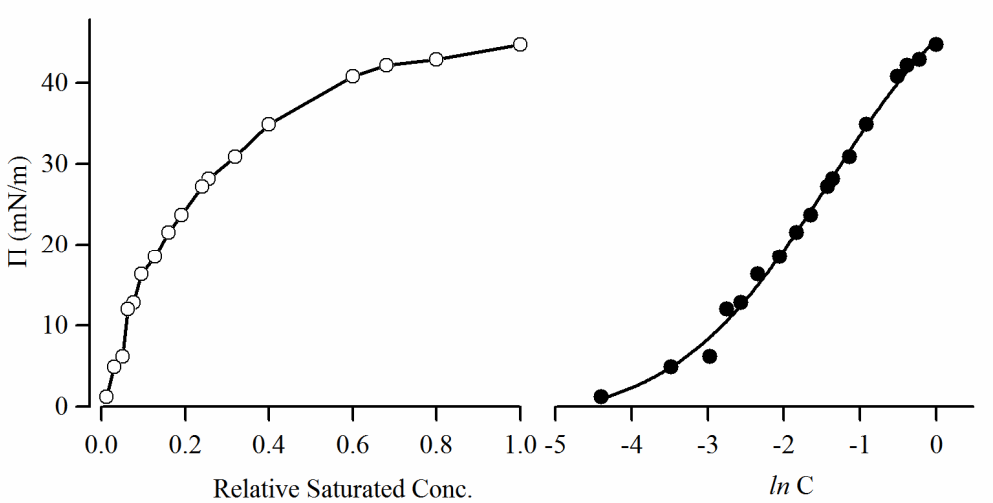

Figure 1.2. Surface pressure isotherm of 1-heptanol at two different concentration scales; relative saturated bulk phase concentration (open circles) and *ln* C (solid circles).

If the adsorbing species are insoluble in the bulk of the subphase, an alternative way of measuring the surface tension is necessary. The measurement can be performed by spreading a known amount of adsorbate monomers at the interface and changing the area available for surfactant molecules to cover. To make these measurements, an instrument known as Langmuir film balance is employed (Figure 1.3).

For experiments carried out in a Langmuir trough, a known amount of surfactant monomers in a spreading solvent is added between the two barriers to the surface of aqueous subphase. A spreading solvent usually consists of a high vapor pressure organic solvent or organic solvent mixture capable of dissolving the surfactants that will adsorb to the air/water interface. For the hexadecanols isotherms, for example, 4:1 hexane/chloroform (v/v) mixture is used. Once the spreading solvent

evaporates, the surfactants remain at the surface and the barriers located in opposite sides of the trough start to move toward each other compressing the dilute monolayer film. As the barriers compress the film, the surface pressure is recorded with a sensor located in the middle of trough. Isotherms for several hexadecanols isomers are shown in Figure 1.4 as examples of the types of data that can result from these measurements.

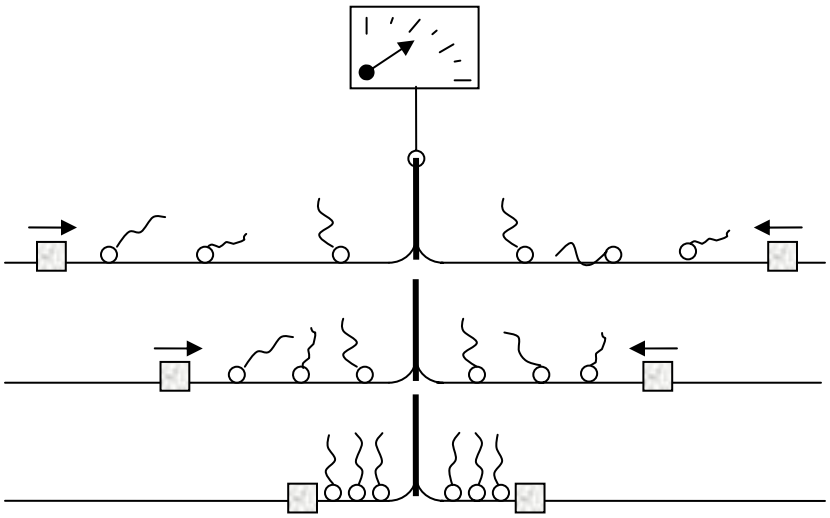

Figure 1.3. Schematic representation of a Langmuir trough compression.

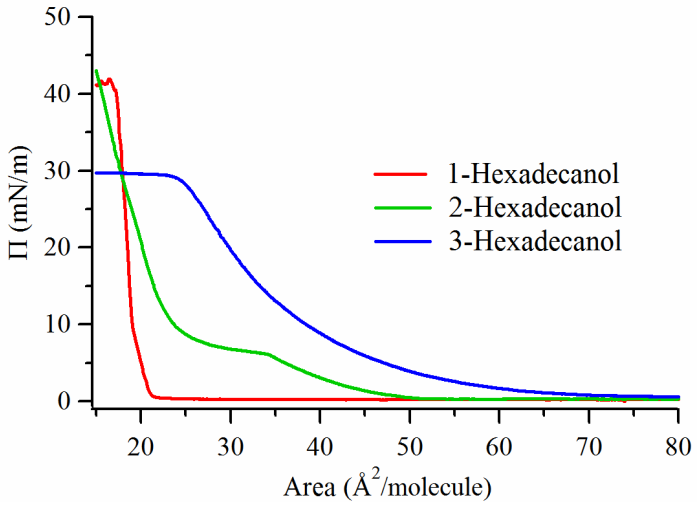

Figure 1.4. Surface pressure isotherms for 1-, 2-, and 3-hexadecanol monolayers.

Surface pressure isotherms of insoluble surfactants provide information about the organization of monolayers during different stages of compression. For example, the 1-hexadecanol monolayer shows signs of different 2-dimensional (2D) thermodynamic phases behaviors at the aqueous/vapor interface. At low surface coverages (corresponding to large areas per molecule) the relatively flat surface pressure indicates limited interactions between the monomers and the monolayer can be described as a 2D gas. As compression forces the molecules closer together the surface pressure starts to rise and the films becomes less compressible. This state of the monolayer is described as a 2D liquid. At the highest compressions corresponding to the highest surface coverages and smallest areas per molecule, the monolayer is in a 2D solid form. Based on differences in their respective isotherms, 2-hexadecanol and 3-hexadecanol have very different 2D phase behavior from 1-hexadecanol. These differences are addressed in much greater detail in Chapter 2.

When measuring a surface pressure isotherm, a fixed number of molecules are constrained to a fixed area and the system is forced to equilibrate under these conditions. A second type of surface pressure measurement performed with insoluble surfactants measures the equilibrium spreading pressure (ESP) of a given soluble surfactant. To make an ESP measurement, a drop of liquid or a solid flake is left at the surface of the aqueous subphase and the system is allowed to equilibrate for up to two days. During the equilibration period, the material spontaneously spreads over the surface due to cooperative interaction between the subphase and the adsorbed monomers. Spreading stops and equilibrium is established when the cohesive forces

between molecules within the solid are balanced by the substrate-monomer and monomer-monomer interactions between those molecules making up the monolayer.

This behavior can be characterized by a general equilibrium between molecules in the solid sample and molecules composing the monolayer film at the aqueous/vapor interface:

$$M_{(s)} \leftrightarrow M_{adsorbed} \tag{1.4}$$

For example, when a flake of phospholipid sample is added into the water surface, the zwitterionic headgroup of the lipid molecules near the flake's surface will eventually be hydrated by water molecules. The solvated headgroups will have different chemical potentials from the unhydrated neighboring molecules. This difference leads to a mass flow of lipid molecules across the interface until the equilibrium surface pressure, known as the ESP, is reached. At ESP, in a dynamic process, the amount of material leaving the solid flake is equal to that sticking back to the flake's surface. And, the added material at the surface serves as an infinite reservoir of surfactant material. The measured surface pressure reflects the monolayer condition when monomers spread at the interface have the same chemical potential as those remaining in the solid sample. By mapping a solute's ESP onto its surface pressure isotherm, we can determine the "natural" organizing tendencies of different constitutional isomers.

1.2.2. Vibrational Sum Frequency Spectroscopy

To study the structure and organization within monolayers formed at the air/water interface we use a surface specific, vibrational spectroscopic technique, Vibrational Sum Frequency Spectroscopy (VSFS). Extensive theoretical background about the technique has been published in the literature.[3-7] Introductory information intended to familiarize readers with the technique will be presented below.

Briefly, this technique requires that visible and infrared optical fields with respective frequencies of ω_{vis} and ω_{ir} be temporally and spatially overlapped on the interface being studied. These two fields couple together through the second order susceptibility tensor, $\chi^{(2)}$, to produce a new field (ω_{sf}) equal in energy to the sum of ω_{vis} and ω_{ir}. Because $\chi^{(2)}$ is a third rank tensor, its elements necessarily change sign upon inversion. Consequently, all elements of the $\chi^{(2)}$ tensor vanish in isotropic media. Only at surfaces where interfacial anisotropy breaks the center of symmetry found in bulk liquids can the $\chi^{(2)}$ tensor assume nonzero values.

Elements of the $\chi^{(2)}$ tensor contain both nonresonant and resonant contributions,

$$\chi^{(2)} = \chi_{NR} + \chi_R(\omega_{IR}) = \chi_{NR} + \sum \frac{A_q}{\omega_{IR} - \omega_q + i\Gamma_q} \qquad (1.5)$$

where χ_{NR} and χ_R are nonresonant and resonant terms, respectively. The resonant term can be further expanded in terms of a mode specific amplitude term (A_q), the resonance frequency of the mode (ω_q), and a damping constant (Γ_q).[4,5]

The intensity of the sum frequency signal is proportional to the square of the surface nonlinear polarization, $P^{(2)}$ induced by the incident infrared and visible beams:

$$I_{sf} \propto \left|P^{(2)}\right|^2 \propto \left|\chi^{(2)}_{NR} + \sum_{\upsilon} \left|\chi^{(2)}_{R_\upsilon}\right| e^{i\varphi_\upsilon}\right|^2 I_{vis} I_{ir} \tag{1.6}$$

there ϕ_v is the relative phase of the v^{th} vibrational mode, I_{vis} and I_{ir} are the intensities of the incoming visible and infrared light, respectively.[5] For the systems compared in this work, careful analysis has shown the nonresonant component of the $\chi^{(2)}$ tensor to be very small compared to the resonant contributions.

For rotationally invariant surfaces, the $\chi^{(2)}$ tensor has 4 independent, nonzero components.[8] These are $\chi^{(2)}_{zzz}; \chi^{(2)}_{xxz} = \chi^{(2)}_{yyz}; \chi^{(2)}_{xzx} = \chi^{(2)}_{yzy}; \chi^{(2)}_{zxx} = \chi^{(2)}_{zyy}$, where z is the direction parallel to the surface normal. Information about molecular orientation can be obtained by isolating two of those 4 elements. The $\chi^{(2)}_{iiz}$ $(i = x, y)$ element is nonzero for vibrational modes having their IR transition dipoles aligned along the surface normal and is the sole element contributing to spectra acquired under $S_{sf}S_{vis}P_{ir}$ polarization conditions (Figure 1.5). Similarly, vibrational modes with IR transition modes in the interfacial plane will appear in the $S_{sf}P_{vis}S_{ir}$ polarized spectrum due to the $\chi^{(2)}_{izi}$ element. Therefore, spectra acquired with these different polarization combinations report information about the average molecular orientation at interfaces.

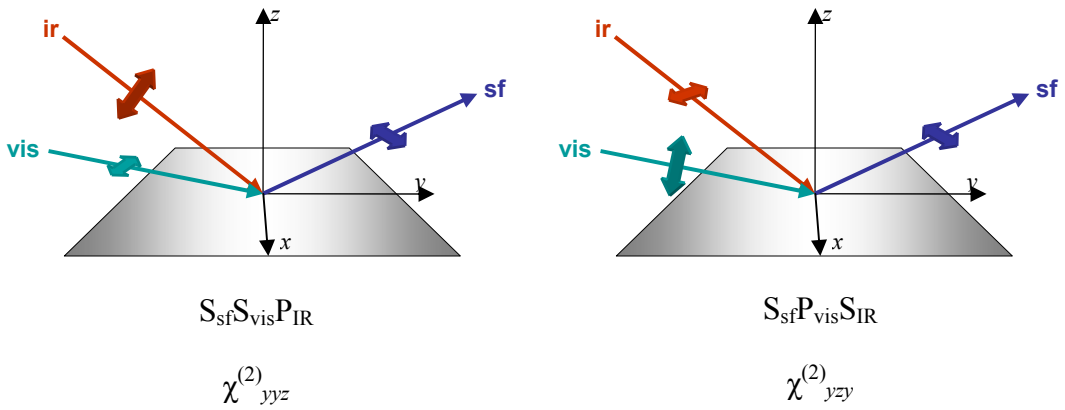

$S_{sf}S_{vis}P_{IR}$ $S_{sf}P_{vis}S_{IR}$

$\chi^{(2)}_{yyz}$ $\chi^{(2)}_{yzy}$

Figure 1.5. Schematic representation of SSP and SPS polarization conditions on interfacial coordinates. The arrows on light beams indicate parallel (S) or perpendicular (P) polarization of the light with respect to the interfacial plane.

Acquisition of polarization dependent VSFS spectra requires that the polarization of IR field be aligned with the IR transition dipole vector of a particular vibrational mode. Thus, the IR field couples with the vibrational transition dipole and the transition contributes into the $\chi^{(2)}$ tensor. The visible field then interacts with the oscillating dipole to create the sum-frequency polarization through an anti-Stokes Raman scattering mechanism. Typically, one interprets VSF spectra with direct correlations between the incoming IR and visible polarizations and orientations of the IR transition dipoles and polarizability tensors for molecular functional groups of interest. For example, in an $S_{sf}S_{vis}P_{IR}$ polarization combination, the "P" polarized IR field having the appropriate frequency excites the methyl symmetric stretch mode if and only if the methyl group has a sizable projection of its local C_3 symmetry axis along the surface normal. If the methyl group, however, is directed parallel to the surface (perpendicular to the surface normal), the resulting VSF spectrum at SSP

polarization combination does not show any contribution from the methyl symmetric stretch.

In general, the intensities of the methyl stretch bands, symmetric (r^+), asymmetric (r^-) and Fermi Resonance (r^+_{FR}), scale with the level of surface coverage of the monomers contributing to the spectra. One can predict that, for example, a monolayer formed by 3-C_{16}OH monomers will have different r^+ intensities in SSP spectra depending on the surface coverage level. A monolayer with a surface coverage corresponding to a molecular area of 40 $Å^2$ will produce significantly larger band intensities compared to a monolayer with that of 60 $Å^2$ (see Figure 1.4). The reasons for this expectation are two-fold. First, the intensity of the sum frequency response scales quadratically with the number of contributing species. Higher surface coverages correspond to more functional groups capable of contributing to the spectrum. Second, $I(\omega_{sf})$ depends on the ensemble averaged orientation of individual functional groups and these orientations will change with surface coverage. At higher molecular areas (corresponding to lower surface coverage), adsorbed monomers will form expanded monolayers leading to smaller, more randomized projections of IR transition dipoles onto the surface normal. As the molecular area gets lower (and surface coverage increases), adsorbed monomers will start to organize more efficiently leading to more well-defined, sharper orientational distributions of the methyl groups onto the surface normal. Thus, larger r^+ intensities are expected at lower molecular areas.[9]

The SFG spectrometer used in our study was built as a part of Dr. Okan Esenturk's Ph.D. research conducted in the Walker Research Group. The

instrumentation is modeled after a first-generation spectrometer first reported by Stephenson and co-workers.[10] Dr. Esenturk's used the instrument he built to study the structure adopted by molecules at neat liquid/vapor interfaces. Specifically, the surface structures of liquid alkanes with varying chain lengths and that of neat haloalkanes, alcohols and ketones were investigated using VSFS.[11,12] The details of the optical setup and instrumentation as well as data collection procedures are reported in Dr. Esenturk's thesis and appeared in the published reports.[13]

1.2.3. Computer Simulations

In recent years, classical molecular dynamics (MD) simulations have emerged as a valuable tool for predicting the properties and the microscopic structure of interfaces. For example, the structure of the charged surfactant SDS adsorbed to aqueous/air and aqueous/organic interfaces have been characterized and compared to extensive experimental results.[14-17] Careful analysis of results helped quantify probable molecular orientations as well as provided detailed pictures of chain disorder within the charged monolayer films. Other examples of MD simulations include the investigation of phospholipid monolayers and bilayers of model biological membranes,[18-26] characterization of bonding phenomena and water interactions at aqueous interfaces,[27-30] dynamics of chemical reactions and solvation at interfaces[31,32] and simulations of common anion and cation surface activity at aqueous/air interfaces.[33,34]

However, results from molecular dynamics simulations can only be as accurate as the potentials employed, and the potentials modeling intermolecular

interactions often are chosen not for generality but rather to reproduce very specific properties such as surface tension, density or viscosity. Simulations are typically not very accurate when differentiating between forces of comparable magnitude that compete to control the monolayer structure and organization at interfaces. One reason for this limitation is often the lack of reliable experimental data for monolayers composed of asymmetric surfactants.

A general pathway to perform MD simulations starts with preparing an input file describing the dimensions of the simulation unit, often called as *simulation box* and the positions of each atom or group inside the box. Physical parameters such as temperature and potentials defining the surfactant-surfactant interactions, surfactant-aqueous phase (subphase) interactions, and the water potential are defined prior to the simulation. Once all the parameters are set, an equilibration run is performed first to search for the most stable energetic conformations that will be used in the production run. The equilibration step is followed by production runs. While an equilibration run requires energy relaxation at frequent intervals, production runs follow dynamics for the equilibrated system. At the end of several nanoseconds of simulation time, the data are averaged and processed. Detailed information about the method we applied will be presented in Chapter 4.

Extensive information about the theoretical underpinnings of classical MD simulations is available in the literature.[35,36] Classical MD simulations operate based on Newtonian mechanics. The potentials defining the interactions of molecules in the box are described using principles of classical mechanics of bodies in motion and any contributions from quantum mechanical effects are not considered. The data obtained

are trajectories of motion described by the change in velocity and position of atoms with time. Simply, by solving the differential equations representing the Newton's Second Law ($F = ma$), one can obtain the trajectories of a simulation.

$$\frac{d^2 x_i}{dt^2} = \frac{F_{x_i}}{m_i} \tag{1.7}$$

From chemical point of view, trajectories can provide information about the structure of molecules through the information of atom positions during the simulation. Relative positions of carbon atoms in alkyl chains, for example, may contain information about the conformational order within individual surfactant monomers adsorbed to a surface. Information about dynamics at surfaces can also be attained by extracting the temporal information from trajectories.

Data presented in this thesis represent the first systematic studies of monolayer films formed by asymmetric surfactants. From the results of our experiments we can begin to understand how hydrophilic and hydrophobic interactions balance to create unique interfacial structures within organic monolayers adsorbed to the aqueous/vapor interface. In order to generalize these findings and develop predictive models, we performed simulations for different soluble alcohol isomers having the same chain length. MD simulations in this study were performed with help and patient mentoring from Professor Ilan Benjamin from University of California at Santa Cruz.

1.3. Systems Studied

1.3.1. Motivation for this Study

At interfaces, the balance between different competing forces acting on adsorbed molecules determines molecular structure and resulting organization. These forces are relatively predictable for symmetric systems, but for more asymmetric molecules, the magnitude and direction of these forces can vary considerably from one system to another. As a result, we have very few principles to help guide our intuition when considering the surface structure of asymmetric molecules and their organization in monolayers.

Understanding the molecular structure and organization within organic monolayers at aqueous/vapor interfaces is the basic motivation of this study. The systems chosen to explore these issues will be discussed in more detail in subsequent chapters. A brief overview, however, is presented below. Relatively simple organic molecules were used to isolate both intermolecular interactions within adsorbed films and the competition between attractive and repulsive forces experienced between monolayer monomers and the aqueous subphase. For example, organization within 1-decanol monolayers is easy to predict because of the simple geometry of the monomer building blocks. Monolayers formed by 2-decanol monolayers, however, are more complicated because of the forces acting on molecules. While the van der Waal's interactions between the longer alkyl chain segments try to keep the molecules as straight as possible, hydrophobic interactions between the C_1 methyl group and the water subphase have a disruptive effect on molecular organization

(Figure 1.6). Therefore, monomers can have a number of possible structures that they can adopt.

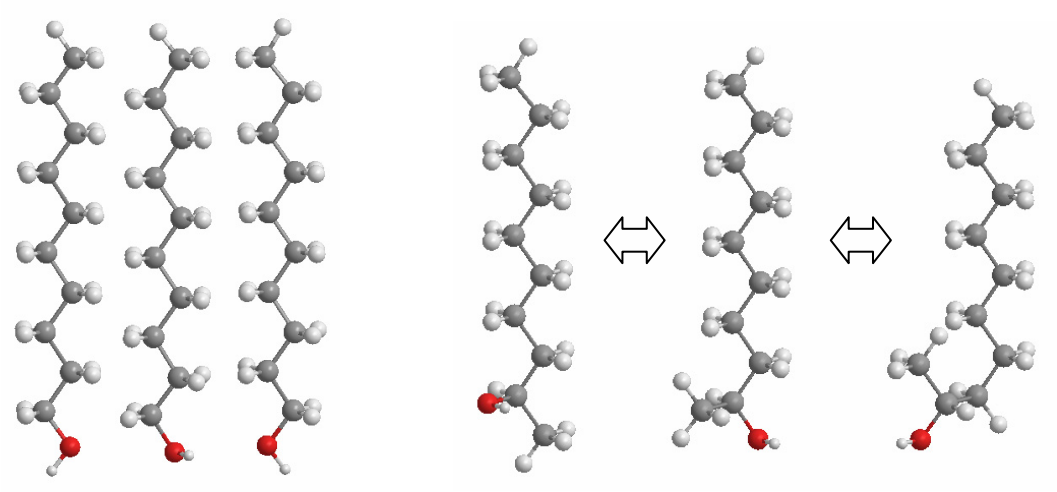

1-Decanol 2-Decanol

Figure 1.6. Possible conformations for 1- and 2-decanol monomers at interface.

Experimental studies (and in some cases MD simulations) allowed us to understand the relationship between the molecular configuration, e.g. constitutional isomerization, and the equilibrium structure within the monolayers.

1.3.2. Alcohols

Alcohols play important roles in many biological processes including fermentation of dairy products and behavioral stimulation of many insects. [37-42] One reason for their common appearance is their amphiphilic structures. Polar headgroups make these molecules prime candidates to form either vesicles and micelles or to intrude into pre-formed biological structures. Competition between these hydrophobic and hydrophilic interactions is also responsible for the equilibrium structure of

monomers adsorbed to the aqueous/vapor interface. For linear alcohols, structure and organization within films adsorbed to the aqueous/vapor interface is easy to intuit. For example, *n*-decanol, a linear, 10-carbon alcohol forms a tightly packed monolayer at the aqueous/vapor interface. This organization allows the alcohol OH group to make strong H-bonds with the water subphase while the hydrocarbon chains interact with each other through attractive van der Waals forces. These interactions lead to the monomers adopting an upright geometry forming a highly ordered monomolecular film.

The story for branched alcohol isomers is more complicated. Structural differences of branched isomers force monomers to choose between the different intermolecular interactions within the monolayer and hydrophilic and hydrophobic interactions with the aqueous subphase. For example, a 2-position alcohol such as 2-decanol has two alkyl chains with different lengths, a methyl group and an octyl group separated by an alcohol at the 2-position. Such a molecule at an aqueous/vapor interface will be subjected to different forces including H-bonding between OH and water, attractive forces between long alkyl chains, and an unfavorable hydrophobic interaction between the shorter alkyl segment and the water subphase. The balance between these forces determines the most probable conformation of monomers within the monolayers. Our studies showed that the interplay between the van der Waals attraction and the hydrophobic repulsion is the primary factor in determining the equilibrium interfacial structures of 2- and 3-position alcohols. Since the magnitude of the van der Waals attractions depends on the chain length of the longer alkyl segment, the balance shifts favoring tightly packed, cohesive organization in

monolayers formed by long-chain, insoluble alcohols (e.g. 2-hexadecanol) but more expanded monolayers with soluble alcohols sharing similar branching patterns (e.g. 2-decanol).

Chapter 2 presents experimental studies that explore the structure and organization of long chain, insoluble alcohol monolayers. Specifically, surface pressure isotherms along with the ESP measurements of different hexadecanol isomers are reported. VSFS spectra acquired at their ESP accompany the thermodynamic data. The data presented allow us to infer equilibrium structures of alcohol monomers within the monolayers.

The surface tension data and VSFS spectra for soluble alcohols are presented in Chapter 3. The experimental results we report reveal equilibrium structures that are significantly different from their corresponding insoluble alcohol counterparts. The differences arise from smaller van der Waals interactions between the shorter "long" hydrocarbon segments in these monomers.

Experimental results obtained provide us important information about molecular structure and organization within the different monolayers. In an effort to model these results we initiated a series of classical MD simulations designed to develop better insight into the equilibrium structures inferred from experiments. Chapter 4 explains the methodology and results of these MD simulations. The results presented belong to simulations run for different constitutional isomers of soluble alcohol monolayers. Specifically, simulations explore the effects of monolayer coverage on the area-conformer relationship of the alcohols within the monolayers.

1.3.3. Phospholipid Monolayers

Chapter 5 of this thesis expands the complexity of systems studied to include the structure of phospholipid films formed in the presence of soluble, charged surfactants. Specifically, role of surfactants in promoting or inhibiting lipid film formation across the aqueous/air interface is discussed. Observations addressing structure of monomers within the mixed monolayers of phospholipids and surfactants are included.

In this thesis, the term "phospholipid" will refer to lipids composed of three parts: a polar or charged headgroup, two nonpolar acyl chains, and a connecting 3-carbon glycero backbone. The acyl chains may contain different number of carbon atoms either in the form of fully saturated or unsaturated hydrocarbon structure. Some examples of phospholipid molecules are shown in Figure 1.7. Work in this thesis focuses on the behavior of DPPC at the aqueous/air interface. DPPC has a zwitterionic headgroup and two saturated sixteen-carbon acyl chains.

Experimental studies of the phospholipid monolayers adsorbed to the aqueous/air interface are presented Chapter 5. The surface pressure isotherms for DPPC on different aqueous subphases are presented with their respective ESP measurements. The effect of SDS and DTAB surfactants on DPPC monolayer formation and monolayer structure were investigated with the help of VSFS measurements. The self driven spreading of DPPC on aqueous surfaces to form monolayers was a matter interest in these experiments. The effect of surfactants as a potentially competing surface active species was explored with a function of

surfactant bulk phase concentration. The results showed significantly different effects depending on whether the surfactant was anionic or cationic.

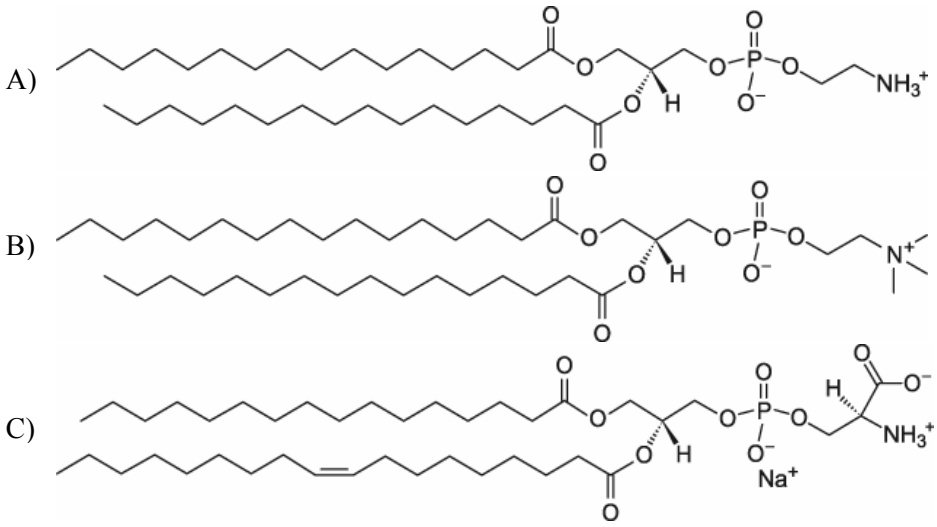

Figure 1.7. Examples of phospholipid molecular structures. A) 1,2-Dipalmitoyl-*sn*-Glycero-3-Phosphoethanolamine (DPPE), B) 1,2-Dipalmitoyl-*sn*-Glycero-3-Phosphocholine (DPPC), and C) 1-Palmitoyl-2-Oleoyl-*sn*-Glycero-3-[Phospho-L-Serine] (POPS)

Chapter 2 and 3 of this dissertation were published in as two separate papers. Parts of Chapter 5 have also been submitted for publication and results presented in Chapter 4 are also in preparation as a journal article. As a result, subsequent chapters will contain some redundant material.

Chapter 2: Insoluble Alcohols

2.1. Introduction

Starting with the seminal experiments of Irving Langmuir more than 75 years ago,[43] a wealth of experimental data and theoretical modeling has led to well honed intuition about the surface properties and structure of symmetric amphiphiles adsorbed to liquid surfaces. Surface tension measurements have characterized the two-dimensional thermodynamic behavior of these systems.[44-46] Neutron and X-ray scattering experiments have resolved with sub-angstrom resolution molecular structure in these monolayers.[47-49] Optical spectroscopy has provided detailed information about the strength and directionality of intermolecular interactions within monolayers as well as between the monolayers and the aqueous subphases.[6,50-53] Increasingly elegant simulations and theory development have continued to refine our understanding of the anisotropic, intermolecular forces responsible for the behavior and properties of alkyl monolayers adsorbed to the water/vapor interface.[14,15,32,54,55] Generally speaking, the high degree of order found within long chain, neutral (or zwitterionic) alkyl surfactants adsorbed to the air/water interface arises from strong hydrogen bonding between surfactant head groups and interfacial water as well as collective van der Waals interactions between chains that lead to close packed, all-*trans* conformations.

Less clear is how asymmetric amphiphiles organize themselves in two dimensions at different surface coverages. Here, the term asymmetric refers to

surfactants having their polar (or zwitterionic) headgroup located in any position other than a terminal carbon. Such structures force surfactants to choose between minimizing hydrophobic interactions with the water by adopting *gauche* defects and maximizing the chain-chain interactions between the longer arms of the surfactants, an attractive interaction requiring an all-*trans* conformation that forces the shorter alkyl segment into the aqueous phase. This competition between cohesive chain-chain attractions and the effective repulsion resulting from hydrophobic effects addresses fundamental questions in colloid science, namely how do molecules at surfaces balance competing forces, and how do the magnitudes of these forces scale with molecular size?

Results presented below mark our initial attempts to answer these questions in a systematic manner. Experiments have examined the two dimensional phase behavior and monolayer structure of a family of hexadecanol isomers with the alcohol functional group in the 1, 2, 3 and 4 positions (Figure 2.1). The linear isomer, 1-hexadecanol (1-C_{16}OH), has long served as a model surfactant for studying self assembly at surfaces, and its inclusion in this work provides an important benchmark for systems that can assemble without any structural constraints.[56-60] The surface pressure isotherm of the 1-C_{16}OH monolayer shows classical Langmuir film behavior, and vibrational spectra of the monolayer at its equilibrium spreading pressure (ESP) reflect a monolayer that is closely packed with very little conformational disorder. In contrast, surface pressure isotherms of 3-C_{16}OH and 4-C_{16}OH monolayers never show any distinctive phase behavior. Correspondingly, vibrational spectra of these systems at their equilibrium spreading pressures reveal

monolayers having considerable degree of disorder and randomization within alkyl chains. The isomer with the smallest degree of asymmetry, 2-C_{16}OH, shows intermediate behavior between these two extremes. A plateau in the surface pressure isotherm suggests a 2-dimensional phase transition from a disordered film to a closely packed monolayer. The ESP of 2-C_{16}OH implies that cohesive chain-chain interactions are strong enough to overcome the energetic cost of solvating the terminal methyl group in the C_1 position. Interestingly, vibrational spectra of the 2-C_{16}OH monolayer show surprising changes in band intensities implying either more disorder than one might expect based on geometric considerations, or destructive interference from oppositely aligned methyl groups. The latter explanation is consistent with ESP data and requires that 2-C_{16}OH at its ESP adopt an all-*trans* conformation forcing the methyl group in the C_1 position to be solvated by the interfacial water.

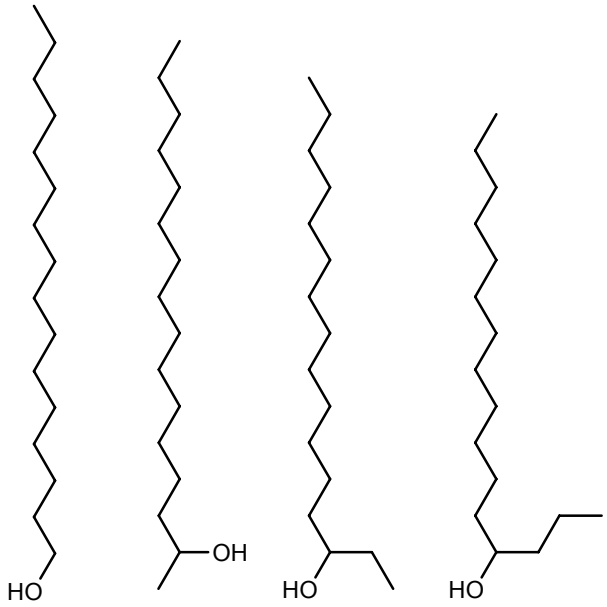

Figure 2.1. Molecular structures of 1-, 2-, 3-, and 4-hexadecanol molecules.

2.2. Experimental

2.2.1. Materials

Hexadecanol isomers used in the study were obtained from Aldrich and ChemSampCo. 1-hexadecanol (1-C_{16}OH, Aldrich, Cat. No: 258741) and 2-hexadecanol (2-C_{16}OH, Aldrich, H6827) both had reported purities of 99%. 3-hexadecanol (3-C_{16}OH, 98%, 3282.80) and 4-hexadecanol (4-C_{16}OH, 98.1%, 3283.00) were ChemSampCo products. Deionized water (Milli-Q, >18 MΩ·cm) was used as the sub phase in these experiments. The asymmetric isomers all are chiral raising interesting questions about whether chirality plays a role in the monolayer structures adopted by different enantiomers. Experiments described in this work used racemic mixtures of each isomer, although related experiments (not reported here) found no discernible difference in the thermodynamic and structural properties of monolayers prepared from pure enantiomers and their corresponding racemic mixtures.

2.2.2. Methods

2.2.2.1. Surface Pressure Measurements

Surface pressure isotherms of the insoluble hexadecanol monolayers were obtained using Langmuir Film Balance (302LL, Nima Technology Ltd., Coventry, England). Monolayers were prepared using a spreading solvent (4:1 hexane:chloroform by volume, 1.0-1.5 mg/mL). Initial monolayer coverages exceeded 200 $Å^2$/molecule. After allowing the spreading solvent to evaporate, the

monolayer was compressed at a rate of 30 cm^2/min. The isotherms of each isomer proved reversible provided that compression was stopped before monolayer collapse. Given the differences in isomer isotherms, monolayers at their ESP were chosen as reference states for comparing differences in molecular structure and organization. Surface tension measurements of ESP's were performed using an analytical balance equipped with a Wilhelmy plate. Samples were prepared by putting a solid flake of the isomer on the water surface and allowing the monolayers to spread across the H_2O surface. At the ESP, the adsorbed hexadecanol surfactants were in equilibrium with the solid "reservoir" floating on the surface. Equilibrium typically required ~3-4 hours to establish itself as evidenced by a constant surface pressure.

2.2.2.2. Molecular Footprint Area Calculations

Calculation of the areas occluded by different isomer conformations at their ESPs employed equilibrium bond lengths: C-C: 1.523 Å, C-H: 1.113 Å, C-O: 1.421 Å and O-H: 0.94 Å. These values were the results of molecular mechanics minimizations of different conformer energies. Every central atom was assumed to occupy a regular tetrahedral center with bond angles of 109.5°. In addition, van der Waals radii (of 1.20 Å for hydrogen and 1.40 Å for oxygen) were used to approximate the boundaries of molecules within a monolayer. Figure 2.2 shows the geometry of a 2-C_nOH molecule with a single gauche defect as an example. With these parameters, cross sectional areas were calculated in two ways: first, molecules were assumed to have circular footprints reflecting complete rotational freedom about the surface normal. This approach necessarily overestimates molecular surface areas

if surfactants aggregate at the surface. The other approach for calculating molecular areas assumes no rotational freedom for the adsorbed surfactants and therefore represents a lower limit to the area occupied per molecule. Despite the ambiguity resulting from these two different limits, the calculated areas from different conformations can serve as useful guides when inferring the equilibrium structure of isomers in monolayers at their ESP.

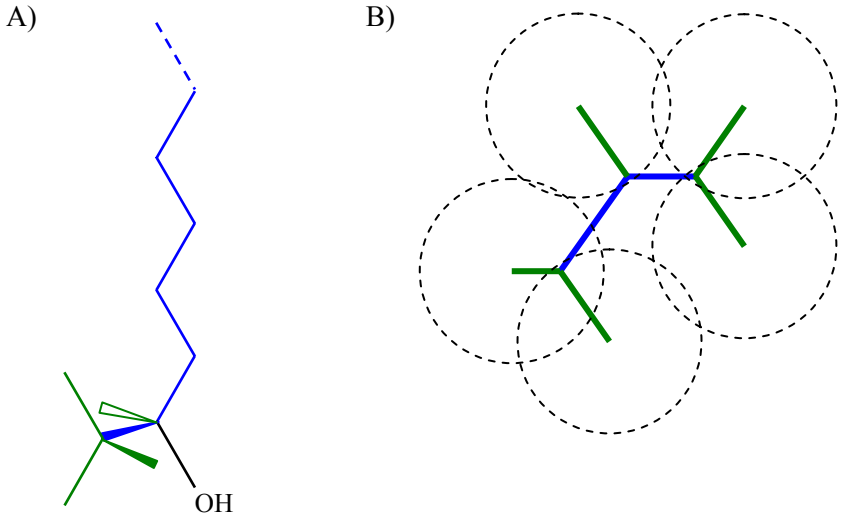

Figure 2.2. Geometry of a 2-C_nOH molecule with a gauche defect around the C_2-C_3 bond axis for molecular footprint area calculations. A) Side view, B) Top view. Blue lines are C–C bonds and green lines are C–H bonds. Circles represent the van der Waals radii for H atoms.

2.2.2.3. Vibrational Spectra Acquisition

The molecular structure of monolayers at their ESP were compared based on surface specific, vibrational spectra acquired using broadband Vibrational Sum Frequency Spectroscopy (VSFS). Theoretical backgrounds of the technique have already been presented in Section 1.2.2. The broad band sum frequency spectrometer

used in these studies has been described in a previous report.[11] The spectrometer uses 775-nm light from a regeneratively amplified Ti:sapphire femtosecond laser system (CPA 2001, Clark MXR) having a bandwidth of ~10 nm, a pulse duration of 130 fs and a repetition rate of 1 kHz and a total output power of 750 mW. About 65% of the total light produced is directed into the tunable optical parametric oscillator (TOPAS, Light Conversion) where ω_{signal} and ω_{idler} are combined via difference frequency mixing to generate IR wavelengths between 2.8 μm – 10 μm. At 3.5 μm, the FWHM of the IR field is ~100 cm^{-1} with a power of ~5 mW immediately before the sample surface. The visible beam is frequency narrowed with an optical stretcher.[61] Typical conditions expand the visible beam to produce a pulse duration of 2 ps pulse and an 8-10 cm^{-1} frequency bandwidth. The corresponding visible beam power on the sample was ~7 mW. Both beams are focused on the sample surface with the aid of a video camera to ensure spatial overlap. The nonresonant SF signal obtained from Au metal and the resonant signal from the symmetric methyl stretch of dimethylsulfoxide (DMSO) surfaces are used to optimize the optical path. The methyl symmetric stretch band of DMSO also provides a reproducible, internal calibrant of system performance that enables the absolute intensities of monolayer spectra to be compared.

The signal detection is done using a 100 x 1340 pixel CCD array (Spec-10:100, Roper Science) following dispersion of the SF signal off of a monochromator grating (Acton, SP300i). Given the IR bandwidth of the TOPAS DFG, multiple spectra must be acquired in order to observe all the vibrational bands in the CH stretching region. This requirement was met by stepping the IR wavelength in 50 nm increments over the region between 3.30 and 3.80 μm and summing the individual

spectra. The wavelength spacing was chosen so that the incident IR energies at any given wavelength were constant after all individual spectra were compiled. Based on the equivalent appearance between spectra acquired with this method and previously reported data (e.g. 1-C_{16}OH on water), this approach appears quite reliable provided that the IR step size is chosen carefully. The composite spectra shown in this work represent the sum of up to ten individual spectra spanning the entire frequency window of interest. DMSO measurements performed before and after each set of spectra ensure stable, reliable system performance and to allow comparisons of absolute signal intensities between spectra from different hexadecanol isomers. Additional details about spectra compilation can be found in a separate report.[11]

2.3. Results and Discussion

2.3.1. Determination of Molecular Area

Surface pressure isotherms of monolayers of various hexadecanol isomers (1 to 4-C_{16}OH) adsorbed to the air/water interface are shown in Figure 2.3. The isotherm of the linear isomer (1-C_{16}OH) remains flat for most of the compression before rising steeply near coverages corresponding to a fully compressed monolayer. This behavior is consistent with other linear, neutral, insoluble surfactants adsorbed to the water/vapor interface. A kink in the isotherm at ~19 $Å^2$/molecule indicates a 2-dimensional liquid-solid phase transition.[44,57]

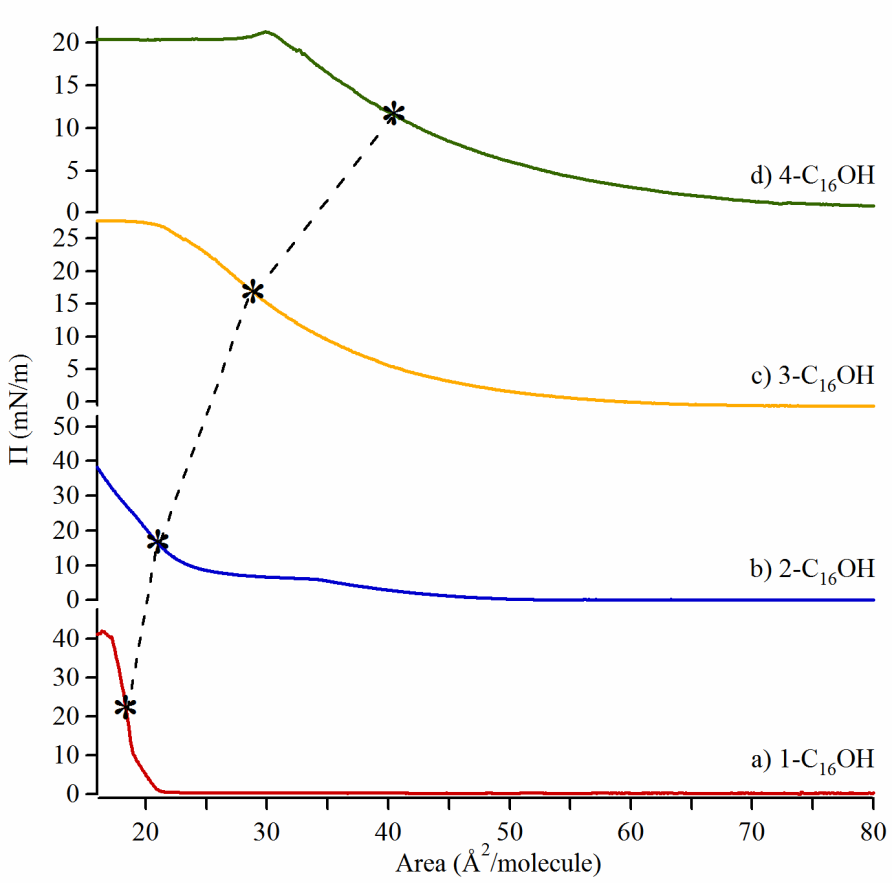

Figure 2.3. Surface pressure isotherms of hexadecanol monolayers. Asterisks show equilibrium spreading pressures. The dashed line is intended as a guide for the eye.

The 2-C_{16}OH monolayer shows distinctly different behavior at the water/vapor interface. The surface pressure begins to rise when the monolayer is more expanded and passes through a plateau between 35 and 25 Å^2/molecule. This feature is characteristic of liquid expanded/liquid condensed transitions commonly observed in monolayers of saturated phospholipids.[62,63] The rise in surface pressure continues until the monolayer collapses at ~14 Å^2/molecule. Compared to the linear isomer, one might expect 2-C_{16}OH to pack less efficiently. The methyl group in C_1 position adds an irregular feature to the molecular structure, forcing the adsorbed

species to choose between optimizing chain-chain interactions and minimizing methyl contact with the underlying aqueous phase. However, the 2-C_{16}OH surface pressure isotherm suggests that this isomer packs just as efficiently as the linear isomer as evidenced by the steep slope at high surface coverage and the high surface coverages at monolayer collapse. The competition between attractive chain-chain interactions and energetically unfavorable hydrophobic forces becomes more pronounced when comparing the surface pressure data from 3- and 4-C_{16}OH monolayers. These two isotherms show no distinguishable phase transitions and the monolayers remain expanded all the way to monolayer collapse at 24 $Å^2$/molecule for 3-C_{16}OH and at 30 $Å^2$/molecule for 4-C_{16}OH.

In order to minimize the interfacial free energy, insoluble, adsorbed alcohol surfactants must balance the strong hydrogen bonding with the water subphase and relatively strong van der Waals interactions between alkyl chains against the hydrophobic interactions of side chains with water and the structural irregularities that prevent efficient packing. For an aqueous surface having constant area and a reservoir of surfactant material, these forces balance when the monolayer reaches its ESP. The measured ESPs of the different hexadecanol monolayers appear in Table 2.1 and are marked on the surface pressure isotherms in Figure 2.3. Predictably, 1-C_{16}OH at its ESP forms the most compact monolayer (with a coverage of < 20 $Å^2$/molecule). A more surprising result is that 2-C_{16}OH also forms a reasonably compact monolayer despite a methyl group in C_1 position that could disrupt chain-chain interactions. 3-C_{16}OH and 4-C_{16}OH form more expanded monolayers at their

ESP reflecting the difficulty in packing together alkyl chains having larger secondary hydrocarbon segments.

Table 2.1. Thermodynamic and spectroscopic data for hexadecanol isomers. ESP and corresponding surface area values are the result of at least 3 replicate measurements.

	ESP (mN/m)	ESP Surface Area (Å^2/molecule)	r^+ intensity[#]	d^+ intensity[#]	r^+/d^+ ratio
1-C_{16}OH	20.8 ± 3.7	18.9 ± 0.3	8560	395	21
2-C_{16}OH	15.1 ± 1.1	21.5 ± 0.3	3800	433	8.7
3-C_{16}OH	15.7 ± 3.4	28.7 ± 2.4	1655	700	2.4
4-C_{16}OH	11.0 ± 1.7	40.3 ± 2.2	675	400	1.7

[#] Arbitrary units extracted by deconvoluting the SSP spectra and scaled to an integrated r^+ intensity of 3.5.

2.3.2. Vibrational Spectroscopy and Conformer Structures

VSF spectra of the hexadecanol monolayers can identify how this balance of forces controls molecular structure within monolayers formed by different isomers. Features appearing in the CH stretching region can be assigned either to methyl groups or methylene groups and these vibrational bands can be very sensitive to alkyl chain conformation and orientation.[64,65] The methyl symmetric stretch (r^+) appears at 2872 cm^{-1} while the doubly degenerate asymmetric stretch (r^-) appears between 2952 and 2957 cm^{-1}. In addition, the CH_3 symmetric stretch can lend intensity to an overtone of CH_3 bending motion (r^+_{FR}) through a Fermi Resonance coupling. This band typically appears at 2935 cm^{-1}. The methylene symmetric stretch (d^+) appears at 2841 cm^{-1}. A broad feature centered at ~2930 cm^{-1} can contain intensity from the r^-,

r^+_{FR} and d^+_{FR}. Notably absent in all spectra presented in this work is a band that can be assigned unambiguously to the methyne (-CH) stretch in the monolayers formed from 2-C_{16}OH, 3-C_{16}OH, and 4-C_{16}OH. Two explanations can explain the methyne group's absence. First, the preferred conformations adopted by the different isomers as deduced below all tend to leave the isolated –CH bond aligned approximately parallel to the surface, meaning that this vibration would not have a strong out-of-plane component (that would be) sampled by the SSP polarization conditions reported in this work. Second, the methyne group itself is expected to have relatively weak VSF activity and therefore would not contribute significant intensity to a VSF spectrum even if it were aligned in the appropriate direction. These findings are consistent with recent work from Lu, *et al.* that reported VSF spectra from the surfaces of neat alcohol liquid/vapor interfaces and failed to identify a distinctive feature that could be assigned to the isolated –CH stretch of the methyne group.[65]

The spectrum of the 1-C_{16}OH monolayer at its ESP shows features due almost exclusively due to the single methyl group in the C_{16} position (Figure 2.4). Very large r^+ and r^+_{FR} bands in the SSP spectrum imply a molecular orientation with the CH_3 C_3 symmetry axis aligned primarily along the surface normal. The large r^- band under SPS polarization combination also supports this picture (Figure 2.5). (SPS spectra from all isomer monolayers at their ESPs appear in Supporting Information.) Low intensity in the d^+ band indicates that the alkyl chains have very few gauche defects, and that the C_2 symmetry axes of the CH_2 groups lie primarily parallel to the surface. The ratio of r^+/d^+ is often used as a signature of conformational order within an alkyl monolayer. Large ratios indicate a well ordered array of all-*trans* hydrocarbon

chains.[66] The 1-C_{16}OH monolayer at its ESP has an r^+/d^+ ratio in excess of 20. (Table 2.1) In addition to the spectral band intensities implying a well ordered monolayer, the molecular surface area at ESP (18.9 ± 0.3 Å^2) is very close to that of all-trans alkyl chains standing normal to the interface. Together, these findings support a molecular structure of linear alcohols at the interface having their chain axes aligned parallel to the surface normal. The difference between the overall chain orientation and the terminal methyl C_3 axis results in a small, non-zero, out-of-plane component of the r^- transition dipole leading to a weak r^- band at 2954 cm^{-1} in the SSP spectrum.

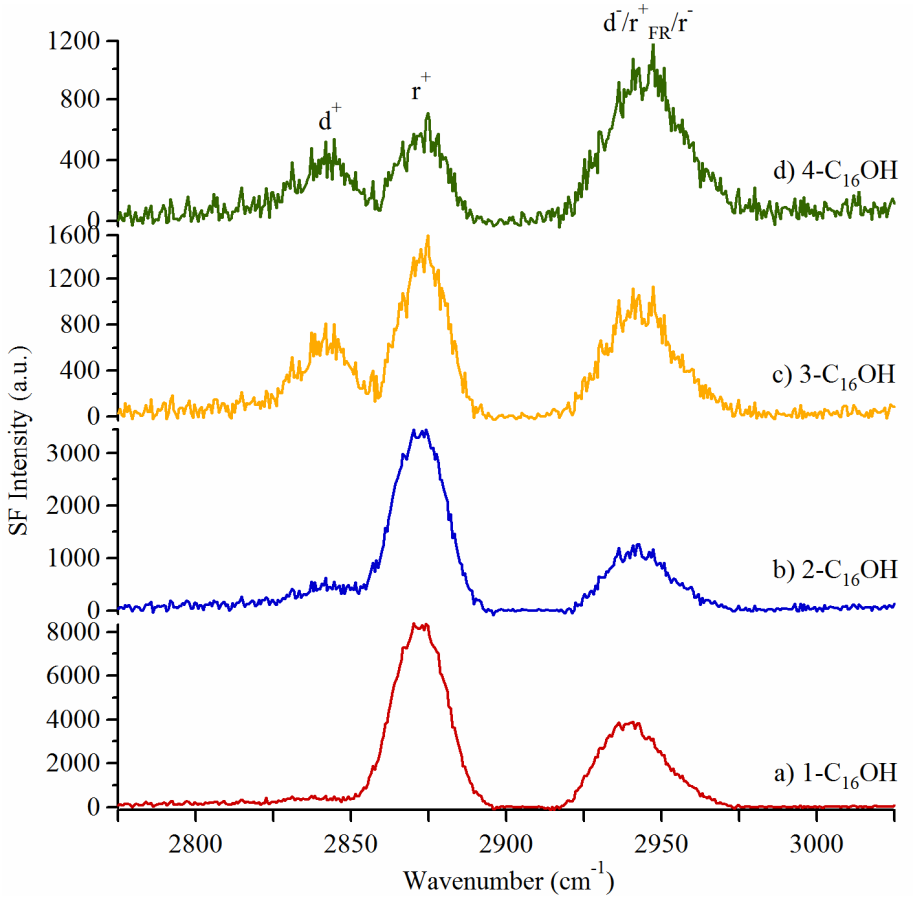

Figure 2.4. VSF spectra of hexadecanol isomers under SSP polarization conditions.

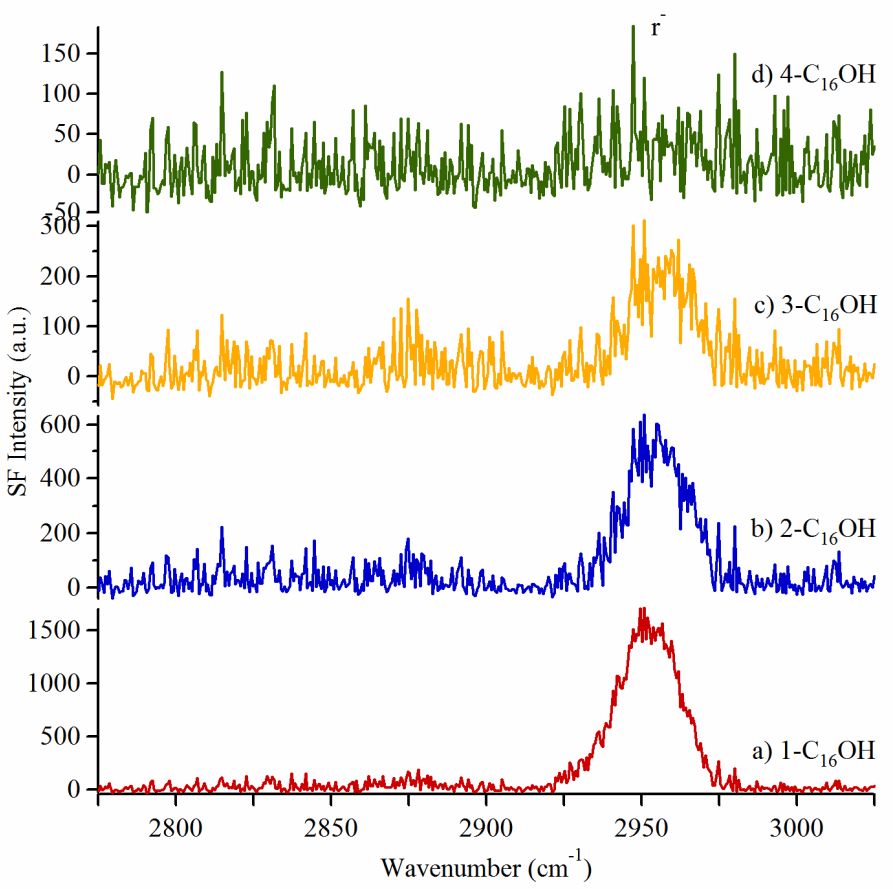

Figure 2.5. VSF spectra of hexadecanol isomers under SPS polarization conditions.

At first glance, the spectrum of 2-C_{16}OH is similar to that of the linear isomer except that the d^+ feature appears slightly more pronounced (Figure 2.4b). Because this measurement is carried out for 2-C_{16}OH at its ESP, we infer that the structure observed in the vibrational spectrum corresponds to a 2-C_{16}OH monolayer having a surface coverage of 21.5 ± 0.3 $Å^2$/molecule. This monolayer is slightly expanded compared to 1-C_{16}OH monolayer at its ESP, meaning that 2-C_{16}OH surfactants have more conformational freedom to adopt gauche defects. Gauche defects allow the d^+ mode to become VSF active. However, careful evaluation of absolute band intensities reveals that the intensity of the d^+ band actually drops only ~20% relative to the d^+

band in the 1-C_{16}OH spectrum. In fact, the observed differences between 1-C_{16}OH and 2-C_{16}OH can be attributed almost entirely to the ~2.5-fold reduction in r^+ band intensity. The absolute intensities of selected bands are listed Table 2.1 and presented in Figure 2.6.

Geometric considerations of the molecular structure help identify the most probable geometry of adsorbed 2-C_{16}OH molecules at the ESP. The van der Waals area covered by a single 2-C_{16}OH molecule having an all-trans conformation along the C-C backbone is calculated to be 22.2 $Å^2$/molecule if the adsorbates held rigidly in place and 26.4 $Å^2$/molecule assuming complete rotational freedom. The lower end of this window is very close to the measured 21.5 $Å^2$/molecule. The all-trans geometry necessarily forces the CH_3 group in the C_1 position into the water in order to maximize interactions between the 14-carbon alkyl chains. A second possible molecular conformation would include a gauche defect that orients the C_3 axis of the C_1 methyl group parallel to the interfacial plane and roughly perpendicular to the molecular C-C backbone. The two cross-sectional areas for this conformation are calculated to be 24.1 and 29.6 $Å^2$/molecule using rigid and rotationally free models, respectively. This window is broader than the all-trans conformation and deviates more from the observed value at ESP. Thus, geometric considerations coupled with experimental data suggest the most likely molecular conformation to be one that has the two methyl groups of 2-C_{16}OH at its ESP pointing reverse directions.

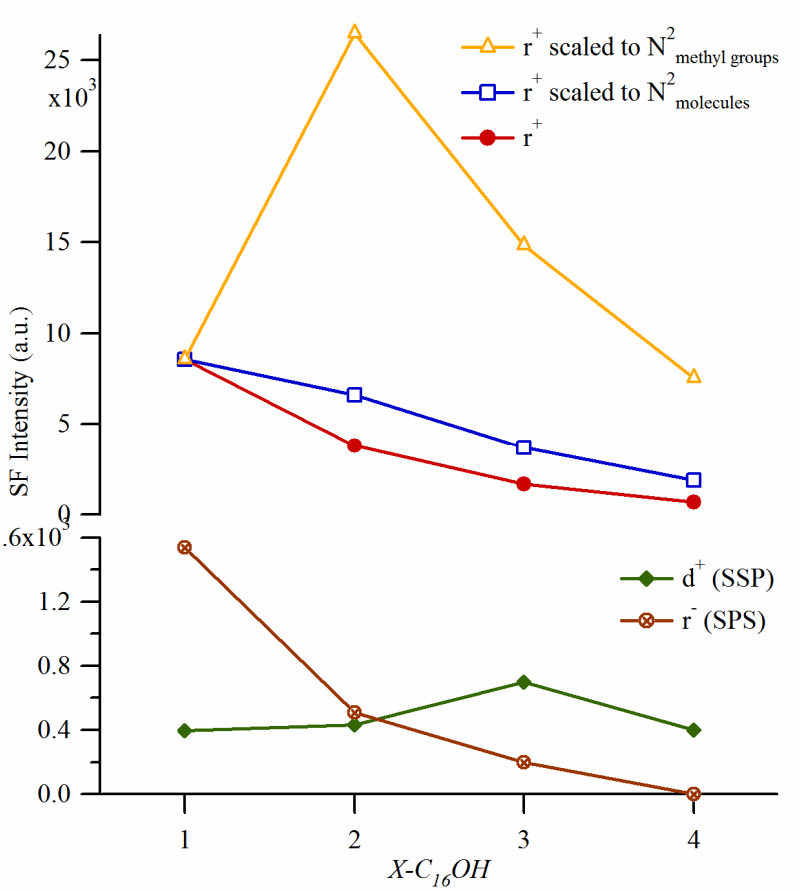

Figure 2.6. Intensity changes in selected vibrational bands with OH registry. Scaled r^+ intensities are calculated using the molecular areas at ESP with respect to the 1-C_{16}OH monolayer. The values are obtained by scaling the r^+ intensity to the number of molecules ($N^2_{molecules}$) and methyl groups ($N^2_{methyl\ groups}$). While the former values assume only one methyl group contributes to each spectrum, the latter values take into account both methyl groups of the isomers and assumes that each methyl group contributes to the spectrum with the same amplitude of the single CH_3 group in 1-C_{16}OH.

This conformation can lead to destructive interference in the r^+ band due to oppositely signed contributions to the $\chi^{(2)}$ tensor from methyl groups aligned opposing directions. If one assumes that only a single CH_3 group contributes to the observed spectrum (due to a gauche defect that directs the C_1 methyl group parallel to

the surface), then one would anticipate r^+ intensity to drop ~20% from the 1-C_{16}OH limit based on surface coverage considerations. However, r^+ intensity diminishes by a factor of ~2.5 (Figure 2.5). Given the symmetry of r^+ band profile destructive interference from oppositely oriented methyl groups would have to result from vibrational transitions having almost perfect spectral overlap. The r^+ vibrational frequency for a methyl group in the α position relative to a R-OH group is reported as ~2870 cm^{-1}, a value that overlaps the frequency of r^+ of the terminal CH_3 group in the C_{16} position.[64,65] These results suggest strongly that destructive interference between two methyl groups is responsible from the signal attenuation observed for r^+ band. A consequence of this destructive interference is that the r^+/d^+ ratio (8.7) is much smaller than one would expect based on simple conformational arguments. In fact at its ESP, 2-C_{16}OH has a CH_3 concentration that is two times that of 1-C_{16}OH, meaning that in principle, twice as many methyl groups *could* contribute intensity to the VSF spectrum. In light of this consideration, the lower r^+/d^+ ratio for the 2-C_{16}OH monolayer further supports the picture of oppositely aligned methyl groups.

The proposed upright geometry for the adsorbed 2-C_{16}OH molecules at their ESP implies that the cohesive van der Waals interactions between C_{14} alkyl chains are strong enough to overcome the energetic cost of solvating at methyl group in the top layers of the aqueous solvent. Furthermore, this conformation at ESP raises an interesting question about the extended plateau observed in the surface pressure isotherm. This region between 35 and 25 $Å^2$/molecule may represent a coexistence between two different conformer populations. As the molecular area diminishes, an increasing number of adsorbed molecules would have to minimize their area by

burying methyl groups into the water. Such a picture is consistent with the geometric arguments presented above and deserves further study.

Figure 2.4c shows the SSP spectrum of the 3-C_{16}OH monolayer at its ESP. Based on the surface pressure isotherm, the measured ESP corresponds to a surface coverage of 28.7 ± 2.4 $Å^2$/molecule. The structural consequences of trying to pack together 13-carbon chains attached to ethyl groups are striking. First, the methylene symmetric stretch, d^+, grows significantly in intensity relative to r^+ (Figure 2.6). The measurable increase in the d^+ band can arise from several sources. Moving the OH group to the C_3 position creates an isolated methylene group at the C_2 position. This isolated methylene group can contribute to the d^+ band regardless of molecular conformation, provided that its C_2 symmetry axis is aligned along the surface normal. Second, the growth of the d^+ band necessarily reduces the r^+/d^+ ratio of this system. Part of this effect can arise from the larger d^+ intensity. In addition, the larger area per molecule allows the 13-carbon alkyl chain to become more disordered, leading to diminished intensity in the r^+ band.

Moving the OH group to the C_3 position creates an interfacial molecular structure controlled by forces different from those responsible for structure within the 1- and 2-C_{16}OH monolayers. While monomers within the 1- and 2-C_{16}OH monolayers adopt primarily all-*trans* geometries, the significantly larger surface area at ESP and differences in spectral band intensities imply that this conformation is not preferred in the 3-C_{16}OH monolayer at the aqueous/vapor interface. Thus the adsorbed 3-C_{16}OH molecules must adopt gauche defects that allow for strong

surfactant hydrogen bonding with the water, while minimizing hydrophobic interactions between the ethyl group and the aqueous subphase.

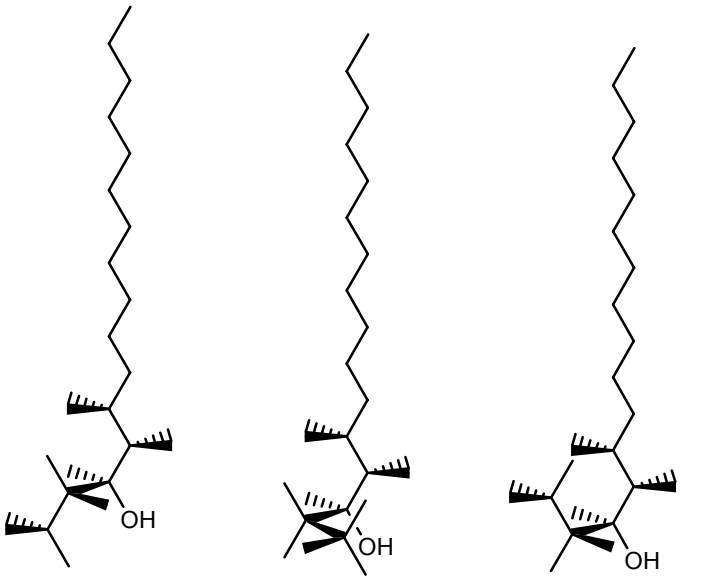

Figure 2.7. Possible conformer structures for 3-C_{16}OH monolayers. Protons on carbon atoms after C_5 are omitted for clarity. Based on surface tension and VSF data, the single gauche defect conformer appears to be the preferred structure of 3-C_{16}OH monolayers adsorbed to the air/water interface at the ESP.

One possible structure for 3-C_{16}OH molecule at the interface is a conformation having a single gauche defect (*g*) around the C_3-C_4 axis (Figure 2.7). The resulting structure decreases the interaction of the C_1-C_3 alkyl segment with the water subphase while still allowing for attractive H-bonding between OH group of alcohol and subphase water molecules. In this conformation, the isolated methylene group in the C_2 position necessarily has an out-of-plane IR transition moment to contribute to the d^+ band in spectrum. The structure also requires the methyl group in C_1 position to be directed toward the water subphase with an out-of-plane

contribution to the $\chi^{(2)}$ tensor that is opposite in sign to the methyl group in C_{16} position. Thus the single gauche defect conformation leads to continued partial destructive interference and reduced r^+ intensity in SSP spectrum. This molecular conformation with a single gauche defect accounts for the band intensities observed in the VSF spectrum and has a calculated molecular area between 30.5 and 42.7 $Å^2$/molecule. Again, the lower end of this window agrees closely with the measured molecular area of 3-C_{16}OH at its ESP (28.7 ± 2.4 $Å^2$/molecule).

Other possible conformations for 3-C_{16}OH molecule require a second gauche defect. The first such conformation has an "L" shaped molecular structure in which the plane containing the C_1, C_2 and C_3 atoms is perpendicular to the plane containing the 12-carbon atom C_5-C_{16} backbone. This structure requires one gauche defect around C_2-C_3 bond axis (*g*) and another one around C_3-C_4 bond (*g*). The scaled van der Waals area for this conformation is calculated to be between 29.4 and 40.8 $Å^2$/molecule. This calculated area is very close to that for 3-C_{16}OH with only a single gauche defect but this conformation directs the symmetry axis of the C_2 methylene group parallel to the surface and does not allow this functional group to contribute intensity to the SSP VSF spectrum. For this conformation, the *β*-position methyl group has an alignment with its C_3 symmetry axis having an in-plane orientation *and* can not contribute (either constructively or destructively) to the r^+ band of the SSP spectrum. The diminished intensity in r^+ band must be attributed solely to the lower coverage and associated alkyl chain randomization.

A second conformation having 2-gauche defects places one gauche defect about the C_2-C_3 bond and a second defect having opposite rotation (*g'*) around the

C_3-C_4 bond. This structure has a calculated footprint (30.5 and 42.7 $Å^2$/molecule) that is virtually identical to that of the gg conformation (29.4 and 40.8 $Å^2$/molecule) and positions the C_2 methylene group so that it can contribute intensity to the d^+ band in an SSP spectrum. With this *gg'* conformation, the methyl group at C_1 position assumes an out-of-plane orientation reducing the interactions with the water subphase. This conformation would be expected to show significant contribution to the r^+ intensity from the C_1 methyl group. However, the SSP spectrum of the 3-C_{16}OH monolayer shows continued evidence of partial destructive interference leading to a decrease in the r^+ signal intensity, albeit not as pronounced as in the 2-C_{16}OH spectrum.

The intensity of r^+ from the 3-C_{16}OH monolayer is ~25% smaller than would be expected based simply on the concentration of CH_3 groups in the 3-C_{16}OH monolayer compared to the 2-C_{16}OH monolayer. In the 2-C_{16}OH monolayer a combination of high surface coverage (21.5 $Å^2$/molecule) and even higher methyl group population (11 $Å^2/CH_3$) coupled with a r^+ intensity that was ~2.5-times less than in the 1-C_{16}OH monolayer led us to consider an all-*trans* conformation of the 2-C_{16}OH surfactants with methyl groups oriented in opposite direction. This arrangement would diminish the overall contribution of methyl groups to the observed intensity in VSF spectra. The 3-C_{16}OH monolayer at its ESP experiences a ~33% reduction in surface coverage compared to the 2-C_{16}OH monolayer. The intensity of the 3-C_{16}OH r^+ band drops ~60% from its level in the 2-C_{16}OH spectrum. Based on the surface coverage alone, we would expect that the r^+ band in the 3-C_{16}OH spectrum should diminish by only 45% compared to the 2-C_{16}OH system.

Along with destructive interferences, alkyl chain randomization will also lead to decreased intensity in the r^+ band. Consequently, the non-quadratic decrease in intensity from 2-C_{16}OH to 3-C_{16}OH monolayer leads us to believe that both methyl group randomization *and* destructive interference contribute to the diminished r^+ signal in the spectrum although quantifying the relative contribution from each effect is difficult.

The final spectrum in Figure 2.4, Figure 2.4d, shows the SSP spectrum of 4-C_{16}OH at its ESP of 11.0 ± 1.7 mN/m corresponding to a surface coverage of 40.3 ± 2.2 Å^2/molecule. While this spectrum looks qualitatively similar to that of the 3-C_{16}OH monolayer, several important differences hint at structural variations between monolayers formed from these two branched isomers. First, the d^+ band diminishes in intensity relative to the d^+ band of 3-C_{16}OH monolayer. This observation could seem surprising if one believed that lower surface coverage should lead to more conformational disorder and a correspondingly larger d^+ feature from both the long and short hydrocarbon segments. However, if the two methylene groups at C_2 and C_3 adopt a conformation where they make equal but opposite contributions to the $\chi^{(2)}$ tensor, then they will not contribute to the VSF spectrum and the "lone methylene" mechanism proposed for d^+ enhancement in the 3-C_{16}OH spectrum no longer applies. Such a condition requires the equilibrium molecular conformation to have one or two gauche defects in the structure. A single gauche defect around C_4-C_5 bond provides a *trans* oriented C_2 and C_3 position methylene groups, but the configuration requires a significant interaction between the resultant propyl group and the water. Based on energetic considerations, this conformation seems unlikely. A

second possible conformation adds an additional gauche defect to the C_3-C_4 axis (*g*) of the molecule leading to an "L-shape" molecular conformation. A third conformation results from a gauche defect around C_3-C_4 axis having the opposite phase, *g'*. This arrangement also leads to oppositely oriented methylene groups. All three conformations have calculated footprints that are equivalent to within experimental uncertainty for both rigid and free rotating models (35.1 to 60.6 $Å^2$/molecule, respectively). Given the lack of structure in the surface pressure isotherm and the relatively large molecular areas occupied by molecules at their ESP, adsorbed 4-C_{16}OH surfactants probably exist in a number of different conformations. The two conformations having two gauche defects appear to be the most likely candidates although other conformations can not be excluded. Despite this ambiguity in possible structures, the isotherm and VSFS data show conclusively that organization in monolayers of 4-C_{16}OH is dominated by hydrophobic interactions between propyl segments and the water subphase. These effective repulsions are strong enough to overcome any chain-chain interactions that would try to bring surfactants closer together.

2.4. Conclusions

To summarize, the structure and organization of monolayers formed from hexadecanol isomers at air/water interface have been investigated using surface tension measurements and VSFS. Data show the monolayers of 1- and 2-hexadecanol isomers pack closely together with all-*trans* conformations *and* average molecular orientations along the surface normal. For 2-C_{16}OH monolayer, the intermolecular

van der Waals interactions are strong enough to keep the chains in straight, all-*trans* conformations, and necessarily solvate the methyl group in the α position with the water subphase. More asymmetric isomers, 3- and 4-$C_{16}OH$, cover significantly larger areas at their ESPs where their conformations are controlled by the interactions of shorter alkyl segments with water subphase. A combination of surface pressure data and vibrational band intensities suggest that 3-$C_{16}OH$ with a single gauche defect is the primary conformer in monolayer at its ESP. In contrast, any one of a number of conformations for 4-$C_{16}OH$ are consistent with the observed ESP and VSFS data.

Chapter 3: Soluble Alcohols

3.1. Introduction

Small, asymmetric organic molecules play a variety of roles in biology, serving as pheromones, reaction byproducts, and essential fragrance components.[40,67] Here, the term asymmetric describes molecules lacking any symmetry elements except for the identity operation (C_1). An important subset of these natural products are asymmetric alcohols where the –OH functional group is not located at a chain terminus. Examples of such species include 3-octanol (~1% of natural spearmint oils), 2-heptanol (component of cheese fermentation), and 2-nonanol (behavioral stimulant for honeybees and other insects).[37-42] In addition to their widespread abundance in different natural systems, these alcohols are also surface active meaning that in an aqueous environment, they will preferentially form monolayers at the water/vapor interface.

This surface activity raises interesting questions about the structure and organization within organic films formed by these soluble alcohols. Linear alcohols (starting with $n \geq 8$) form tightly packed, well ordered monolayers at the air/water interface. (Monolayers formed by linear alcohols having 7 or fewer carbons have lower surface coverages.) This behavior can be understood based on the strong hydrogen bonding known to occur between the terminal –OH of the alcohol and the aqueous subphase coupled with the strong, collective van der Waals interactions between the alkyl chains. In contrast, the monolayer structure of asymmetric, soluble

alcohols is not easy to intuit. These isomers can still form strong hydrogen bonds with the water. However, in order for the longer alkyl segments of these molecules to pack together efficiently, the chains must adopt trans conformations that direct the shorter alkyl segments into the aqueous phase. Such a structure requires paying a hydrophobic penalty for solvating these hydrocarbon groups. For monolayers formed from insoluble, hexadecanol isomers, this tradeoff between attractive van der Waals forces and repulsive, hydrophobic interactions is readily apparent.[68] 2-C_{16}OH at its equilibrium spreading pressure (ESP) forms a tightly packed monolayer with the chains adopting primarily all-trans conformations with the methyl groups on either end of the molecule oriented in opposite directions. On the other hand, 3-C_{16}OH forms a more expanded monolayer with gauche defects directing the short, ethyl segment along the surface thus decreasing hydrophobic interactions with the underlying water subphase.

This question of how asymmetric molecules organize themselves in two-dimensions has important consequences for a number of fields. First, lipid monolayers are often used as model membrane systems for examining peptide conformation, enzyme activity and anesthetic action.[8,69-71] Most of these studies use monolayers formed from saturated phosphocholines as the membrane mimic. Real membranes, however, consist of complex mixtures of saturated and unsaturated phospholipids (as well as cholesterol, proteins and other species).[72] Unsaturated phospholipids will pack together differently than their saturated counterparts, yet the way in which these monomers organize remains poorly understood. Studies presented

in this work begin to identify how monomer molecular structure influences extended structure in films at surfaces.

Second, understanding how molecular structure affects organization within organic films adsorbed to the water/vapor interface may have important consequences for a number of atmospheric processes involving aerosols, including uptake of volatile organic and inorganic molecules, evaporation and condensation, and heterogeneous catalysis.[1,73-79] Organic films on aerosols have even been proposed as important sources of prebiotic macromolecules necessary for the creation of life.[80] Organic films on aqueous, atmospheric aerosols will form initially from available surfactants. As these films age, unsaturated species on the surface will be oxidized, eventually forming saturated carboxylic acids.[81] The rate at which monomers in these films are oxidized and the selectivity of oxidation will depend sensitively upon monolayer structure, density, and thickness. All of these factors depend, in turn, upon the structure of the monomers themselves. Consequently, understanding how naturally abundant, asymmetric molecules adsorb to surfaces is important for formulating accurate, predictive models of aerosol reactivity and stability.

Experiments described below begin to address questions about structure and organization in soluble alcohol monolayers using surface tension measurements and surface specific, vibrational sum frequency spectroscopy (VSFS). Data show that linear alcohols form packed monolayers with chain axes directed along the surface normal. As the constitutional branching along the chain begins, the molecules start adopting molecular conformations different from an all-trans geometry. The equilibrium structures of most 2- and 3-position alcohols have two gauche defects

allowing adsorbed monomers to direct both of their methyl groups away from the aqueous phase. These findings demonstrate that the hydrophobic repulsion between the water phase and the shorter alkyl segment assume the dominant role in controlling the structure within the monolayer. Unlike the 2- and 3-C_nOH monolayers, 5-C_nOH monolayers show less consistent behavior among the different chain lengths likely implying a fundamentally different surface organization and, perhaps, more dispersed conformational structures.

3.2. Experimental

3.2.1. Materials

Chemicals used in these experiments and their reported purities are as follows: 1-heptanol (1-C_7OH, Aldrich, Cat. No. H2805, 98%), 2-heptanol (2-C_7OH, Aldrich, H3003, 98%), 3-heptanol (3-C_7OH, Aldrich, 109363, 99%), 1-octanol (1-C_8OH, Sigma, O4500, 99%), 2-octanol (2-C_8OH, Aldrich, R-(-) 147990, 99% and S-(+) 147982, 99%), 3-octanol (3-C_8OH, Aldrich, 218405, 99%), 1-nonanol (1-C_9OH, Aldrich, 131210, 98%), 2-nonanol (2-C_9OH, Aldrich, N30307, 99%), 3-nonanol (3-C_9OH, Fluka, 74295, ≥95.0%), 5-nonanol (5-C_9OH, Fluka, 74308, ≥99.5%), 1-decanol (1-C_{10}OH, Aldrich, 23976-3, 99+%), 2-decanol (2-C_{10}OH, Aldrich, 118311, 98%), 3-decanol (3-C_{10}OH, TCI, D1176, 98+%), 5-decanol (5-C_{10}OH, TCI, D1381, 96+%), 1-undecanol (1-C_{11}OH, Aldrich, U1001, 99%), 2-undecanol (2-C_{11}OH, TCI, U0027, 98+%), 3-undecanol (3-C_{11}OH, TCI, U0028, 95+%), 5-undecanol (5-C_{11}OH, TCI, U0039, 98+%) 1-dodecanol (1-C_{12}OH, Aldrich, 443816, 98+%), 2-dodecanol (2-C_{12}OH, Aldrich, D221503, 99%). All alcohol reagents were used without any

further purification. The water sub phase came from a deionized source and had a resistivity of >18 MΩ·cm (Milli-Q).

3.2.2. Methods

3.2.2.1. Determination of Surface Area

Surface tension measurements were performed to measure the limiting surface areas at terminal coverage for each isomer. Data were used to infer how different soluble alcohol isomers organized themselves at the aqueous/vapor interface. Data consisted of surface pressure measurements as a function of aqueous phase alcohol concentration. The alcohols themselves showed varying degrees of surface activity depending on their structure, but all adsorbed spontaneously to the aqueous/vapor interface. Alcohol concentration was varied through successive dilutions of saturated samples, and interfacial tensions were measured using a platinum Wilhelmy plate. Experiments were performed at temperature of 22.5 ± 1.5 °C. Detailed information about the surface tension measurements were given in Section 1.2.

3.2.2.2. Calculation of Molecular Footprint Area

The footprint area of different alcohol structures were calculated using simple molecular geometry calculations. Details of the calculations have been presented in Section 2.2.2.2.

3.2.2.3. Vibrational Spectra Acquisition

The molecular structures of different isomers at their terminal monolayer coverages were compared based on surface specific, vibrational spectra acquired using broadband Vibrational Sum Frequency Spectroscopy (VSFS).[10,11,82] Theoretical background of the technique have been given in Section 1.2.2. The details of the spectrometer used in our experiments and the experimental parameters have been summarized in Section 2.2.2.3. Additional details about spectra compilation can be found in separate reports.[11,12]

3.3. Results and Discussion

3.3.1. Determination of Molecular Area

Representative surface pressure data for four nonanol isomers are shown in Figure 3.1. The steeper slope for the linear isomer indicates a higher monolayer surface excess and a smaller surface area per molecule. The isotherms of asymmetric isomers, 2-, 3- and 5-C_9OH, show shallower slopes denoting smaller surface concentrations and correspondingly larger surface area values at saturated monolayer coverages. Based on these observations, one might expect monolayers formed by branched alcohol molecules to show less organization at the water/vapor interface and have greater variability in chain conformation.

Results of terminal monolayer surface coverages for all of the soluble alcohols studied are presented in Table 3.1. Several trends stand out. First, the data show that the linear C_n alcohols with $n \geq 8$ form tightly packed monolayers at the aqueous/vapor interface. With molecular areas of ~20 $Å^2$/molecule, the surface area data for linear

isomers are largely independent of alcohol chain length meaning that monolayers of these linear molecules will likely adopt similar structures at the air/water interface.

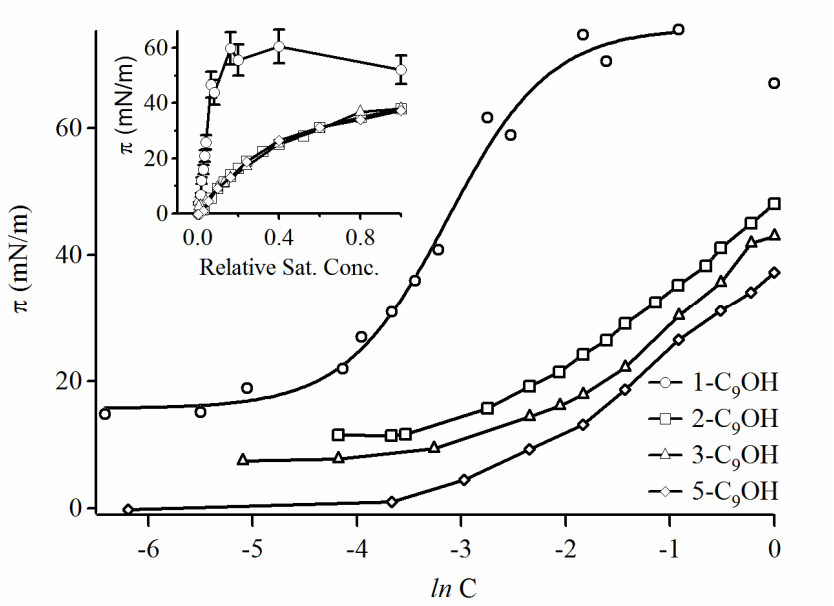

Figure 3.1. Surface pressure isotherms for the nonanol isomers: 1-C_9OH, 2-C_9OH, 3-C_9OH, and 5-C_9OH. (Data for 1-, 2-, and 3-C_9OH are displaced vertically for clarity.) Inset figure shows the surface pressure as a function of relative saturated bulk solution concentration.

Table 3.1. Surface area values for the alcohol isomers (Å2/molecule) at terminal monolayer coverage.

	X-C_nOH			
C_nOH	**1**	**2**	**3**	**5**
7	33.8 ± 1.4	39.5 ± 1.7	45.4 ± 1.3	N/A
8	17.4 ± 3.2	40.6 ± 1.8	45.3 ± 1.8	N/A
9	20.5 ± 2.4	39.0 ± 2.7	38.7 ± 2.7	38.5 ± 3.8
10	23.9 ± 1.8	39.1 ± 0.9	41.1 ± 1.2	54.6 ± 2.1
11	21.8 ± 1.5	40.7 ± 1.3	50.9 ± 3.3	63.0 ± 4.6
12	19.4 ± 0.9	49.2 ± 5.3	-	-
16	18.9 ± 0.3	21.5 ± 0.3	28.7 ± 2.4	-

The footprint molecular area of an alcohol molecule with an all-*trans* geometry is calculated to be 18.7 $Å^2$/molecule. This value compares favorably to results from X-ray scattering studies.[47] Furthermore the calculated limiting area is very similar to the molecular areas calculated from surface pressure data. Thus, we conclude that intermediate length, soluble, linear alcohols form tightly packed monolayers having molecules aligned primarily along the surface normal similar to what one observes in monolayers of saturated, linear, insoluble alcohols adsorbed to the water/vapor interface.[68] Again, such results are expected based on previous reports of various long-chain linear alcohols adsorbed to the aqueous/vapor interface.[51,83,84] 1-C_7OH, despite its similar spectroscopic data (*vide infra*), has a significantly larger surface area, 33.8 $Å^2$/molecule at full monolayer coverage. The reduced surface coverage reflects the shorter alkyl chain and the resulting weaker intermolecular van der Waals interactions. Even larger areas at terminal monolayer coverage are observed for shorter chain alcohols. (Data not shown.)

3.3.2. Vibrational Spectroscopy and Conformer Structures

Complementary information about the inferred interfacial structure comes from vibrational spectra of the soluble monolayers. From polarization-dependent, vibrational band intensities, VSF spectra of the alcohol monolayers enable us to deduce the average structure of molecules in these monolayers. Data presented in this work focus on the CH stretching region of the vibrational spectrum, a region where relative band intensities contain a wealth of information about chain conformation and orientation.[56,64,65] Features appearing in the CH stretching region can be assigned

primarily either to methyl groups or methylene groups.[85,86] The methyl symmetric stretch (r^+) appears at 2872 cm^{-1} while the doubly degenerate asymmetric stretch (r^-) appears between 2952 and 2957 cm^{-1}. In addition, the CH_3 symmetric stretch can lend intensity to an overtone of CH_3 bending motion (r^+_{FR}) through a Fermi Resonance coupling. This band typically appears at 2935 cm^{-1}. The methylene symmetric stretch (d^+) appears at 2841 cm^{-1}. A broad feature centered at ~2930 cm^{-1} can contain intensity from r^-, r^+_{FR} and d^+_{FR}. The weak feature observed at ~2908 cm^{-1} of some branched isomer spectra is assigned to a second d^+_{FR} band, although isolated methine (–CH) groups can also appear in this region.[65,87]

VSF spectra of linear alcohol monolayers acquired using two different polarization combinations are presented in Figure 3.2. The SSP combination describes a perpendicularly polarized (P) IR field and samples out-of-plane components of the IR transition dipoles, while the SPS polarization combination is sensitive to vibrational modes having in-plane IR transition moments. As expected, the spectra of all linear isomers have virtually identical sets of SSP and SPS spectra. Both sets of spectra are dominated primarily by bands assigned to methyl group transitions. A large r^+ band and a small d^+ band in the SSP spectra and a dominant r^- band in the SPS spectra characterize the vibrational structure of each monolayer. The strong r^+ band in SSP spectra implies that the C_3 symmetry axis of the methyl group has an average orientation directed along the surface normal. Correspondingly, this average orientation is also responsible for the large r^- band in the SPS spectra. The observation of a weak d^+ feature in the SSP spectrum requires that adsorbed alcohols

exist in primarily all-*trans* conformations. Based on high surface excess calculated from π–A isotherms, the qualitative appearance of these spectra is not surprising.

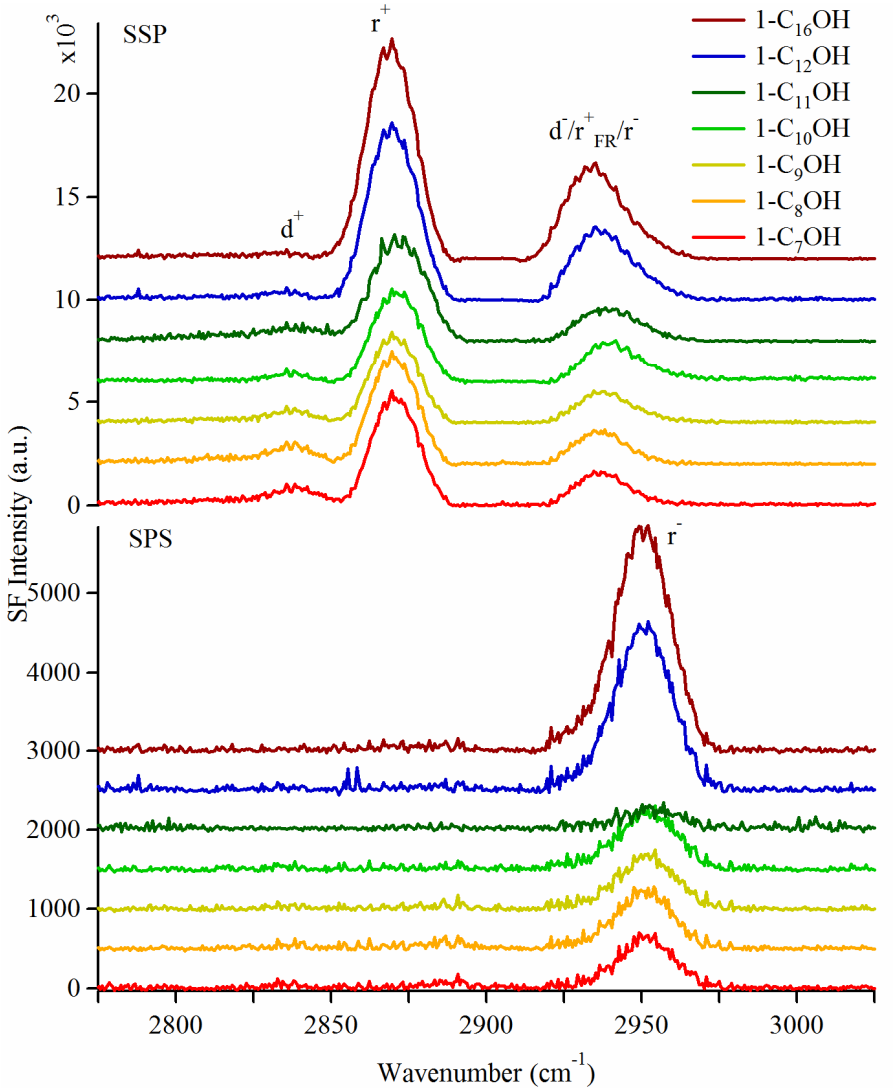

Figure 3.2. VSF spectra of the linear alcohol monolayers under SSP (top) and SPS (bottom) polarization conditions. Experimental conditions, geometries, and vibrational assignments are discussed in text.

The VSF spectra coupled with the small footprint area determined from the surface tension data (except 1-C_7OH monolayer) support the structure of a highly organized monolayer where soluble linear alcohols at the air/water interface adopt

primarily all-*trans* conformations with chain axes aligned along the surface normal. Although this molecular arrangement should, in principle, show no methylene band in an SSP spectrum, the d^+ band is always observed, albeit weakly. The appearance of the methylene symmetric stretch indicates either a small average tilt of the alkyl chains relative to the surface normal or occasional gauche defects.[88,89] One interesting observation is that the intensity of the d^+ band generally diminishes as the chain length increases (Table 3.2). In contrast, the r^+ band begins to grow large, especially for 1-C_nOH where $n \geq 12$. For comparison, the insoluble 1-C_{16}OH monolayer at its ESP has an r^+ intensity that is about two-fold larger than the shorter chain alcohol monolayers despite having similar surface coverage.

The behaviors of the r^+ band intensities with varying alkyl chain length are shown in Figure 3.3. The monolayers formed from 1-C_{12}OH likely exist in a two dimensional (2D) solid at the temperatures where the studies were conducted. Numerous accounts have shown that r^+ intensity in a VSF spectrum rises discontinuously when a monolayer undergoes surface freezing.[84,90-92] For the experiments presented in this work, the temperature is kept constant, thus adsorbed monolayers will assume their most thermodynamically stable phase given the ambient conditions. In a previous report, we showed that 1-C_{16}OH monolayers at their ESP exist as a 2D solid.[68] With a surface freezing temperature of ~39 °C, monolayers of 1-C_{12}OH will also exist in 2D solids. The surface freezing temperature of 1-C_{11}OH – reported as ~27 °C[93] – is close to ambient temperatures. Given the local heating can result from the absorption of IR light *and* the similarities between 1-C_{11}OH spectrum and those from shorter length linear alcohols, we conclude that the 1-C_{11}OH

monolayers studied in this work exist in 2D liquid state. (The surface freezing temperature of 1-C_{10}OH is ~14 °C as determined by both VSF measurements and X-ray scattering studies.[91,94])

Table 3.2. Spectroscopic data for the alcohol isomers. The intensities are the normalized peak maximum intensities with respect to the DMSO signal. Uncertainties vary between 12 and 20%.

		X-C_nOH			
C_nOH		**1**	**2**	**3**	**5**
7	r^+	5392	2177	3186	N/A
	d^+	796	835	1216	
8	r^+	5333	2176	2685	N/A
	d^+	813	305	469	
9	r^+	4351	2380	2530	1918
	d^+	593	309	386	180
10	r^+	4598	3013	1581	1374
	d^+	499	694	471	271
11	r^+	5067	2465	1438	1172
	d^+	599	468	530	258
12	r^+	8684	2444	-	-
	d^+	518	466		
16	r^+	10708	2534	1112	-
	d^+	444	307	475	

Traditionally, the rise in intensity in linear alkyl surfactants that accompanies surface freezing is attributed to enhanced conformational order. However, this explanation is difficult to reconcile with the fact that terminal monolayer coverages of these linear alcohols do not vary significantly from n = 8-16. For example the

terminal monolayer coverages of 1-C_{12}OH and 1-C_{16}OH (at ESP) are 5.15×10^{14}/cm^2 and 5.29×10^{14}/cm^2, respectively. Based on number densities and assumed similarities in conformational order, one would expect the intensity of r^+ in the 1-C_{16}OH SSP spectrum to rise by ~5% relative to the same band in the equivalent 1-C_{12}OH spectrum. Instead, r^+ intensity rises by more than 20%. These unexpected changes in VSF band intensities may, instead, reflect dynamic or reorientation effects where shorter length alkyl chains will experience greater motional freedom that serves to reduce the observed nonlinear signal.[95] These effects deserve further investigation.

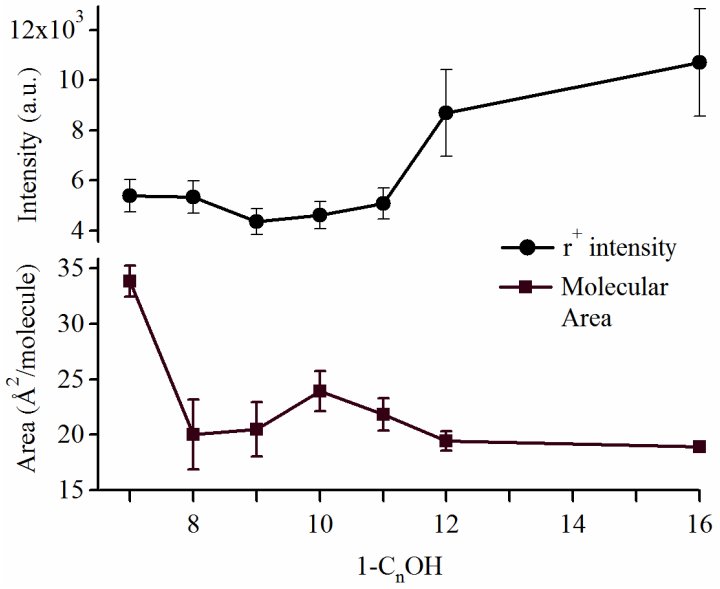

Figure 3.3. Spectroscopic data and surface coverages for linear alcohol isomers with varying chain length. Intensities result from fitting data from SSP spectra in Figure 3.2 to Equations 1.4 and 1.5. The r^+ refers to the methyl symmetric stretch (at 2872 cm^{-1}). Uncertainties include the day to day variation in measured intensities scaled to a DMSO standard as well as instrumental contributions.

From the surface tension and VSF data, we conclude that monolayers formed by linear alcohol molecules have average orientations along the surface normal with

varying packing efficiencies. Monolayers formed by the linear alcohol chains with lengths between 8 and 11 carbon atoms behave similarly in terms of packing efficiency as evidenced by spectral and thermodynamic data (Figure 3.3). Monolayers formed from 1-C_{12}OH have significantly higher spectral band intensities and represent a crossover between soluble and insoluble monolayer structures.

Moving the location of the OH group from the chain terminus to the 2-position creates an alcohol structure having the smallest degree of asymmetry. The VSF spectra of monolayers formed by 2-C_nOH molecules are shown in Figure 3.4. The spectra are qualitatively similar to those of the linear isomers indicating a high degree of conformational order. However, the intensities of the dominant features in the SSP spectra are significantly smaller. One explanation for the differences in spectral intensities comes from the surface tension data. Despite the relatively small change in molecular structure as inferred from the VSF data, the molecular areas at full monolayer coverage show an approximate two-fold increase. Such a drastic change in surface coverage means that the interfacial molecular conformations and the resulting monolayer organization are likely to be quite different for linear and branched alcohol isomers. The 2-C_nOH alcohol molecules can adopt one of two general conformations: if the van der Waals interactions between the long chain segments are strong enough, adsorbed molecules can have all-trans conformations and pack loosely together at the interface. This arrangement leads to relatively high surface coverage and requires paying an energetic cost for solvating the methyl group in the C_1 position. Monolayers of 2-C_{16}OH organize themselves in this way.[68] Alternatively, if the cost of solvating the C_1 methyl group exceeds the stability

resulting from chain-chain interactions, then the adsorbed monolayers will include gauche defects that minimize hydrophobic interactions and reduce surface coverage. This situation clearly describes the behavior of the 2-C_nOH alcohols for n = 7-12.

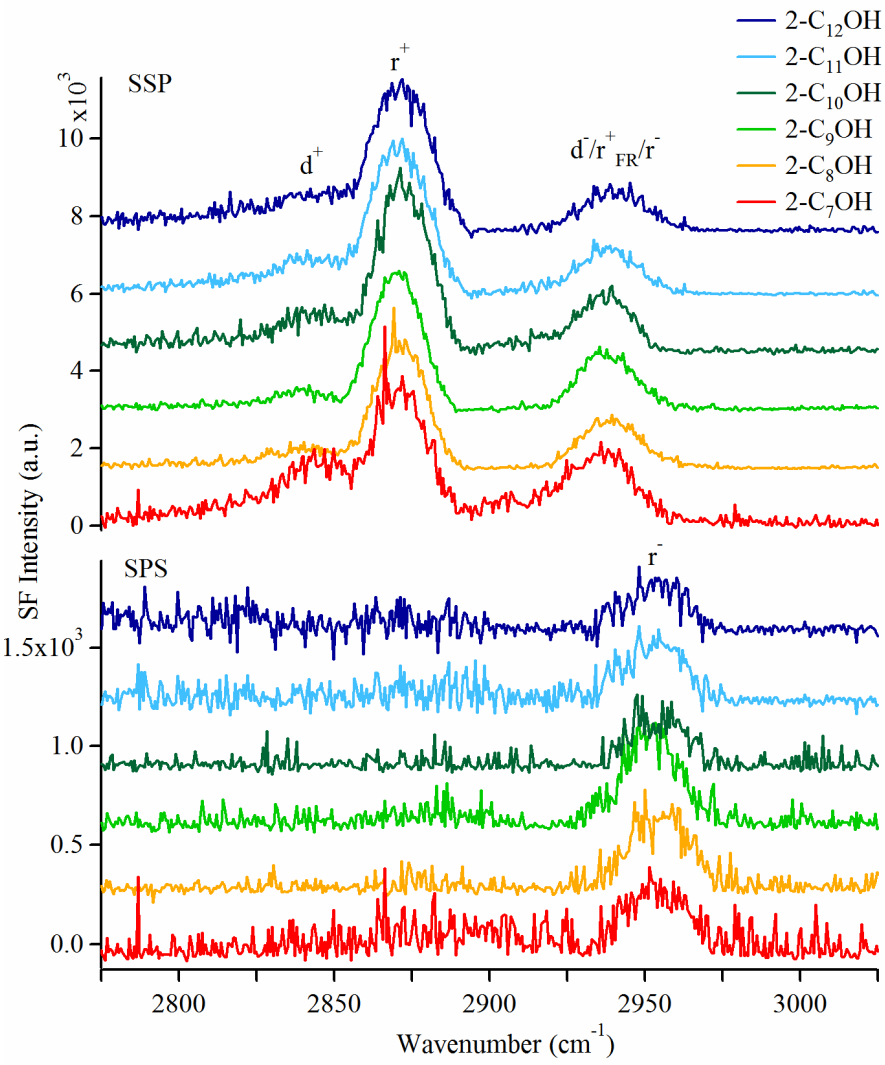

Figure 3.4. VSF spectra of the 2-C_nOH monolayers under SSP (top) and SPS (bottom) polarization conditions. Experimental conditions, geometries, and vibrational assignments are discussed in text. The VSF spectra for the two enantiomers of 2-C_8OH monolayers are reported in Appendix A.

Possible conformers for 2-C_nOH alcohols and corresponding molecular areas are shown in Figure 3.5. The all-*trans* conformation has the smallest footprint at the

interface with an area of 26.4 $Å^2$/molecule assuming complete rotational freedom. If not free to rotate, the footprint shrinks to 22.2 $Å^2$/molecule. While this conformation optimizes packing of the longer alkyl segments, it is not consistent with the surface tension and the VSF data from these systems. A second conformation with a gauche defect around C_2-C_3 bond axis gives the C_1 methyl group an in-plane alignment leading to a molecular area of 29.6 $Å^2$/molecule assuming that the longer alkyl chain backbone has an all-trans conformation. Although, this conformation reduces the hydrophobic interaction between the terminal methyl group and the water, it still requires a more tightly packed monolayer than is observed. A third possible conformer has two gauche defects having opposite rotation about the C_2-C_3 and C_3-C_4 bonds has a footprint area of 42.7 $Å^2$/molecule. In the literature this structure is denoted as gg'.[86] The value is close to the observed molecular areas for the 2-C_nOH isomers having different chain lengths. Furthermore, the gauche-gauche conformation allows both methyl groups to make partial contributions to the r^+ intensity in SSP spectra (where "partial" refers to the fact that each —CH_3 group has only part of its IR transition dipole projected onto the surface normal). Such a conformation maximizes the relatively strong hydrogen bonds between the adsorbed alcohols and the aqueous subphase while minimizing interactions of the alkyl segments with water. (A "gg" conformer where both defects involve equivalent rotations about consecutive dihedral angles directs the 1-position methyl group parallel to the surface and can not account for the intensity variation observed in the r^+ band.)

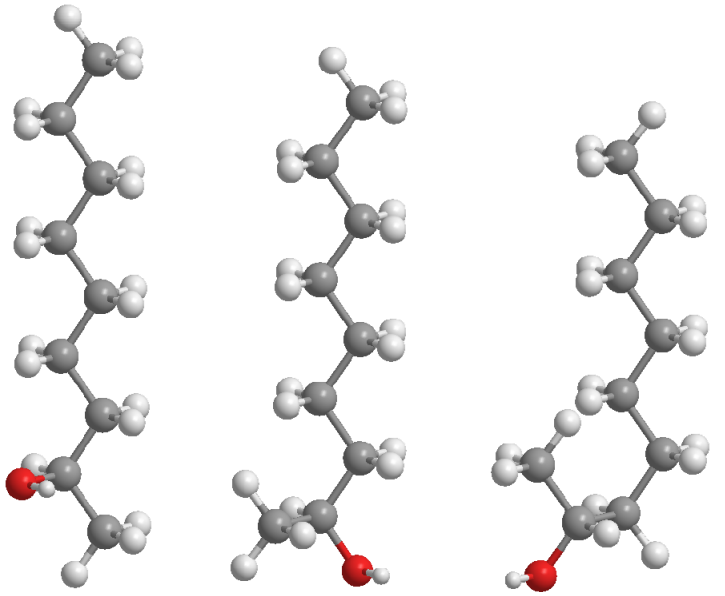

Figure 3.5. Structures of different 2-C_9OH conformers and corresponding calculated circular footprint areas resulting from free rotation of monomers adsorbed to the interface.

To understand the quantitative change in r^+ intensity with changing isomer structure, one should recognize first that linear isomers have the highest r^+ intensities in SSP spectra due to the high degree of conformational order and not due to methyl group surface coverage. For example, knowing that the surface area of 2-position alcohols is approximately twice that of linear isomers, we would expect the r^+ intensity to be ~25% of that from the linear isomer monolayer if only one methyl group per molecule contributed to the spectrum. However, 2-C_nOH isomers have two methyl groups per molecule. If both methyl groups of the isomer contribute to the spectrum, then the intensity would remain approximately the same as for the linear

isomer provided that both methyl groups from the 2-alcohol isomer shared the same orientation as the individual methyl groups of linear chains.

Figure 3.6 shows how the intensities of r^+ bands change with the position of the -OH group for the family of nonanol isomers. Similar plots can be seen for other alcohol families in the Supporting Information. Figure 3.6 contains the measured r^+ intensities as well as how one would expect the intensities of the r^+ band to scale with X-C_9OH surface coverage. Two limits are shown. If both methyl groups of the branched nonanols share the same orientation as the single methyl group of the 1-C_9OH, the absolute intensity of the r^+ band will rise slightly because the methyl surface concentration is approximately 5% higher for the branched isomers. These predictions are denoted by the open circles in Figure 3.6. If only a single methyl group per branched isomer (or an equivalent linear combination of both methyl groups) shares the same projection of its C_3 axis along the surface normal as the linear isomer, the r^+ band intensity will scale simple as $(N_{X-C_9OH} / N_{1-C_9OH})^2$ (open triangles in Figure 3.6). Of course the "1-methyl group response" does not represent a true "limit" given that excessive chain randomization *and* destructive interference can lead to even lower observed r^+ intensities. Nevertheless these considerations provide a useful framework for comparing r^+ intensities observed in monolayers formed from different isomers. These comparisons can prove particularly helpful when attempting to identify likely conformers of adsorbed species as will be shown below.

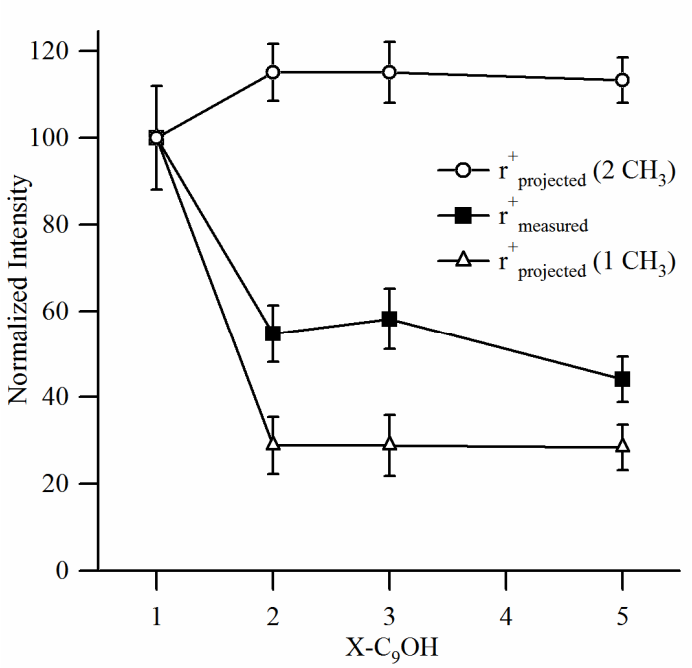

Figure 3.6. r^+ intensities of the monolayers from nonanol isomers. Projected intensities are expected, scaled intensity values with respect to surface area values as described in the text.

For the 2-C_9OH monolayer, data show that the intensity relative to the linear isomer decreases by ~45% from the response of r^+ from 1-C_9OH monolayer: This result falls between the 10% increase anticipated from two contributing methyl groups and the 75% decrease that would result from just a single contributing methyl group. A 2-C_9OH molecule in its all-*trans* conformation would have its CH_3 group at the C_9 position aligned with the surface normal. Given the relationship between surface coverage and VSF intensity, this conformer should lead to an r^+ intensity of no more than ~25% of the r^+ intensity from monolayers of linear isomers. In fact, the all-trans conformation would likely lead to an even smaller r^+ band due to destructive interference by oppositely aligned methyl groups (as is observed in monolayers of 2-C_{16}OH).[68] As discussed above, a conformer having two gauche defects has a

footprint area closest to the observed molecular area determined from the surface tension measurements. This conformation simultaneously optimizes adsorbed alcohol/water interactions *and* directs both methyl groups to project their r^+ transition dipole along the surface normal. Thus, the magnitude of the r^+ band from this conformation is anticipated to be larger compared to other conformer structures. The observed r^+ intensity from a 2-C_nOH monolayer can be best related to this conformer. Supporting this picture are classical molecular dynamics simulations of sodium dodecyl sulfate (SDS) monolayers adsorbed to the air/water interface. SDS is a water soluble anionic surfactant that forms monolayers having terminal surface coverages of ~45 $Å^2$/molecule. From their simulation results, Berkowitz and coworkers found that SDS monomers have a 50-60% probability of adopting a gauche defect about the C_2-C_3 bond axis.[15,17] The probability of gauche defects appearing about successive bond axes drops to 25% for the rest of the chain. The authors interpreted strong driving force to adopt gauche defects close to the strongly associating functional group (-OSO_3^- for simulations, -OH in this work) as reflecting the need for adsorbed surfactants to maximize van der Waals interactions with the adjacent aqueous subphase. Note that this tendency to integrate disorder close to the aqueous phase will disappear if adsorbates can pack more closely and adopt trans conformations to maximize chain-chain interactions.

The SSP and SPS spectra of 3-C_nOH monolayers are presented in Figure 3.7. Again, the spectral features are qualitatively similar to those of the 2-C_nOH isomers. Specifically, r^+ and d^+ bands dominate the low frequency part of the CH stretching region. Similar to the 1- and 2-C_nOH monolayers, the r^- band is the most significant

feature in SPS spectra of 3-position alcohols. The SPS spectrum of 3-C_7OH, the alcohol having the shortest alkyl segments in this study, also contains appreciable intensity in the r^+ band.

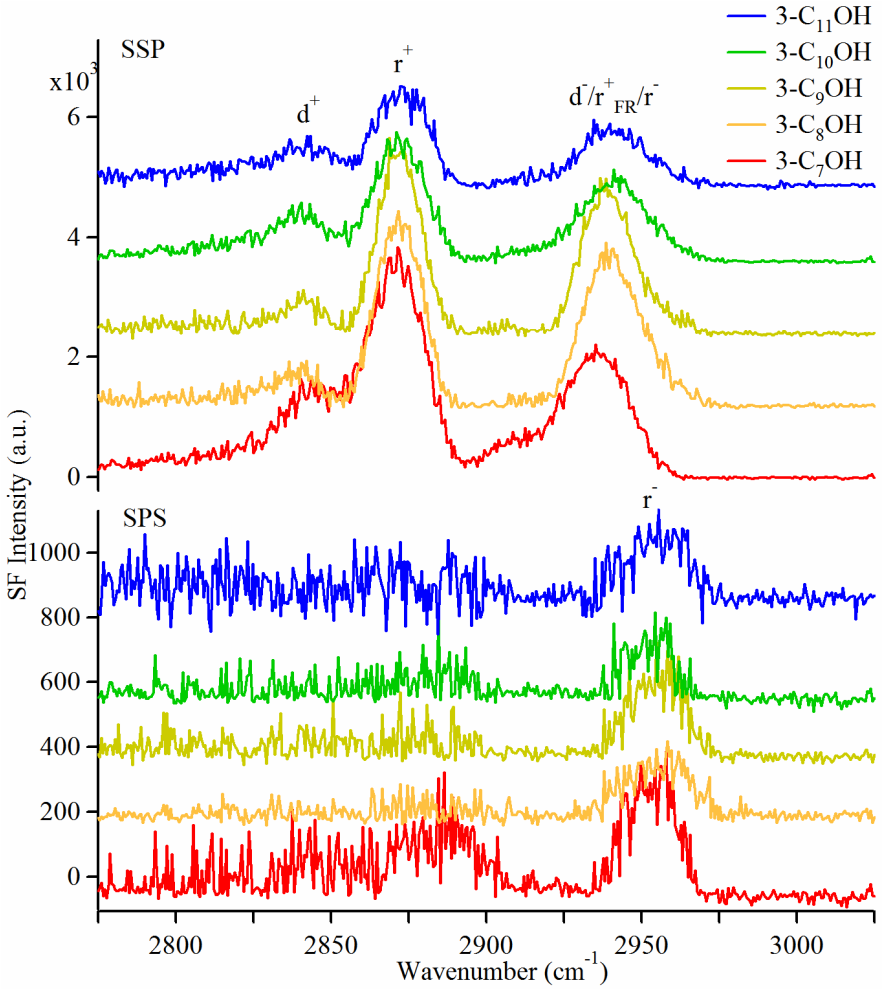

Figure 3.7. VSF spectra of the 3-C_nOH monolayers under SSP (top) and SPS (bottom) polarization conditions. Experimental conditions, geometries, and vibrational assignments are discussed in text.

The monolayer structure for alcohol isomers of the 3-C_nOH structure can be inferred from the thermodynamic and spectroscopic data in a way similar to 2-C_nOH alcohols. The surface tension data for 3-position isomers show that the molecular area

values range from 38.2 to 45.4 $Å^2$/molecule except for 3-C_{11}OH with an area of 50.9 $Å^2$/molecule (Table 3.1). These values are similar to those of the 2-position isomers. Recalling that the equilibrium structure at terminal monolayer coverage is controlled primarily by a competition between chain-chain interactions and hydrophobic forces at the interface, one might expect average conformations of adsorbed species to vary with compositional isomer structure. However, the data suggest that 3-C_nOH monolayers share many structural similarities with 2-C_nOH monolayers.

Similar to the 2-C_nOH alcohol monolayers, 3-position alcohol isomers are assumed to adopt a small number of preferential conformations at the water/vapor interface. The OH group in the 3-position is expected to interact with water subphase through relatively strong hydrogen bonding interactions. To accommodate this interaction, adsorbed molecules will adopt gauche defects to minimize hydrophobic interactions between the short ethyl segment and the water. A single gauche defect around the C_3-C_4 bond produces a conformer structure that simultaneously enables hydrogen bonding and decreases the unfavorable interaction. The circular footprint area for this conformation is calculated as 42.7 $Å^2$/molecule, a value in agreement with the average molecular area of ~40 $Å^2$/molecule (Figure 3.8). However, this conformation still requires some solvation of the shorter alkyl segment in the subphase. Moreover, the structure still requires that the in-plane methyl group in the C_1 position be deflected slightly towards the water phase. Such a conformation should lead to at least a 75% reduction in the observed r^+ intensity relative to the spectrum from the linear alcohol system. However, the intensities of 3-C_nOH monolayers

diminish by 40 - 70% compared to the linear isomers meaning that this conformer is unlikely to be the predominant equilibrium structure of adsorbed 3-C_nOH species. A second conformer with two gauche defects in the structure directs the C_1-C_3 alkyl segment parallel to the interface. This structure also can not explain the observed intensity variation with respect to the linear isomer since this conformer has only one methyl group contributing to the spectrum.

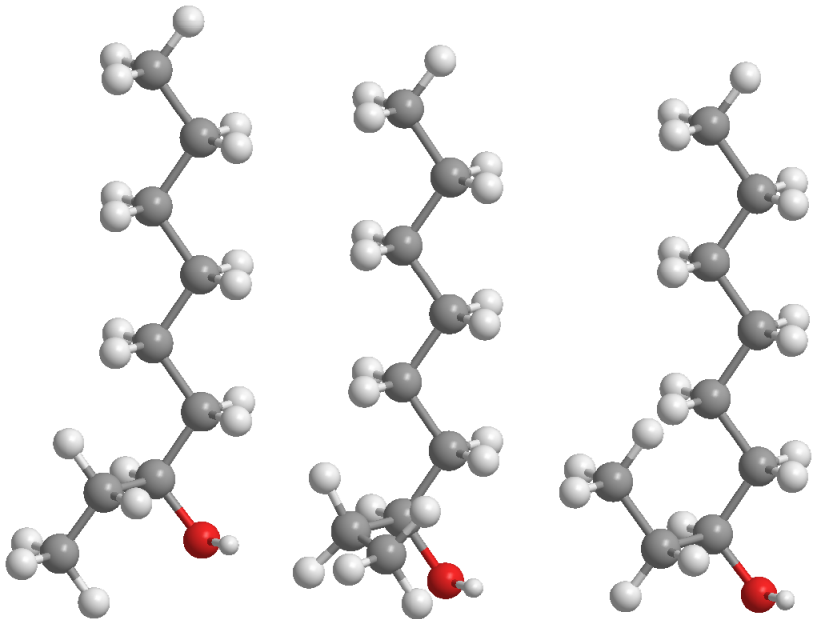

Single gauche defect	Two gauche defects (gg)	Two gauche defects (gg')
42.7 Å^2/molecule	40.8 Å^2/molecule	42.7 Å^2/molecule

Figure 3.8. Structures of different 3-C_9OH conformers and corresponding calculated circular footprint areas resulting from free rotation of monomers adsorbed to the interface.

A third conformer (gg') is produced by two gauche defects having opposite rotation about the C_2-C_3 and C_3-C_4 axes. This structure has the same carbon backbone geometry as the two-gauche defect conformer structure for 2-C_nOH in Figure 3.5

except that the OH group is moved to the C_3 position. The structure has the same footprint area as the corresponding 2-position alcohol conformer (42.7 $Å^2$/molecule) and matches the area determined from surface tension measurements. For 3-C_9OH, the measured r^+ response requires contributions from both methyl groups of the molecule. This gg' conformer provides such an opportunity with both methyl groups contributing constructively to the SSP spectrum. Consequently, we propose that this structure is the primary conformer for soluble 3-C_nOH molecules at air/water interface. The isolated methylene group for this structure at C_2 position has an out-of-plane alignment that can be responsible for a small but measurable increase in d^+ intensity.

Quantitative comparisons of the r^+ band intensities for different 2-C_nOH and 3-C_nOH monolayers show trends implying modest chain length dependent structural changes within the monolayer. Variations in the ratios of measured r^+ intensities to the scaled intensities for 2- and 3-C_nOH isomers are shown in Figure 3.9. Here, scaled intensity ratios plotted on the y-axis refer to ratio of the measured r^+ signal relative to the anticipated response from a single, perpendicularly aligned methyl group per adsorbed alcohol aligned along the surface normal scaled by their surface excess concentrations. In this context, an r^+ ratio > 1.0 means that the measured intensity must contain constructive contributions from both methyl groups of the adsorbed 2- or 3-C_nOH molecules, a condition requiring conformers to have two gauche defects and C_1 methyl groups projecting some component of their r^+ transition dipole onto the surface normal (Figure 3.5 and 3.8). An r^+ ratio $\leq$ 1.0 means that

either the methyl groups have become randomized or that the methyl groups are oriented in opposite directions and interfere with each other destructively.

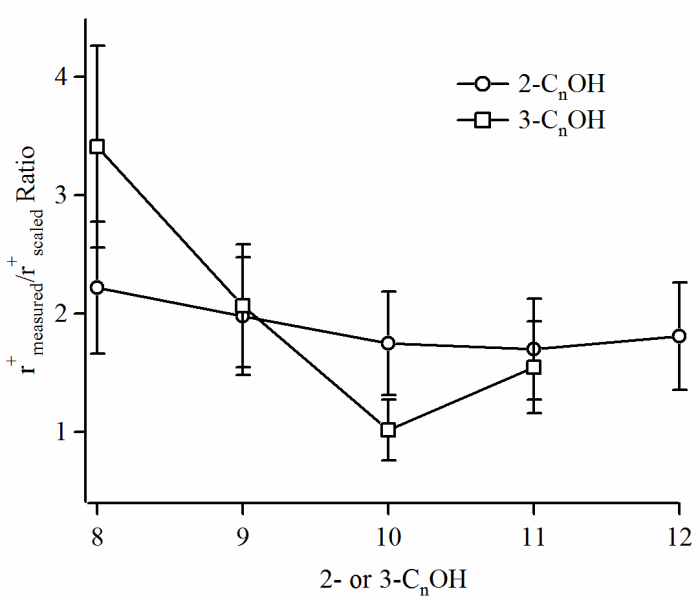

Figure 3.9. Comparison of $r^{+}_{measured}/r^{+}_{scaled}$ ratios of different 2-C_nOH and 3-C_nOH monolayers. Scaled intensities are obtained by scaling the r^{+} intensity from the appropriate linear isomer spectrum by differences between the branched and linear isomer surface coverages. (For reference, these ratios were 0.57 and 0.36 for insoluble monolayers of 2-C_{16}OH and 3-C_{16}OH, respectively.)

Figure 3.9 shows this measured-to-scaled ratio to be greater than 1.0 for all 2-C_nOH alcohols. These data further support the proposed primary gg' conformer structure for soluble 2-C_nOH monolayers. For comparison, in 2-C_{16}OH monolayers, alkyl chain cohesion overcomes hydrophobic repulsion leading to a tightly packed monolayer with monomers having all-trans chain conformations. The measured to scaled ratio for r^{+} band in the 2-C_{16}OH monolayer is calculated to be 0.57 indicating destructive interference between the two oppositely oriented methyl groups. For the soluble alcohols, the observed/projected r^{+} ratios show a decreasing trend with

increasing n for both 2-C_nOH and 3-C_nOH alcohols. The data suggest that the primary conformer structure for shorter chain alcohols is likely to be the gg' conformation (Figure 3.8) with two methyl groups directed away from the water surface. As the longer alkyl segment lengthens, stronger chain-chain interactions will induce stronger association between monomers leading to a smaller number of gg' conformers and a smaller $r^+_{measured}/r^+_{scaled}$ ratio. (Not shown are the data for the C_7 alcohols. The ratios for 2-C_7OH and 3-C_7OH do not follow the general trends shown in Figure 3.9. However, rather than reflecting systematic differences in monolayer organization, we believe that the variance reflects the anomalously low surface coverage of the linear heptanol isomer.)

Interpreting the surface tension and VSFS data is more challenging for the 5-C_nOH monolayers (Figure 3.10). First, the terminal surface coverage of 5-C_9OH leads to a molecular area in the range of 40 $Å^2$/molecule. Compared to the 2- and 3-C_nOH alcohols, one might expect the 5-C_9OH molecules to have conformer structures with significantly larger molecular areas since the position of the –OH group is far from a chain terminus. However, the data do not support such a picture. Second, unlike the 2- and 3-position alcohols whose coverages show little variation with chain length, the terminal surface coverage of 5-C_{10}OH jumps to 55 $Å^2$/molecule and increases again to 63 $Å^2$/molecule for 5-C_{11}OH. Finally, the SSP spectra of the three 5-C_nOH isomers studied show surprisingly weak d^+ bands relative to the r^+ feature that dominates each spectrum.

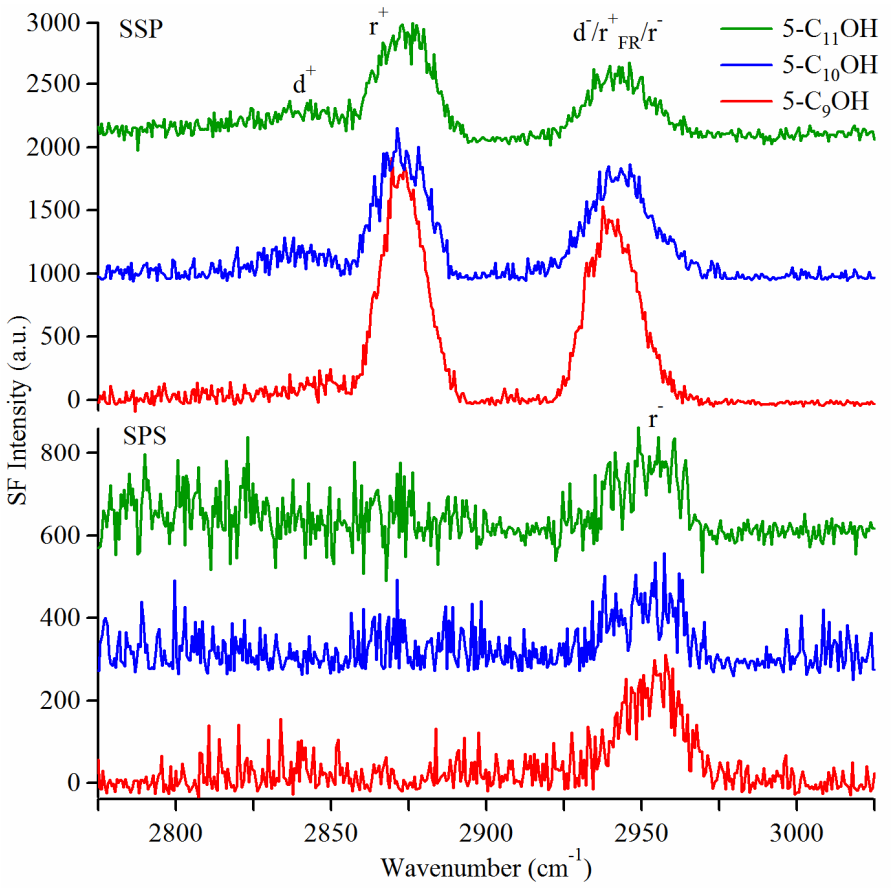

Figure 3.10. VSF spectra of the 5-C_nOH monolayers under SSP (top) and SPS (bottom) polarization conditions. Experimental conditions, geometries, and vibrational assignments are discussed in text.

The alkyl segments in 5-C_9OH, 5-C_{10}OH and 5-C_{11}OH have chain lengths between 4 and 6 carbons. Based on data from solutions of 1-C_7OH (a linear alcohol with a 6 carbon alkyl segment), we assume that inter-chain van der Waals interactions are too weak to drive the adsorbed alcohols to form highly ordered assemblies at the water/vapor interface. Moreover, the position of the OH group in the chain makes strong chain-chain interactions even less likely. Thus, the adsorbed species should adopt conformations that minimize hydrophobic interactions. One way to minimize hydrophobic interactions for both segments is to adopt gg (or gg') conformation(s) on

either side of the –OH position at C_5. Such a structure would have a large molecular area due to the significant in-plane projections of both alkyl chains. Based on the spectra from the 2- and 3-C_nOH isomers, however, we would expect methylene groups from these conformers to generate significantly larger intensities in the d^+ band. The spectra, however, show little support for this supposition. Surprisingly weak intensity of the d^+ band from all three isomers might be attributed to the local cancellation of the nonlinear susceptibility, possibly from overlapping or interdigitated monomers at the surface, although this conclusion remains highly speculative.

These data further reinforce how subtle shiftings in the balance of hydrophobic and hydrophilic forces at the air/water interface can have a large impact on the structure and organization within the resulting monolayer. For example, increasing chain length does not significantly influence the molecular areas of most 2- and 3-C_nOH monolayers. Except for 3-C_{11}OH and 2-C_{12}OH, monolayers formed from the 2-C_nOH and 3-C_nOH have an average surface coverages corresponding the molecular areas between 39 and 45 $Å^2$/molecule. The 3-C_{11}OH and 2-C_{12}OH monolayers are 50.9 ± 3.3 and 49.2 ± 5.3 $Å^2$/molecule, respectively. In contrast, the terminal monolayer coverages of the 5-position isomers increase by more than 50% as the overall chain lengthens from 9 to 11 carbons. Collectively, these observations emphasize that the structure of monolayers formed from asymmetric surfactants depends sensitively on the structure of the molecules themselves. Small changes in molecular structure can lead to changes in monolayer organization, but this correlation does not follow simple, easily summarized patterns. Careful studies

including the use of isotopically labeled reagents and controlled surface coverages will continue to improve our understanding of how molecular structure controls surface activity and organization in these organic films.

3.4. Conclusions

Studies of structure and organization of soluble alcohols at air/water interface showed that linear alcohols formed tightly packed monolayers with all-trans conformations aligned with the surface normal while 2-C_nOH monolayers did not pack efficiently but instead adopted gauche defects. For these monolayers, the cohesive chain-chain interactions were not strong enough to alter the hydrophobic forces to solvate the C_1 methyl group within the water phase. A two gauche defect conformation with both methyl groups have out-of-plane alignments was assigned to the primary structure at the interface. Similarly, 3-C_nOH monolayers adopted two gauche defect conformations and formed monolayers with molecular areas twice as great as linear isomers. Further studies are necessary to better characterize the primary conformer structures formed in 5-C_nOH monolayers.

Chapter 4: Molecular Dynamics Simulations

4.1. Introduction

The studies of insoluble and soluble alcohol monolayers described in the preceding chapters have shown that small changes in molecular structure can lead to large changes in interfacial monolayer structure and organization. Apart from the well organized linear alcohols, the structure and organization of monolayers formed by branched alcohol monomers depends on a balance of different competing forces having comparable magnitudes. Our experimental results showed that this competition leads to different interfacial conformations for the soluble and insoluble alcohols of the same general chain structure. 2-position alcohols, for example, can adopt a variety of conformations including all-trans or structures having one, two or more gauche defects. (Figure 4.1).

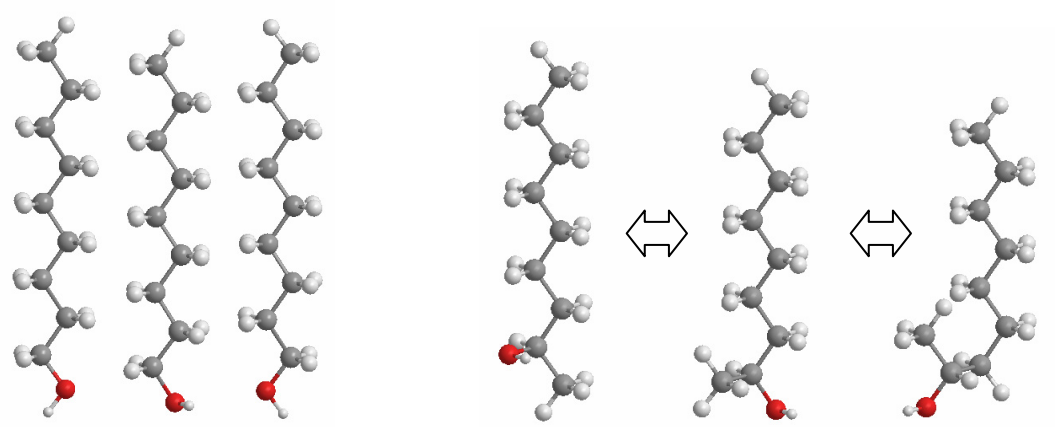

1-Nonanol 2-Nonanol

Figure 4.1. Possible conformations for 1- and 2-nonanol monomers at aqueous/vapor interface.

Our studies showed that while insoluble, long chain 2-C_{16}OH monomers prefer the all-trans conformation, the shorter, soluble alcohol monomers generally adopt a conformation having 2-gauche defects. The reason for preferentially adopting these structures is explained by differences in the magnitude of van der Waals interactions between the long alkyl segments of the molecules. Stronger van der Waals interactions between the 2-C_{16}OH molecules overcome the hydrophobic interactions associated with solvating the C_1 methyl group in the water subphase and the chains remain closely packed. Smaller van der Waals interactions between the long segments of the shorter chain alcohols can not offset the energetic cost of solvating the methyl group, so monolayers are more expanded and the monomers have a more disordered structure.

Experimental studies of structure and organization within alcohol monolayers were performed using surface tensiometry and surface specific VSFS. Although these methods are very useful when gathering information about the surfactants at interfaces, our understanding of monolayer structure and organization is restricted only to the specific constitutional isomers studied. Our data do not allow us to generalize and create models capable of predicting *a priori* how surfactants having different molecular structures will organize spontaneously at the aqueous/air interface. Developing molecularly based insight and microscopically accurate models requires computational tools that not only confirm previous results but also anticipate how new systems balance different competing forces to create unique interfacial structures.

Classical MD simulations have long been used to model surfactant monolayers at aqueous interfaces.[14,17,20,23,26,96-101] These simulations provide important and otherwise inaccessible data that complement the experimental studies. For example, molecular structures of charged, soluble surfactants at aqueous surfaces have been reported by a number of authors.[15,97,100,102,103] Studies that focus on surfactants with neutral, polar headgroups or zwitterionic headgroups are even more common.[14,19,23,26,32,99,104-106] However, none of these studies included an examination of how and why asymmetric molecules adopt preferred conformers at the aqueous interface. Here asymmetric is used to define molecules that can only have C_1 point group symmetry. In this study, we employed MD simulations to explore the predicted equilibrium structures of soluble alcohol isomers at the air/water interface. Simulations varied both isomer structure and surface coverage of a given isomer. In carrying out these simulations, we needed to overcome a number of challenges previously unencountered by researchers by who have focused on structure and organization in monolayers formed by more symmetric monomers. Our motivation for this work resulted from our desire to model our experimental results with detailed "pictures of molecules" at interfaces and to identify different energetic contributions to monolayer organization that might prove general enough to formulate predictive models.

This chapter describes our efforts to simulate monolayers of branched alcohol adsorbed to the air/water interface. Simulations focused on the behavior of constitutional isomers of nonanol at different surface coverages corresponding to full monolayer coverage (experimental conditions), 2/3 of full monolayer coverage and

1/3 of full monolayer coverage. Surface coverage was varied in order to observe how cooperative interactions between monomers develop as more and more molecules adsorb to the surface. Technical details of the simulations including potentials, structures and procedures are given in Section 4.2. The results of the simulations are summarized in Results and Discussion section of this chapter (Section 4.3). This work was initiated through a collaboration with Professor Ilan Benjamin at University of California at Santa Cruz. Professor Benjamin and his group have written all of the code used for these simulations and Professor Benjamin continues to provide guidance and advice.

Findings presented in this chapter should be viewed as work in progress. Given the very long times required for equilibration and limited computational resources, our simulations have begun to identify those quantities that are most important in controlling monomer structure within monolayers, but the lack of agreement between experimental results and predictions from simulations imply that potentials used in the simulations may need adjustments.

4.2. Methods

The linear alcohol molecules studied in these simulations can be represented as semi-flexible chains composed of methylene groups, terminal methyl groups and a single, uniquely positioned -OH group. For simplification and to save processor time, each methylene group is represented by a united atom with a mass of 14 a.m.u. and a 15-a.m.u. united atom models a methyl group. For branched alcohols, the methylene

group to which the -OH is attached is replaced with a united mass of 13. The oxygen and hydrogen atoms of the alcohol OH group are included explicitly.

Intramolecular potentials defining stretching and bending motions are modeled as harmonic oscillators. Physical properties of important coordinates used are listed in Table 4.1. The parameters were based on those used by Jorgensen (1986) and include the constants for bond lengths, bond angles and vibrational force constants for alcohol chains under investigation.[107]

Table 4.1. Physical constants defining the structure of alcohol molecules used in the study. (Jorgensen, 1986)

Property	**CC**	**CO**	**OH**
Bond Length (Å)	1.53	1.43	0.945
Force constant (kcal/mol/Å^2)	520.0	640.0	1106.0
	CCC	**CCO**	**COH**
Bond Angle (degree)	112.0	108.0	108.5
Force Constant (kcal/mol/rad)	126.0	100.0	110.0

4.2.1. Potential Energy Parameters

The water potential used in these simulations is described by flexible simple point charge (SPC) water model.[108] This model is attractive for molecular dynamics simulations at interfaces given its simplicity and proven structural and thermodynamic accuracy.[101,109,110] Intramolecular parameters of water molecules in the model are adjusted in the manner described by Kuchitso and Morino.[111]

The intermolecular potential between water molecules is defined by a sum of Lennard-Jones and Coulomb potentials.

$$U(r) = \sum_{i<j} 4\varepsilon_{ij}\left[\left(\frac{\sigma_{ij}}{r_{ij}}\right)^{12} - \left(\frac{\sigma_{ij}}{r_{ij}}\right)^{6}\right] + \frac{q_i q_j}{r_{ij}} \qquad (4.1)$$

where r_{ij} is the distance between the closest sites of molecules, q_i and q_j are fixed charges on sites i and j, and σ_{ij} and ε_{ij} are Lennard-Jones parameters defined by the SPC model. This potential function with different Lennard-Jones parameters also defines the interactions between water molecules and alcohol molecules at the interface.

Finally, the intermolecular interactions between the hydrocarbon chains of alcohol were defined by Lennard-Jones potentials (the first term of Eq. 4.1). The Lennard-Jones parameters, σ_{ij} and ε_{ij}, were calculated using the expressions,

$$\varepsilon_{ij} = \sqrt{\varepsilon_i \varepsilon_j}, \sigma_{ij} = (\sigma_i + \sigma_j)/2 \qquad (4.2)$$

The parameters defined for CH_3, CH_2 and CH groups are as follows: σ_{CH_3} = 3.86 Å, $\sigma_{CH_2} = \sigma_{CH}$ = 3.98 Å, ε_{CH_3} = 0.181 kcal/mol, and $\varepsilon_{CH_2} = \varepsilon_{CH}$ = 0.114 kcal/mol. The intermolecular interactions were adjusted smoothly to zero when the distance between the two sites (r_{ij}) is in the range between 19.5 and 21.5 Å.[32,106]

4.2.2. Torsional Potentials

The torsional energy responsible for carbon chain deformations of alcohol molecules is represented by an expression containing three terms:

$$U(\alpha) = Vt_1(1+\cos(\alpha)) + Vt_2(1-\cos(2\alpha)) + Vt_3(1+\cos(3\alpha)) \qquad (4.3)$$

Here, α is the dihedral angle between the four consecutive atoms and Vt_1, Vt_2 and Vt_3 are coefficients Fourier terms of the equation. These coefficients for CCCC, CCCO and CCOH dihedral angles are listed in Table 4.2.

Table 4.2. The coefficients for intramolecular rotational energy functions (units are in kcal/mol). (Jorgensen, 1986)

	Vt_1	Vt_2	Vt_3
CCCC	0.7055	-0.1355	1.50725
CCCO	0.5	-0.1	1.0
CCOH	0.417	-0.058	0.3735

With these parameters, the torsional potentials for the different dihedral angles are plotted in Figure 4.2. As seen in the graph, the system is in its lowest energy state when the angle α is π (180°). The global minimum at α = 180° is flanked by 2 local minima at 60° and 300°. These orientations correspond to local gauche defects. In the case of the CCOH dihedral angle, for example, the energy associated with a gauche defect lies only 0.87 kcal/mol above the all-trans ground state and the barrier for interconversion is quite small. When a conformational change requires moving heavy atoms exclusively, however, the barrier becomes larger. Rotation about the CCCO dihedral requires overcoming a barrier of 2.1 kcal/mol and barrier for rotation about the CCCC dihedral is even larger (3.2 kcal/mol).

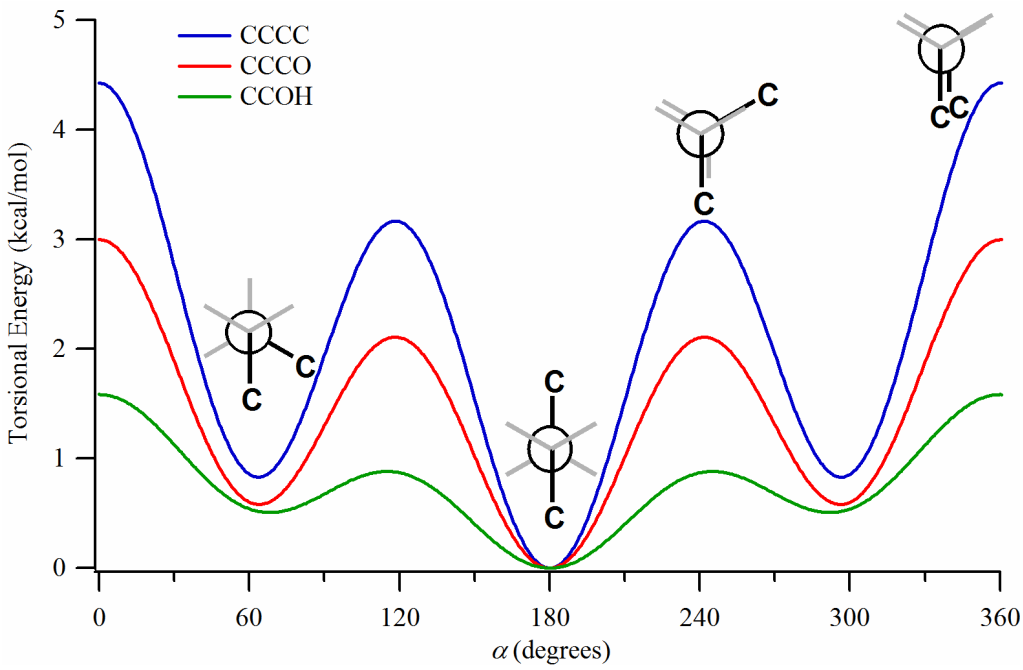

Figure 4.2. Plot of torsional energies as a function of CCCC, CCCO and CCOH dihedral angles. Inset molecular structures correspond to the energy minima and maxima for specific internal rotations of CCCC dihedral angle.

4.2.3. Simulations

The computer code written for running the MD simulation requires an input file defining the physical shape of the simulation media and the positions and properties of the particles (atoms and molecules) involved in the simulation. For simulations of the different monolayers, the simulation *box* is defined as a rectangular cube having dimensions 43 × 43 × 150 Å ($x \times y \times z$ where the z-axis is normal to the interface). This box contains alcohol molecules as well as the water subphase. Periodic boundary conditions are imposed along the x and y axes.

The middle of the z-axis, Z = 0, is defined as the interface between the water subphase (d = 1.0 g/mL) and air. Approximately 900 water molecules are placed at

the lower part of the simulation box. Alcohol molecules are placed in the upper part starting from the water surface (Z = 0). Chains start having all-trans conformations ($\alpha = \pi$ for all CCCC dihedral angles) with the C_1 carbon closest to the water. This conformation is reasonable for linear ROH but, as was inferred from experimental studies presented in Chapter 2 and Chapter 3, almost certainly not the correct structure for the branched alcohols other than 2-C_{16}OH. Consequently, we expect that the initial starting structure will need to undergo significant relaxation and conformational change in order to equilibrate.

All simulations were based on an initial box created for a 1-C_{16}OH monolayer. The interfacial region with a cross-sectional area of 43 × 43 $Å^2$ was filled with 88 alcohol monomers prior to equilibration. This monomer density corresponds to a 21.0 $Å^2$ area per molecule in order to match the experimentally measured average linear alcohol molecular area (~20 $Å^2$) observed for virtually all linear alcohol surfactants at terminal monolayer coverage. Slight differences in surface coverage from system to system are well within the typical uncertainty limit of MD simulations and experimental data.

The input files for the branched alcohols were created using the equilibrated 1-C_{16}OH simulation box in two steps. First, 2-, 3-, 4-, and 5-C_{16}OH input files were created by sliding the OH group along the carbon backbone. The specific procedure requires putting an electron vacancy on the carbon atom to which the -OH group will be attached and equilibrating the resultant box in small time steps to avoid any irreversible changes or a collapse in structure. For instance, the 3-C_{16}OH input file was built from the pre-equilibrated 2-C_{16}OH file by adjusting the potentials on C_2 and

C_3 carbon atoms prior to the equilibration step. Then, during the equilibration step, the -OH group moves from the C_2 carbon atom to C_3 to stabilize the energy.

In the second step, the length of the carbon chain is adjusted by the cutting the hexadecanol chain from the carbon atom that will form the terminal methyl group of the new chain and deleting the remaining piece. For example, the 5-C_9OH input file was created from the equilibrated 5-C_{16}OH input file by deleting C_{10}-C_{16} carbons and converting the C_9 into a methyl group. For simulations examining correlations between surface coverage and organization, the number of molecules at the interface is also adjusted accordingly by selecting the number of molecules necessary to have a given average molecular area and then removing the remaining molecules on the surface.

The useful information from a MD simulation comes from the production run. The production run refers to the simulation that gives results of an equilibrated system that evolves over time subject to the laws of Newtonian mechanics. Before a production run is performed, the generated input files were first equilibrated in order to ensure that the simulation started from an optimized, energetically stable arrangement of conformers. The equilibration runs were performed in two steps. The first step randomized the distributions of alcohol monomers across the surface of the box. For example, the molecular area in any hexadecanol isomer input file including the source files for branched alcohols, starts with a maximum surface coverage of 21 $Å^2$/molecule.

When a lower surface coverage is needed for the branched alcohol, the appropriate number of molecules are removed from one side of the box leaving the

remainder still having a local coverage of 21 $Å^2$/molecule concentrated on the other side of the box. In order to uniformly spread the molecules over the entire interfacial area, intermolecular forces are defined by repulsive interactions between the hydrocarbon chains. This condition induces the molecules to spread during the first equilibration step. The torsional potentials are also turned off to obtain a homogeneous distribution of different molecular conformations. In the second step of the equilibration run, the intermolecular interactions are returned to normal and the torsional potentials are reactivated (Table 4.2). This step organizes the molecules in what one hopes is an equilibrium geometry prior to the simulation run. For example, Figure 4.3 shows the distribution of 30 oxygen atoms for a 5-C_9OH monolayer when the box created and at the end of equilibration runs. Here, the oxygen atom positions represent the anchor for the molecular footprint of alcohol chains. 30 molecules at the interface correspond to 2/3 of the full monolayer coverage meaning that average molecular area is ~60 $Å^2$. At the end of the equilibration run, although the molecules are not homogeneously distributed over the interface, the procedure clearly helps spread the monomers. Also, the actual footprints of the molecules are larger than the points showing oxygen atom positions in the graph. Thus, the efficiency of molecule distribution across the interface is better than might be inferred from the distribution of oxygen atoms. The actual simulation (= production run) is then carried out using this configuration as the starting point and enabling the inter and intramolecular interactions defined earlier.

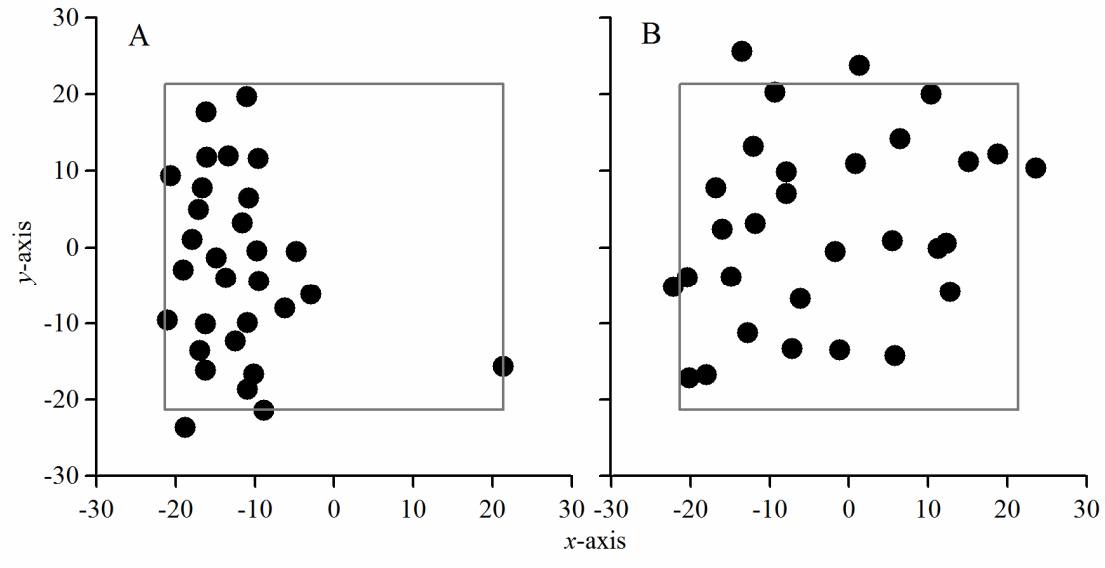

Figure 4.3. Distribution of 5-C_9OH O atoms over the *xy*-plane of the simulation box A) when the input file created, B) after the equilibration run. Gray lines define the boundary of the simulation box for 2/3 of full monolayer coverage.

All simulations were performed at 300K. A 1.0 fs time step was used for each snapshot of the equilibration run and a complete configuration was calculated after every sequence of 500 steps. The structure is randomized to reduce the temperature to 300K. Each equilibration run consisted of 200 randomizations.

The equilibrated configuration is then used as the input configuration for the production run. The same time step as the equilibration run (1 fs) is used, and the complete ensemble configuration is calculated at the end of each 25 fs interval. A trajectory is composed of 1000 configurations and corresponds to a 25 ps integration time. The physical quantities printed for each trajectory include density profiles for carbon atoms and water along the *z*-axis, the orientation of the methyl group(s) as well as the overall chain orientation, dipole orientation and OH bond orientational distribution for water. Finally, the results also contain information about the torsional

distributions along the C_1-C_n chain. The results from at least 40 trajectories were used to generate the average result corresponding to a 1 ns simulation time.

4.3. Results and Discussion

4.3.1. Linear Alcohols

Structure and organization within monolayers formed by linear alcohols have been examined in greater detail in Chapter 2 and Chapter 3. Namely, the molecules were found to align parallel to the surface normal allowing the OH groups interact with the water subphase. This organization leads the monomers to cover the smallest area possible at the interface as inferred experimentally by the footprint of 20 $Å^2$/molecule.

Results of MD simulations for 1-C_9OH at experimental surface coverage are presented in Figure 4.4. As mentioned earlier, the simulations provide data about the positions of particular atoms/groups along the box dimensions. Of particular interest are the statistical distributions of each carbon atom within the chains as well as the OH of the alcohol and subphase molecules along the z-axis (perpendicular to the interfacial plane). Data in Figure 4.4 show that the water subphase extends up to the interface and terminates over a distance of ~5 Å along the z-axis. The OH of the alcohol and the first five carbon atom positions appear in a highly ordered distribution in the outer boundary of the water subphase. The symmetric distribution of each methylene group and the equal spacing between methylene group positions show that the alkyl chains are aligned primarily along the surface normal. The more narrow distribution of the oxygen density from the OH group can be related to the strong

interaction of the group with the water subphase through H-bonding. The small increase in the H_2O density at the interface (Z = -1.5 - 0 Å) may also be related to the H-bonding between the alcohol OH groups and the water molecules.

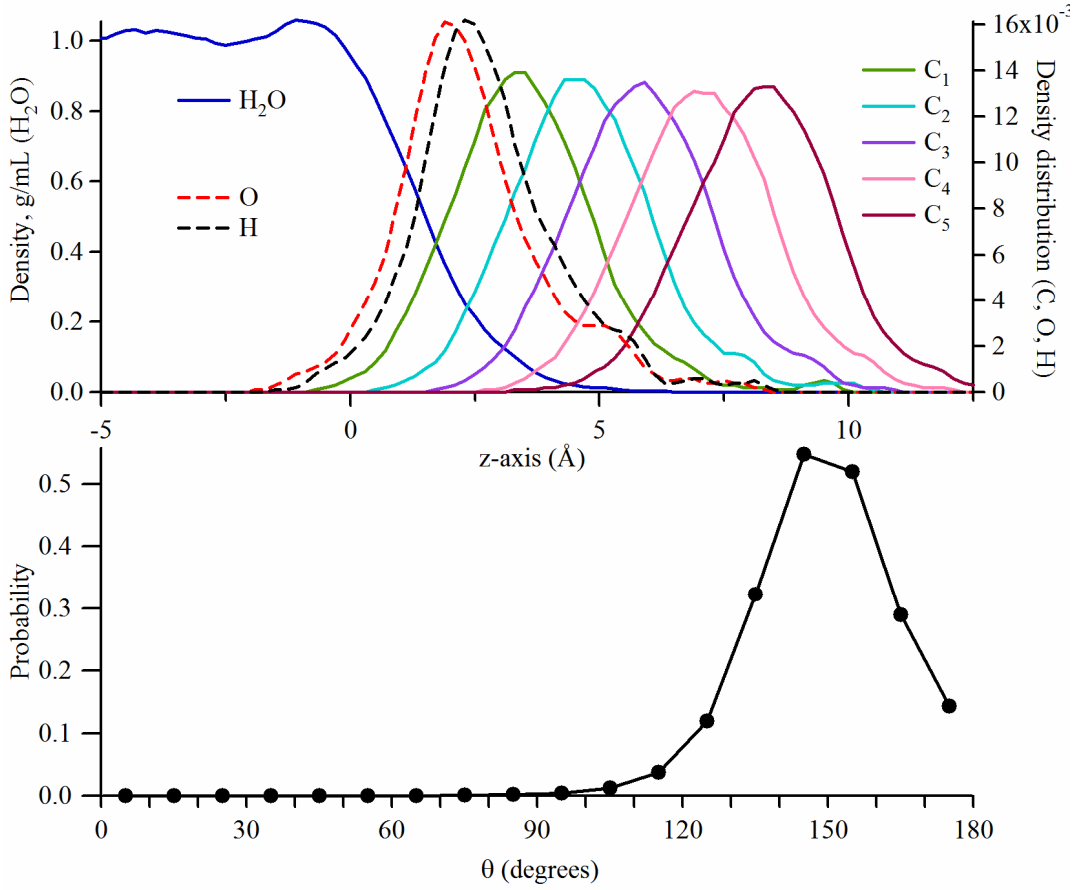

Figure 4.4. Density profiles for H_2O and C, O and H of alcohol chains along the *z*-axis for 1-C_9OH simulation at experimental surface coverage (top). Orientation distribution of methyl group of 1-C_9OH (bottom).

The distribution of the methyl group orientations for the 1-C_9OH monolayer is also shown in Figure 4.4. These data are particularly important because they correlate directly with features measured in VSF spectra. Here, the angle θ defines the angle between the surface normal and the C_3-axis of the methyl group. For example, when θ is 0 degrees, the methyl is aligned toward the water subphase, and if θ = 180°, the

methyl is directed away from the surface. The angle for the lone methyl group of 1-C_9OH is oriented ~150° with the surface normal. This angle corresponds to the molecular geometry where the carbon backbone is aligned with the surface normal and the terminal methyl C_3-axis is directed ~30° away from the normal due to the tetrahedral geometry of the bonding of carbon atoms. In conclusion, the data showing the distribution of methyl group orientations fits into the picture drawn by the experiments and complete the density profile data of the linear chains.

4.3.2. 2-C_9OH Simulations at Various Surface Coverages

Simulations for branched alcohol monolayers have been performed in different surface coverages in order to vary the contribution of different parameters in the overall system's energetics. Varying the molecular area primarily affects the balance of intermolecular interactions between monomers adsorbed to the surface and the interactions between these same monomers and the aqueous subphase. Results of MD simulations for 2-C_9OH monolayers at three different surface coverages are presented below.

The methyl group orientations for 2-C_9OH monolayers at 1/3 of full monolayer coverage (~120 Å^2/molecule) are shown in Figure 4.5. The figure shows that the C_9 methyl group of the 2-C_9OH monomers has an average angle of 115° corresponding to an orientation which is directed slightly above the interfacial plane. This distribution changes little at higher surface coverages. The C_1 orientation shows an overall distribution centered around 90°, although the distribution has a bimodal appearance. Thus, the two methyl orientations approximately parallel to the surface

plane suggest that the 2-C_9OH molecules at dilute surface concentrations lie flat on water. Since the molecular area is only 1/3 of full monolayer coverage, the molecules have enough room to stay in an all-trans conformation.

At 2/3 full monolayer coverage, the C_1 methyl distribution is significantly different than in the 1/3 full coverage case. The C_9 methyl group distribution resembles closely the distribution observed for full monolayer coverage. The broad C_9 methyl distribution has a maximum at 125° corresponding to an average orientation slightly above the interfacial plane. More dramatic changes are observed with the C_1 methyl orientation. Although this distribution has more than one maximum in the distribution profile, the most probable orientation falls at 0° meaning that the C_1 methyl group points towards the water subphase. The other two significant local maxima in the C_1 methyl distribution occur at 115° and 165° corresponding methyl distributions resulting from gauche defects in the structure that have been proposed in Chapter 3. These conformations are the ones most likely to reproduce vibrational band intensities observed in VSF spectra at terminal monolayer coverage. Additional analysis presented below shows that a significant part of the chain lies mainly parallel the interface. In conclusion, the simulations of 2-C_9OH at 2/3 of full monolayer coverage show that the molecules are likely to adopt a number of different conformational structures.

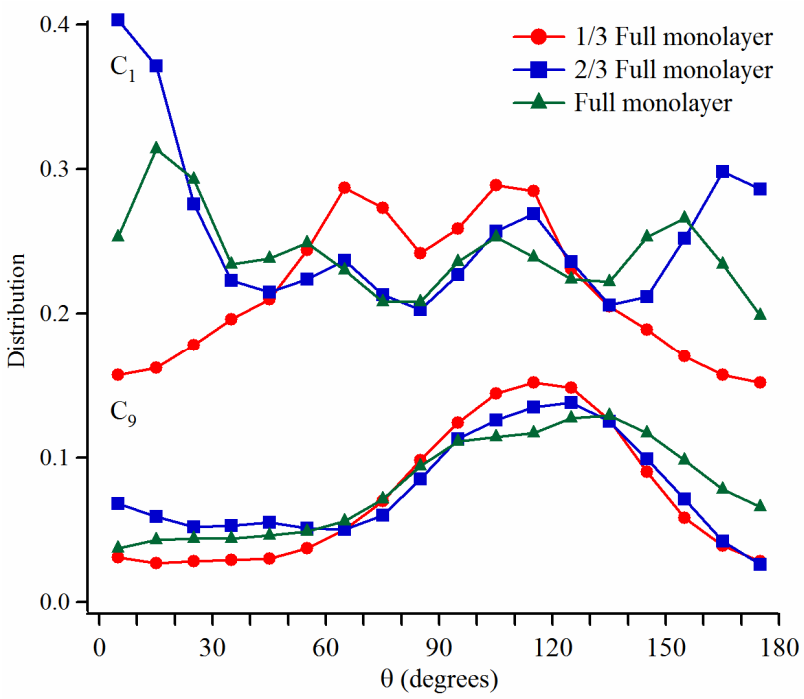

Figure 4.5. Methyl orientation distributions for 2-C_9OH monolayers at various surface coverages. The data for C_1 methyl orientation are vertically offset for clarity.

To evaluate the C_1 methyl orientation distribution, we assume that –OH hydrogen bonding is the strongest interaction between the monomers at the surface and the underlying subphase. If this assumption is true then the C_1 methyl group should have well defined orientations relative to the –OH in the 2-position. Depending on conformation we would expect the C_1 methyl group distribution to have up to 4 different orientations consistent with the simulation data. If the most probable orientation of the C_1 methyl group appears to be 0° or directed down into the water means, Lewis projections predict that the –OH will be directed away from the water leaving the oxygen well positioned to accept (but not donate) hydrogen bonds.

Methyl orientation distributions from MD simulations of 2-C_9OH monolayers at experimental, terminal monolayer coverages are also shown in Figure 4.5. In

general, the orientation profiles for both methyl groups of 2-C_9OH are similar to that at 2/3 of the full monolayer coverage. Again the C9 methyl group has an average orientation of 120° but the distribution is broad and shows signs of a bimodal character. The distribution of methyl group at C_1 position again shows 4 maxima at 15°, 55°, 105° and 155°. The two smaller angles correspond to orientations where the methyl group points towards the water subphase while the maximum at 105° shows an orientation mostly parallel to the surface. The maximum at 155° corresponds to a chain orientation along the surface normal. The most noticeable difference between the 2/3 and full monolayer coverage C_1 distributions is that orientation probabilities are much more evenly distributed in the full monolayer coverage situation. When combined with the C_9 methyl orientation distribution, the data show that 2-C_9OH monomers at full monolayer coverages adopt a number of different conformer structures at the interface. One such structure is an all-*trans* conformation pointing the methyl groups in opposite directions. This result is inconsistent with experimental observations and hints that the potentials used in these simulations may not be properly scaled.

The methyl orientation distributions resulting from simulations of 2-C_9OH monolayers present a general picture showing conformational variation of monomers within the monolayers. We began these simulations hoping to shed light on the specific balance of interactions between monomers and between monomers and the subphase that gave rise to monolayers having well defined vibrational structure. As a result of our analysis, we predicted that monomers should, on average, have a certain number of gauche defects to account for the observed molecular areas and vibrational

band intensities. The distributions presented above show hints of the appropriate conformations but the structures anticipated from experimental data represent a minority of those predicted by the simulations. Specifically, the C1 methyl distributions have to show greater probability in the maxima located at 105° and 155° and less probability at 15° and 65°. Such a shifting of the probability distribution will require stronger –OH/water interactions, and/or slightly weaker torsional potentials to make conformational flexibility more favorable.

Another approach to analyzing the simulations is to locate the gauche defects by examining the dihedral angles along the carbon chain. Torsional (dihedral angle) distributions of 2-C_9OH chains are shown in Figure 4.6. Similar to the methyl orientation distribution profiles, torsional distributions do not indicate any significant difference between the full monolayer and 2/3 of full monolayer coverages. One clear result shown by the data is that all C-C dihedral angles have a maximum at 180°. This result implies that all parts of the chain are primarily in *trans* conformations. One exception to this trend is the observable peak at ~70° of C_1-C_4 dihedral angle profile. A peak in distribution profile at this angle means that there is a gauche defect around the C_2-C_3 bond. This gauche defect necessarily flips the positions of C_1 methyl group and the oxygen atom, and orients the methyl group out of the plane defined by the rest of carbon atoms. This small chance of a gauche defect also shows up as a small increase in O-C_4 torsional distribution at angles around π. The large peak at ~65° of O-C_4 distribution also, again, shows that the chains are primarily in all-*trans* conformation.

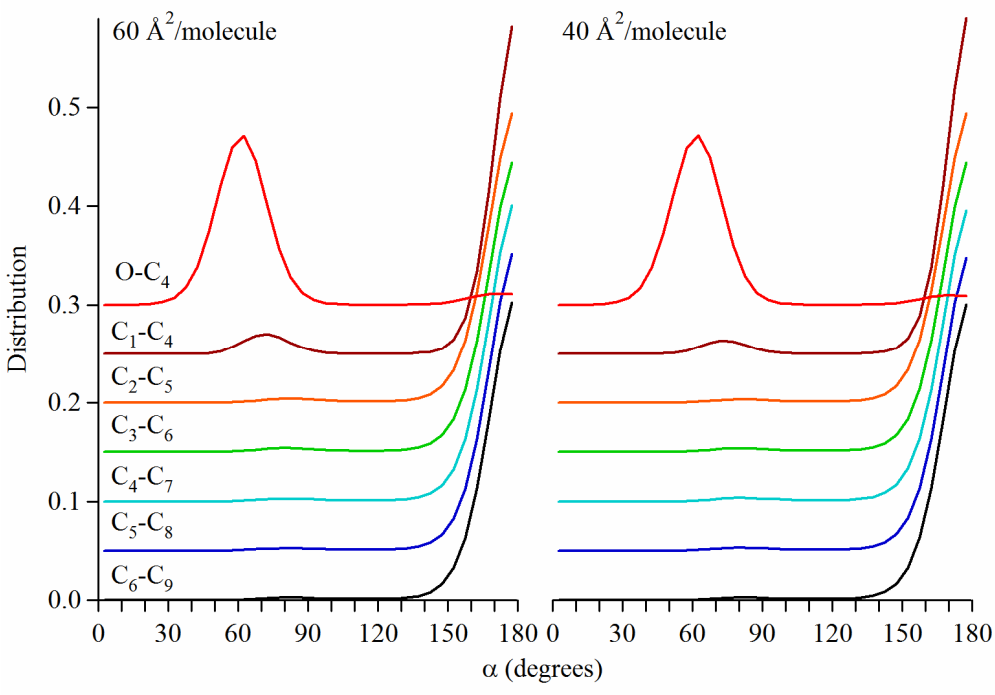

Figure 4.6. Torsional (dihedral angle) distributions of 2-C_9OH monomers at two different surface coverages corresponding to molecular areas of 60 and 40 Å^2/molecule. The data are vertically offset for clarity.

The structures shown by the torsional distribution show evidence of conformers that would match those predicted by our experimental findings but the dominant calculated conformations are inconsistent with experimental results. The simulation data predict that at high enough surface coverage (≥ 2/3 monolayer coverage) the 2-C_9OH monomers exist primarily in all-*trans* conformations. Our experimental studies predict that gauche defects around C_2-C_3 and also around C_3-C_4 bonds should be much more common. In addition methyl orientation distributions point strong possibility of gauche defects in carbon chains. The disagreement between the data may be partly attributed to the distribution of molecules in z-direction of the simulation box.

Figure 4.7 shows the density profiles of hydrogen, oxygen and the first five carbon atoms of 2-C_9OH molecules as well as water molecules along the *z*-axis at full monolayer coverage. The first observation is that the distribution of atoms in the alcohol chain is dramatically different than those observed for linear alcohols (Figure 4.4). Specifically the alcohol molecules are grouped into two distinct domains separated along the *z*-axis by almost 2 nm. Such a structure is consistent with bilayer formation. Within both domains, the alkyl chains show very little preferential ordering. For the chains localized closer to the water, the –OH groups show a broad distribution indicating H-bonding between monomers as well as with the subphase. The very narrow distribution of –OH groups in the outer domain indicates a very compact, tightly bonded network.

Another observation resulting from this representation of the simulation data is that density in the water region decays over longer distances (8 Å) compared to the linear alcohol system. (~5 Å) Given that the monomers themselves begin distributed across the interface all sharing the same orientation, the restructuring that occurs to form this bilayer architecture likely represent an energetic minimum in monolayer organization. However, the disagreement between experimental results and calculated methyl orientations, forces us to be cautious when interpreting these calculated structures. More work is needed to test the sensitivity of the calculated structures to changes in inter and intramolecular potentials.

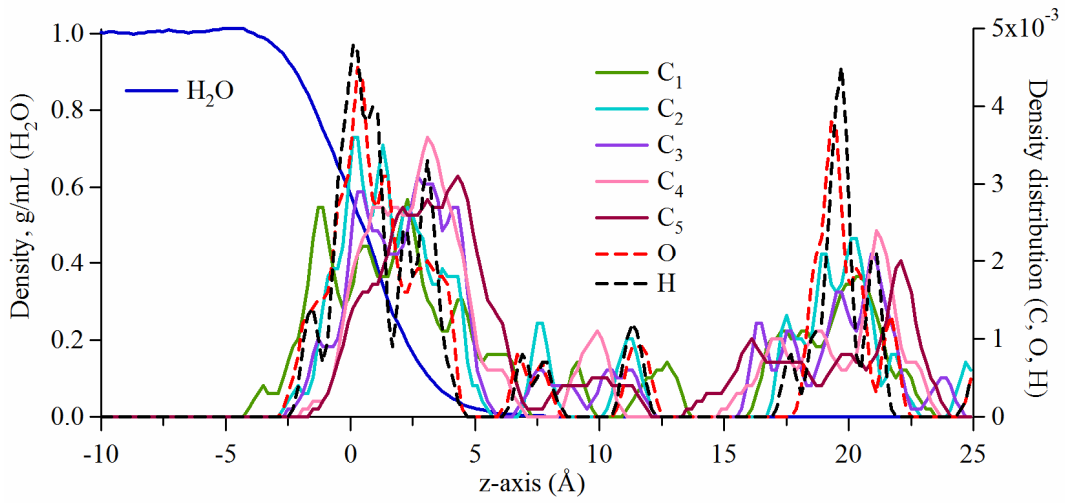

Figure 4.7. Density profiles for H_2O and C, O and H of alcohol chains along the *z*-axis for 2-C_9OH simulation at experimental surface coverage.

In conclusion, the density distributions of 2-C_9OH monolayer at different surface coverages show that the simulations predict molecular organizations having considerable variation in conformation and position along *z*-axis. Such an organization may not accurately simulate the real picture at the aqueous/vapor interface. One limitation of the simulations performed is the way in which the monolayers are formed compared to experiments. In an experiment, monomers adsorb to the interface from bulk, but in a simulation, all monomers are already present at the surface meaning that the original monolayer may find a local energy minimum that is not the global minimum.

4.3.3. 3-C_9OH Simulations at Various Surface Coverages

The distribution of methyl orientations for 3-C_9OH monomers are shown in Figure 4.8. The methyl orientational distributions are quite different from those for the

2-C_9OH monomers. The small difference in methyl orientations comes from a single gauche defect in the carbon chain that allows the –OH group in C_3 carbon atom to contact the water subphase. If the monomer is otherwise in an all-*trans* conformation, such an orientation requires both methyl groups to be directed along the surface with some inclination angle toward the bulk. Thus, like the 2-C_9OH, 3-C_9OH monomers at low surface coverages also have primarily all-trans conformations with average molecular orientations along the interfacial plane to optimize both –OH/subphase hydrogen bonding and van der Waals contact between the chain and the underlying water.

The 3-C_9OH molecule at its 2/3 of monolayer coverage shows a number of possible different molecular orientations. First the C_1 methyl group has two maxima in the distribution profile corresponding to orientation angles of 85° and 155°. While the distribution at 85° correspond to and average orientation along the surface, the latter value results from orientations mainly along the surface normal. On the other hand, the distribution of C_9 methyl group orientation appears to be approximately constant for all angles with a slight enhancement in probability near 35°. Thus, the orientational distributions of methyl groups at 2/3 monolayer coverage does not show any clear preferential orientation. Compared to the 2/3 monolayer coverage, methyl groups at full monolayer coverage have more well defined orientations. While the C_1 methyl group has a maximum at ~50°, the C_9 methyl group has a broad distribution with a maximum at ~130°. In general, these orientations indicate all-trans conformations along the surface normal. However, similar to the 2-C_9OH

simulations, the results shown by torsional and density distributions data do not show any predominant conformational structure.

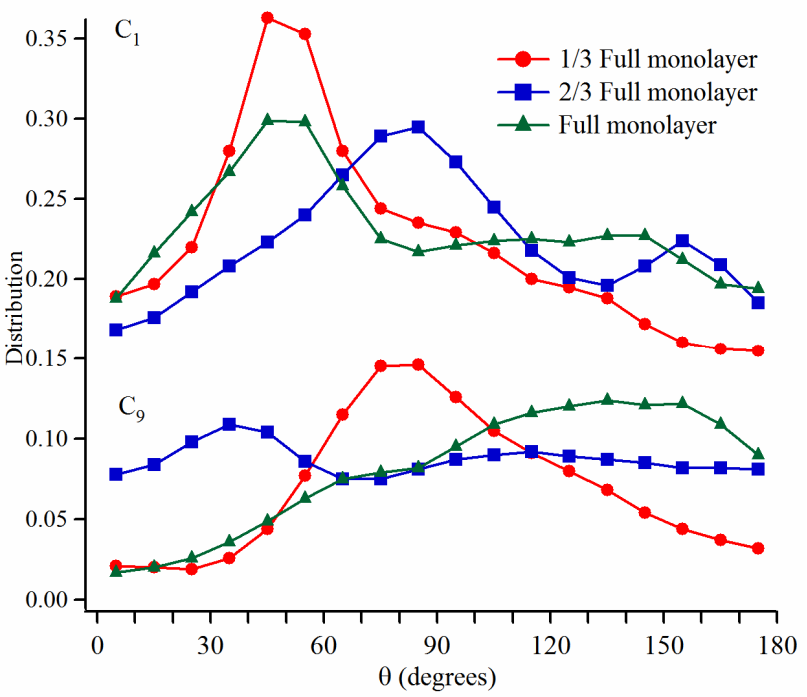

Figure 4.8. Methyl orientation distributions for 3-C_9OH at various monolayer coverages. The data for C_1 methyl orientation are vertically offset for clarity.

Figure 4.9 shows the distribution of dihedral angles for 3-C_9OH monomers at experimental surface coverage. The distributions are quite similar to those obtained in the simulations for 2-C_9OH except for the position of small gauche defect probability. At full monolayer coverage, a small increase at C_2-C_5 dihedral angle shows the probability of a gauche defect around C_3-C_4 bond. Similar to the 2-C_9OH torsional distributions, the O-C_5 dihedral angle distribution completes the picture drawn by C_2-C_5 dihedral angle. Although, such a structure appears in the distributions as a possibility, it remains a minority conformer as most of the chains remain in mostly all-trans conformations as evidenced by the large distributions at angles around 180°.

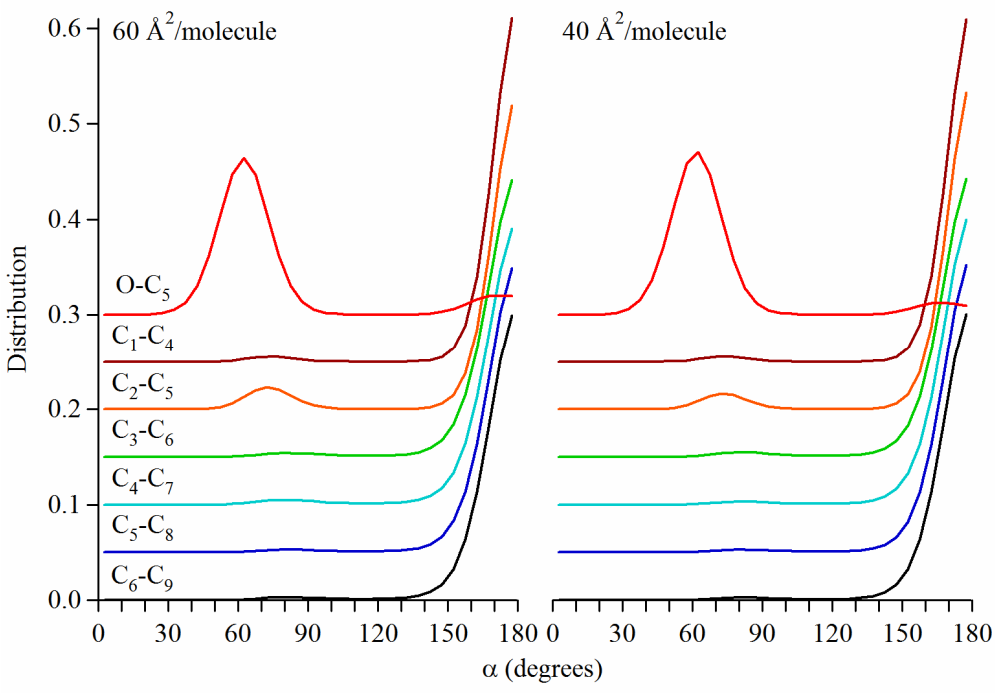

Figure 4.9. Torsional (dihedral angle) distributions of 3-C_9OH monomers at two different surface coverages corresponding to molecular areas of 60 and 40 Å^2/molecule. The data are vertically offset for clarity.

The density profiles of hydrogen, oxygen and the first five carbon atoms of 3-C_9OH molecules, and the water subphase molecules at full monolayer coverage are shown in Figure 4.10. Similar to the 2-C_9OH case, the molecules appear split into two domains separated along *z*-axis. Although the ordering with the domains seems very poor, the approximate, relative positions of atoms within each domain may provide information about different orientational preferences. While the –OH group appears to have a maximum on lower part of the domain which is closer to the water subphase, the outer domain shows a relatively symmetric distribution. However, it is difficult to assign these small differences to preferential structures for each domain.

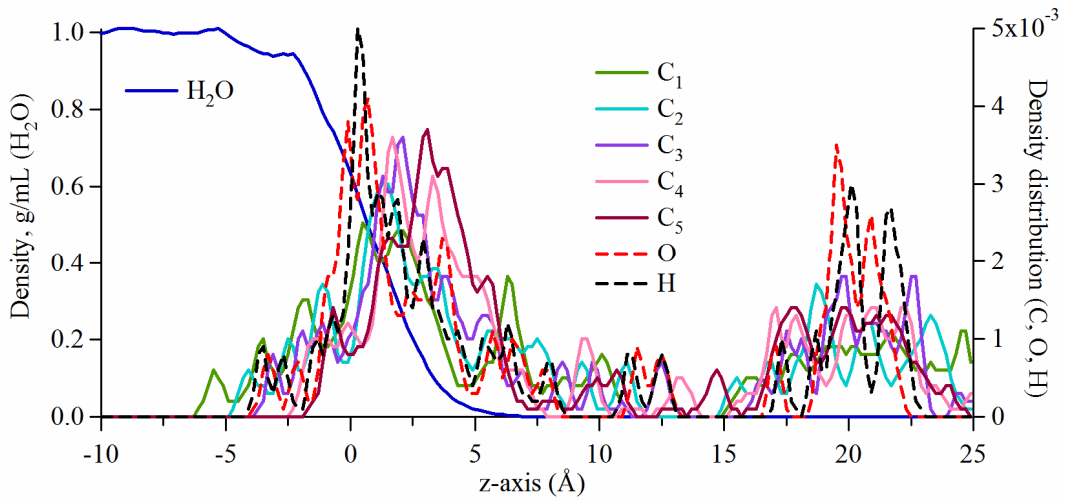

Figure 4.10. Density profiles for H_2O and C, O and H of alcohol chains along the *z*-axis for 3-C_9OH simulation at experimental surface coverage.

4.4. Conclusion

In conclusion, the MD simulations carried out thus far have highlighted difficulties associated with attempting to model systems whose structure is controlled by multiple competing forces having comparable magnitudes. Calculated monolayer organization at experimental surface coverage leads to functional group distributions that are inconsistent with experimental results. Discrepancies suggest that specific potentials may over or underestimate interactions between monomer and between monomers and the subphase. New simulations will attempt to identify those interactions responsible for the minority populations that appear more consistent with experimental observation.

Chapter 5: Phospholipid Monolayers

5.1. Introduction

Structure and organization of organic films at liquid surfaces figure prominently in a host of environmental and biological systems. Examples include monolayers controlling uptake, evaporation, and heterogeneous catalysis at aerosol interfaces [1,74-76,78] and the spreading and compression of lung surfactant on the surfaces of alveoli.[57,58,112] Phospholipid films on aerosol surfaces have even been proposed as possible precursors to very first biological cells.[80] While the importance of these organic films can not be disputed, surprisingly little is known about the properties of films having mixed composition. These issues are particularly relevant as most biologically-important, self assembled systems consist of multiple surface active components. Nowhere is this heterogeneity more apparent than in the composition of cell membranes.

Cell membranes – also referred as plasma membranes – can contain up to 25 different types of lipids although typically only 3-4 dominate a given membrane's population.[113,114] The specific distribution of lipids in a plasma membrane depends on the type of the cell. Human heart cell plasma membranes are rich in 1,2-distearoyl-*sn*-glycero-3-phosphoethanolamine (DSPE) while 1,2-dipalmitoyl-*sn*-glycero-3-phosphocholine (DPPC) is the major phospholipid structure in red blood cell membranes.[115,116] Phospholipid organization in two dimensions relates directly to issues of cell membrane structure and stability.[117] Of particular importance is the

ability of phospholipids to mix with other surface active species and the relative degree of order/disorder found within lipid assemblies having varying composition. Detailed studies have characterized properties such as miscibility and phase behavior of mixed phospholipid systems,[118,119] but considerably less is known about how simple surfactants impact lipid organization and structure. Some simple surfactants are known for their ability to solubilize membranes and induce/promote domain formation within the membranes.[120-122]

While the properties of DPPC monolayers adsorbed to air/aqueous interfaces are well characterized,[66,123-125] only recently have studies begun to examine the interfacial behavior of mixed monolayers where DPPC is the primary component.[112,126-129] Of particular relevance to the work presented below is a recent report from Allen and coworkers that used surface specific, vibrational sum frequency spectroscopy (VSFS) to study the structure of condensed DPPC monolayers deposited on the neat air/water interface and on the surface of solutions containing 2 mM sodium dodecyl sulfate (SDS).[130] Based on changes in vibrational structure and clever isotopic labeling schemes, the authors concluded that the anionic surfactant competes with DPPC for available surface sites and that the combination of surfactant and lipid leads to greater conformational order within the mixed monolayer system. Such surfactant-lipid interactions raise a host of questions about how soluble surfactants influence the self-assembling tendencies of biological amphiphiles.

Experiments described below examine the effects of simple, soluble surfactants on the ability of DPPC to form monolayers spontaneously at the air/aqueous interface. Surface pressure measurements coupled with surface-specific

vibrational spectroscopy show that very dilute surfactant solutions inhibit the tendency of DPPC to spread at the air/aqueous interface and that this effect is general for both anionic and cationic surfactants. Increasing concentrations of anionic and cationic surfactants lead to different monolayer organizations having varying degrees of conformational order.

5.2. Materials and Methods

5.2.1. Materials

DPPC consists of two saturated, 16-carbon acyl chains attached to a 3-carbon glycero backbone and a zwitterionic choline headgroup (Figure 5.1). This lipid represents the primary component of the lung surfactant mixture that allows alveoli to expand and contract during respiration and also constitutes the primary building block in many cell plasma membranes.[131] Surfactants used in the experiments discussed below were sodium dodecyl sulfate (SDS), an anionic surfactant, and dodecyl trimethyl ammonium bromide (DTAB), a cationic surfactant. Both surfactants have saturated, 12-carbon chains and CMCs in excess of 8 mM. Experiments examining the ability of DPPC to form monolayers spontaneously in the presence of these surfactants used surfactant solutions having bulk concentrations of 1, 100 and 500 μM. All experiments were carried out at 295 ± 1 K.

All solutions were prepared using pure water, Milipore Milli-Q (>18 MΩ·cm resistivity, pH = 5.5). DPPC was purchased from Avanti Lipids (Cat. No. 850355P) and used as received. SDS and DTAB samples were purchased from FisherBiotech (BP166-100) and Sigma (D8638), respectively. Deuterated SDS (d_{25}) and DTAB (d_{34})

reagents came from Cambridge Isotopes (DLM-197-1) and ISOTEC Inc. (684260-SPEC), respectively.

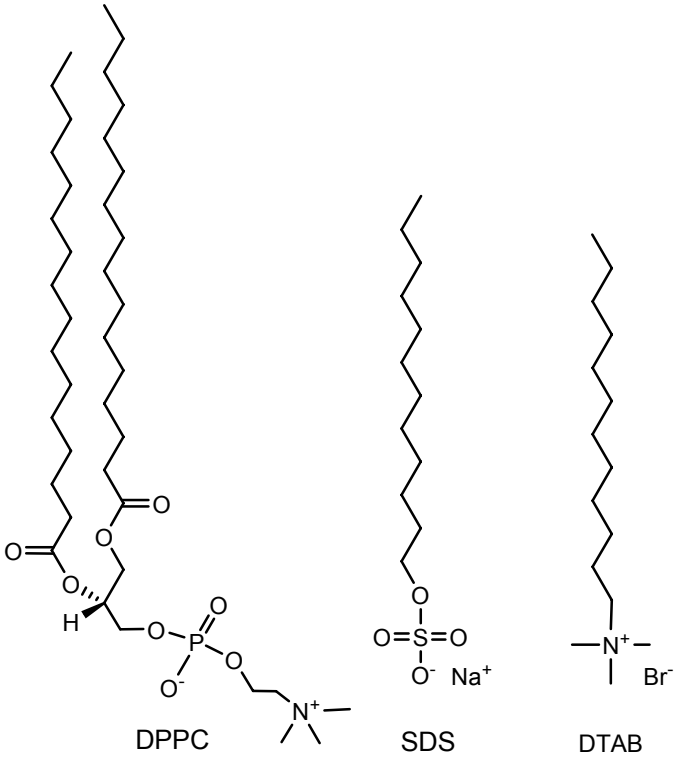

Figure 5.1. Molecular structures of DPPC, SDS and DTAB.

5.2.2. Surface Pressure Measurements

A Nima Langmuir-Blodgett trough (Model 302LL) was used to measure isotherms of phospholipid films adsorbed to the air-water interface. Phospholipid films were prepared by adding 10 μL of ~1 mg/mL DPPC:chloroform spreading solvent on the surface of an aqueous solution inside of the two barriers. Experiments began 20 minutes after deposition to allow chloroform to evaporate and for DPPC molecules to spread across the surface. The film was compressed with a constant

speed of 10 cm^2/min. This compression proved reversible as evidenced by a lack of hysteresis in subsequent expansions and re-compressions of the pure monolayer.

Equilibrium spreading pressure (ESP) measurements were carried out by placing a small, solid flake of DPPC onto the surface of a given subphase and then allowing the system to equilibrate for at least 24 hours. Monolayer formation ceases when the chemical potential of the monomers on the water surface becomes equal to the chemical potential of monomers in the "infinite reservoir" of material provided by the solid sample. By measuring the surface pressure of the monolayer at its ESP, one can determine the monomer coverage by mapping the ESP onto the surface pressure isotherm.[68]

5.2.3. Vibrational Sum Frequency Spectroscopy

A detailed description of vibrational sum-frequency generation has appeared in numerous sources. Briefly, SF generation is a nonlinear optical process that occurs when two high intensity optical fields with frequency ω_{ir} and ω_{vis} overlap at the vapor/liquid interface to generate a third frequency ω_{sf} equal in energy to the sum of ω_{ir} and ω_{vis}. The intensity of the SF response, I_{sf}, is proportional to the square of second-order nonlinear susceptibility tensor ($\chi^{(2)}$) and the intensities of the infrared (I_{ir}) and visible (I_{vis}) beams:

$$I_{sf} \propto \left|\chi^{(2)}\right|^2 I_{ir}\, I_{vis} = \left|\chi^{(2)}_{NR} + \chi^{(2)}_{R}\right|^2 I_{ir}\, I_{vis} = \left|\chi^{(2)}_{NR} + \sum_q \frac{A_q}{\omega_{ir} - \omega_q + i\Gamma}\right|^2 I_{ir}\, I_{vis} \qquad (5.1)$$

where $\chi^{(2)}_{NR}$, $\chi^{(2)}_{R}$, A_q, ω_q, and Γ are the nonresonant and resonant susceptibility,

amplitude, vibrational center frequency, and linewidth for a given mode q, respectively. Previous studies of similar systems showed that the nonresonant contribution is negligible for alkane systems. Consequently, evaluation of the spectra shown below does not include this term.

Although the $\chi^{(2)}$ tensor has 27 elements, due to rotational invariance at the interface there are only three independent components: $\chi^{(2)}_{yyz}, \chi^{(2)}_{yzy}, \chi^{(2)}_{zzz}$. Different polarization combinations sample different elements of the $\chi^{(2)}$ tensor. SF spectra in this work were collected using an $S_{sf}S_{vis}P_{ir}$ polarization combination to sample those vibrational modes having the net transition moment aligned along the surface normal ($\chi^{(2)}_{yyz}$). More details about the system and spectra collection procedures were given in previous reports.[12,68,132]

5.3. Results and Discussion

Surface pressure isotherms for SDS and DTAB are shown in Figure 5.2. Data agree well with previous published reports, and a Gibbs analysis shows terminal monolayer coverages of 2.5 x 10^{14} /cm^2 (SDS) and 2.9 x 10^{13} /cm^2 (DTAB). The experiments described below focus on the ability of these soluble surfactants to either promote or inhibit monolayer formation by DPPC at the liquid/vapor interface. In particular we choose solutions having three different concentrations corresponding to different surface excess concentrations. At bulk concentrations of 1, 100 and 500 μM, solutions of SDS have aqueous/vapor surface pressures of 0, 0.6 and 2.7 mN/m corresponding to surface excess coverages of ~1 x 10^6, >1000 and ~100 Å^2/molecule,

respectively. For 1, 100 and 500 μM solutions of DTAB, the surface pressures (and coverages) are 0.6 mN/m (>500 Å^2/molecule), 9.2 mN/m (123 Å^2/molecule) and 22.7 mN/m (76 Å^2/molecule), respectively.

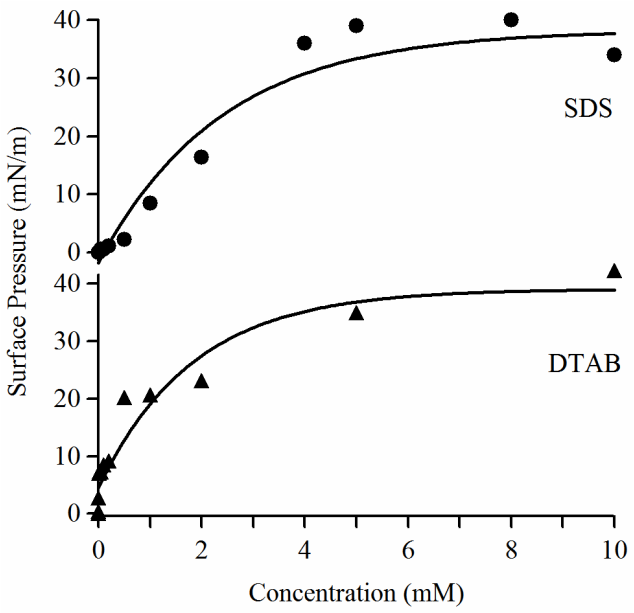

Figure 5.2. Surface pressure isotherms of SDS and DTAB. Data are fitted with an exponential function (solid lines).

5.3.1. Surface Area Measurements DPPC

Figure 5.3 shows the surface pressure isotherm of DPPC adsorbed to the air/water interface. The isotherm was acquired by compressing an expanded film of DPPC monomers. The well-studied DPPC isotherm on pure water shows a surface pressure lift-off at ~90 Å^2/DPPC monomer, a liquid expanded/liquid condensed coexistence region between 55-70 Å^2/monomer and a condensed, incompressible film between 40-50 Å^2/monomer.[133-135] Isotherms of DPPC on 1 and 100 μM solutions of SDS and DTAB are similar but not identical to that of DPPC on pure water. One small but reproducible noticeable difference between the DPPC on pure water and

DPPC on the 100 μM SDS solution is that the pressure lift-off occurs at a higher monomeric area on the SDS containing solution. Correspondingly, the length of liquid expanded/liquid condensed coexistence region increases by ~ 10 $Å^2$. Similar but less pronounced behavior is observed for isotherms acquired for 1 and 100 μM DTAB solutions. On 500 μM surfactant solutions, lift off occurs at DPPC monomer areas > 160 $Å^2$/molecule for both SDS and DTAB. With SDS, the DPPC liquid expanded phase extends over a very large 70 $Å^2$ window (160-90 $Å^2$) and the liquid expanded/liquid condensed coexistence region occurs at a higher surface pressure.

The rising pressure associated with the liquid condensed to solid phase transition is virtually equivalent for DPPC on pure water and all SDS solutions implying that SDS is reversibly squeezed out of the monolayer at high pressures. In the case of 500 μM DTAB, coexistence occurs at approximately the same surface pressure as lower concentrations but at considerably expanded DPPC monomer areas. The overall shift to larger areas of the DPPC isotherm on the 500 μM DTAB solution implies that the cationic surfactant is integrated into the DPPC monolayer irreversibly. Here, the molecular area values are given in terms of area per DPPC monomer. The surface pressures of DPPC isotherms acquired from the surface of surfactant containing solutions are reported relative to the equilibrated surface pressures of each surfactant solution in the absence of DPPC.

An important point to remember is that isotherms of surfactant solutions acquired in the absence of DPPC never show a measurable change in surface pressure. As the area between the barriers shrinks, any excess soluble monomers on the surface resolvate back into solution only to re-adsorb to the expanding area

outside of the trough barriers. If the surfactants were not interacting with the lipid, DPPC isotherms on surfactant containing solutions would mirror the isotherms of DPPC on pure water. The fact that lift off occurs at lower DPPC monomer concentrations (= larger area/monomer) indicates strong, non-ideal attractive interactions between the surfactant and the lipid.

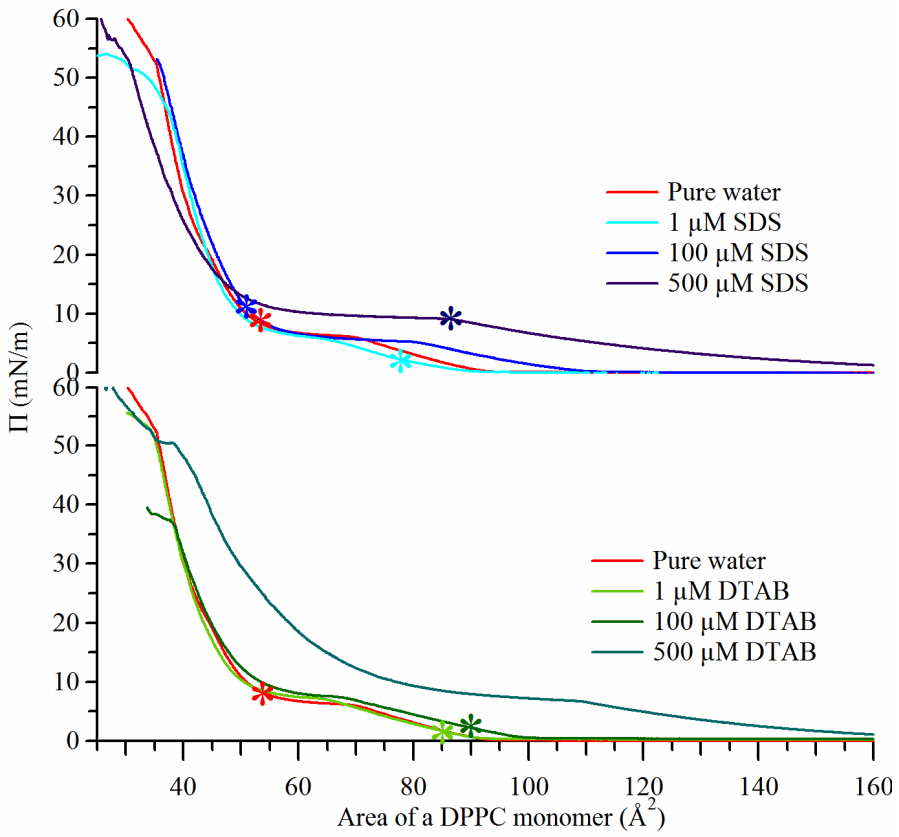

Figure 5.3. Surface pressure isotherms of DPPC on pure water and 1, 100 and 500 μM SDS and DTAB solutions. Asterisks show ESP values for each experiment. In the case of 500 μM DTAB, the measured surface pressure is negative relative to 22.7 mN/m, the surface tension of the surfactant solution without DPPC. See text for more details.

Also marked on the isotherm are the ESPs of DPPC on sub-phases of pure water, 1 and 100 μM SDS and DTAB. At room temperature on pure water, DPPC

spreads to form a monolayer having an ESP of 8 ± 2 mN/m (Table 5.1). This value corresponds to a DPPC monolayer on the high coverage side of the LC/LE coexistence region with an area of 53 $Å^2$/DPPC monomer. One recent study by Mansour and Zografi reported that the DPPC does not spread on a Tris buffer solution (pH = 7.4) containing 150 mM NaCl.[136] The difference between our observation and the reported DPPC behavior on the Tris buffer is related to the difference in subphase composition and the resulting tendency of DPPC to spread across the surface. Studies in our own lab have reproduced the Tris results, and the precision of the DPPC measurements on unbuffered (pH = 5.5) water show that the slightly acidic nature of Millipore water plays an important role on DPPC spreading at the aqueous/vapor interface.

On a 1 μM SDS solution, DPPC forms a monolayer that is much more expanded compared to the monolayer formed on pure water. The ESP measurement of 3.5 ± 1.0 mN/m on SDS corresponds to surface coverage of 77 $Å^2$/DPPC monomer. On more concentrated SDS solutions, DPPC spreads more readily with surface pressures of 10.9 mN/m on 100 μM SDS solutions and 9.1 mN/m on 500 μM SDS solutions. These values correspond to areas of 50 $Å^2$/DPPC monomer and 56 $Å^2$/DPPC monomer, respectively. Within experimental uncertainty, these areas/DPPC monomer are almost equivalent and bracket the DPPC itself at its ESP on pure water. Again, we note that these surface pressures are referenced to the surface tensions of the respective solutions in the absence of DPPC. For example, the surface tension of a 100 μM SDS solution is 71.7 mN/m corresponding to a surface pressure of 0.6 mN/m relative to the neat water/vapor interface (γ_0 for pure water at 295 K is

72.3 mN/m). With DPPC present (in the form of a solid flake), the surface tension drops to 61.2 mN/m resulting in the reported surface pressure of 10.5 mN/m ($= \gamma_0 - \gamma$ and $\gamma_0 =$ 71.7 mN/m for 100 μM SDS solution).

Table 5.1. Surface pressure data for DPPC monolayer on pure water and on SDS and DTAB surfactant solutions. All values are in mN/m.

Subphase	**Surfactant solution surface pressure**	Π_{H_2O} *	$\Pi_{surfactant}$ #
Pure water	-	7.9 ± 2.3	-
SDS			
1 μM	0	3.5 ± 1.0	3.5 ± 1.0
100 μM	0.6	11.5 ± 0.6	10.9 ± 0.6
500 μM	2.7	11.8 ± 2.8	9.1 ± 2.8
DTAB			
1 μM	0.6	< 1.0	< 1.0
100 μM	9.2	11.7 ± 0.7	2.5 ± 0.7
500 μM	22.7	10.6 ± 0.6	-12.1

* ESP of DPPC or DPPC/surfactant relative to pure water surface tension.

ESP of DPPC/surfactant system relative to surfactant surface tension.

One important observation is that the effect of DPPC spreading is to lower the surface tension of the system relative to the individual SDS surfactant solutions. Solutions having low surfactant concentrations (1 μM), however, appear to inhibit DPPC spreading relative to DPPC behavior at the neat aqueous/vapor interface. Higher concentrations promote slightly the formation of mixed monolayer films compared to the behavior of DPPC at the aqueous/vapor interface in the absence of surfactants. The ability of SDS to either inhibit or promote DPPC spreading

depending on the bulk anionic surfactant concentration suggests a competition between surfactant adsorption and DPPC spreading. Furthermore, results imply that the balance between these two phenomena changes as surfactant concentration varies. These issues are explored in greater detail below through an examination of the surface vibrational spectra of these systems.

On a solution of 1 μM DTAB, the measured DPPC ESP value of < 1.0 mN/m shows that the DPPC does not spread to any measurable extent. This surface pressure corresponds to an area of > 85 $Å^2$/monomer. In comparison to SDS, the low surface excess coverage of DTAB more efficiently inhibits monolayer formation by DPPC. This behavior is accentuated with higher bulk concentrations of the cationic surfactant. Due to its more hydrophobic headgroup, DTAB is more surface active than SDS, and a 100 μM solution of cationic surfactant has a surface pressure of 9.2 mN/m relative to pure water at the solution/vapor interface. When DPPC is added to the system (in the form of a solid flake of material), the surface pressure rises to 11.7 mN/m (relative to pure water, Π_{H_2O}) for an effective change of only 2.5 mN/m. Mapping this result into the surface pressure isotherm shown in Figure 5.3, we see again that DTAB effectively reduces the ability of DPPC to spread across the interface.

Unusual behavior is observed when the DTAB concentration is increased further. The surface pressure of a 500 μM DTAB solution exceeds 20 mN/m. Adding DPPC to the system (in the form of a solid flake on the solution surface) leads to an *increase* in surface tension and a corresponding *negative* surface pressure (of -12.1 mN/m). Naively, one might interpret this result to mean that DPPC serves as a

"drain" on DTAB monomers at the surface, reducing the surface excess coverage of all species and causing the surface tension to increase. However, VSFS data show that DPPC does spread across the surface of this solution – albeit slightly – meaning that the reduction of DTAB surface excess is accompanied by an increase in DPPC surface coverage.

5.3.2. Vibrational Spectra and Monolayer Organization

Surface pressure measurements contain substantial information about the thermodynamic states of monolayers, but the data provide no insight into the structure of the mixed films that form. To examine molecular structure and conformation within the monolayers themselves, we employ VSFS, a technique with inherent surface and molecular specificity.[50] Within the dipole approximation, VSFS experiments probe the vibrational structure of surface species without contributions from the underlying isotropic solution.

Figure 5.4 shows VSF spectra of the DPPC/SDS monolayers adsorbed to the air/aqueous interface. Included are spectra acquired with both hydrogen-containing and deuterated surfactants. Comparing the two otherwise equivalent systems enables one to distinguish between contributions to the observed vibrational structure from DPPC and from the surfactants. Spectra were acquired under $S_{sum}S_{vis}P_{ir}$ polarization conditions meaning that only those vibrational modes having a net out-of-plane projection of their IR transition moments contribute to the spectrum. Band assignments are based on previous reports from surface studies of DPPC.[66,137] Of particular importance are the two bands centered at ~2840 cm^{-1} and 2873 cm^{-1}. These

two features correspond to the acyl chain CH_2 symmetric stretch (d^+) and CH_3 symmetric stretch (r^+), respectively. The relative r^+ and d^+ band intensities are often used as a measure of chain order/disorder within monolayers.[7,11,12] A large r^+/d^+ ratio is associated with a well-organized monolayer structure due to all-trans hydrocarbon chains with methyl C_3 axes projected along the surface normal and the C_2 axes of methylene groups directed parallel to the surface. In contrast, a small ratio (and correspondingly large d^+ band) indicates a chain structure with gauche defect(s) and correspondingly poor organization within the monomers composing the monolayer.

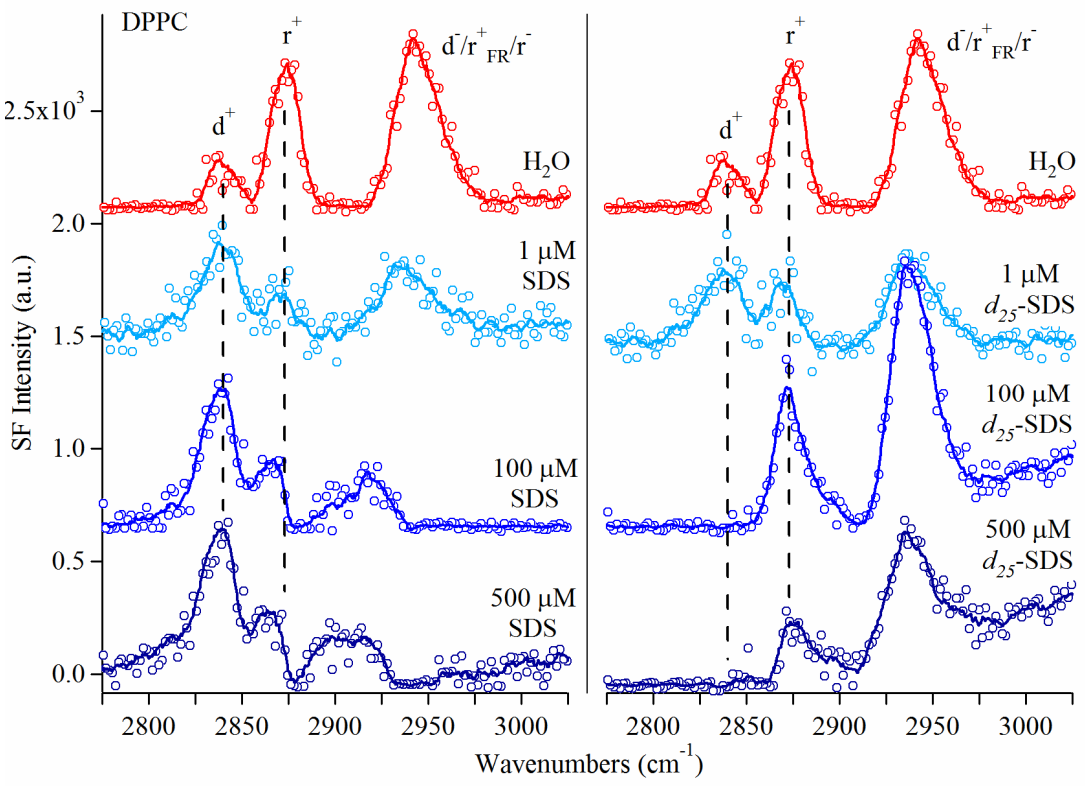

Figure 5.4. SFG spectra of DPPC on pure water and 1, 100 and 500 μM SDS solutions. The circles appear in every 3rd data point for clarification. The lines are obtained by box averaging of 5 consecutive data points. The spectra are offset vertically for clarity.

The DPPC monolayer on pure water appears well organized as evidenced by a large r^+/d^+ ratio. This result is consistent with the ESP measurement that shows the DPPC to be in a mostly liquid-condensed state. The VSF spectrum of DPPC in the presence of 1 μM SDS shows a much smaller r^+/d^+ ratio meaning that collectively DPPC and SDS monomers are more disorganized than DPPC by itself. The spectrum acquired from the 1 μM d_{25}-SDS solution appears qualitatively similar to that acquired from the solution having the hydrogen containing surfactant. Taken together, the ESP measurement coupled with the VSF spectra show that small amounts of SDS (1 μM bulk solution concentration) are capable of suppressing DPPC's ability to spread spontaneously at the aqueous/vapor interface and that the resulting mixed monolayer is largely disordered.

The cationic surfactant DTAB appears to be even more effective at inhibiting DPPC spreading given the VSF spectra shown in Figure 5.5. While the 1 μM concentration, mixed monolayer spectrum shows features in the –CH stretching region (with an r^+/d^+ ratio indicating considerable disorder), all of the intensity appears to come from DTAB monomers. Repeated experiments using d_{34}-DTAB show no measurable signal across the CH stretching region. The low concentration DTAB results further support conclusions drawn from surface pressure measurements. Namely, low concentrations of surfactants in solution are very effective at inhibiting DPPC spreading at the air/aqueous interface. Curiously, the DPPC and DTAB must enjoy some limited cooperativity in forming a film at the air/water interface. VSF spectra of just the surfactant solution show no measurable intensity in the CH region. (Data not shown.) Thus, while spectra from the

DPPC/d_{34}-DTAB system are consistent with data from the surface pressure measurements, the small, non zero intensity observed in the DPPC/DTAB VSF spectra imply a small amount of poorly organized surfactant at the aqueous/vapor interface.

VSFS spectra of 100 and 500 μM SDS solutions are shown in Figure 5.4. Considering DPPC's relatively large ESP (of 10.5 mN/m) on the 100 μM SDS solution, the VSF spectrum from this system shows surprisingly high levels of disorder. In contrast, the spectrum of DPPC on the solution of 100 μM d_{25}-SDS is distinguished by an absence of intensity in the d^+ region and a strong r^+ band. Based on simple r^+/d^+ considerations we might interpret the data in the following way: spectra from DPPC on surface of solutions having higher surfactant concentrations create disorganized monolayer films but the disorder can be attributed entirely to the soluble surfactant. When the soluble surfactant can no longer contribute to the observed vibrational spectrum (because of deuteration) the relative vibrational band intensities imply highly ordered alkyl chains. This picture would be consistent with islands of tightly packed DPPC monomers separated by regions of disordered soluble surfactants. Such structures have been observed in microscopy studies of DPPC films (without surfactants) across the liquid expanded/liquid condensed coexistence region.[138,139] VSF data from DPPC on 500 μM SDS solutions follow the trends established by the 100 μM SDS system as well as observations from the surface tension measurements. Absolute intensity differences between spectra acquired from solutions having different surfactant concentrations are less important qualitatively and should be evaluated as being with the uncertainties in the measurements.

Complicating this interpretation is the increasingly large signal from water on the high frequency side of spectra acquired with d_{25}-SDS. This contribution arises from anisotropic water oriented by the double layer formed when charged soluble surfactants adsorb to the water surface. The adsorbed surfactants create a sheet of charge and leading the counter ions to self assemble spontaneously some distance away from the surface. The resulting electric field forces water molecules to adopt a preferred alignment. The Debye-Hückel theory relates the thickness of double layer region (Debye length, $1/\kappa$) to the ionic strength of the solution through the expression

$$\frac{1}{\kappa} = \left(\frac{\varepsilon_r \varepsilon_0 RT}{4\pi F^2 \sum_i z_i^2 M_i} \right)^{1/2} \tag{5.2}$$

where ε_r and ε_0 are the relative dielectric constant of the solution and that of vacuum, respectively. *R, T, F, z* and *M* are the gas constant, the absolute temperature, the Faraday constant, and the charge and the molar concentration of each ion, respectively. By this expression, we can predict that for a 100 μM surfactant solution, the electrical double layer extends ~30 nm into a 1:1 surfactant solution and ~13 nm into a 500 μM surfactant solution.[45,140] These numbers are only approximate, however, given that we do not know whether the mixed DPPC/surfactant film is homogeneously or heterogeneously distributed across the interface. Large water signal from double layer formation implies that the monolayer has acquired a net charge. Such effects are not observed for neutral monolayers (such as alcohols or acids) nor do zwitterionic headgroups create an electrical double layer across the interface. Considering the fact that the electrical double layer results in preferential

alignments of water molecules at the interface, observed trends in VSF spectra of mixed monolayers formed by DPPC and soluble, charged surfactants likely include destructive and constructive interference interactions between the double layer's electrical field and individual vibrational bands of the lipid and surfactant. These effects will be discussed in more detail in Section 5.3.3.

These interferences at higher and lower frequency regions can affect the relative peak intensities in both the 100 and 500 μM SDS/DPPC spectra. The interference appears to have opposite phase depending on whether SDS is hydrogenated or deuterated. While the low frequency region of the spectrum for h_{25}-SDS containing solutions is enhanced by constructive interference, the features on the higher frequency side of the CH region are diminished by a destructive interference. These effects are reversed for the solutions containing d_{25}-SDS. A relatively flat region at lower frequencies and a large and increasing background signal at higher frequencies show the destructive and constructive effects, respectively. The asymmetric shapes of the r^+ band in the SDS spectra imply that this feature is influenced strongly by interference effects. The d^+ band will also be strongly affected by interference effects meaning that r^+/d^+ band comparisons may not be accurate measures of conformational order and organization within the mixed monolayers. Again, these issues and the possible origin of the interference effects are addressed in Section 5.3.3.

Spectra of the DPPC monolayers on the 100 μM solutions of DTAB and d_{34}-DTAB are shown in Figure 5.5. The spectra are qualitatively similar for both DTAB and d_{34}-DTAB solutions showing poor surface organization evidenced by very

large d^+ intensities. This behavior contrasts sharply with observations made for the higher concentration SDS solutions just described. Despite ambiguities resulting from surface pressure measurements about the composition of mixed films on DTAB solutions, VSF spectra show the coexistence of both molecules at the interface. Molecular organization within the mixed monolayer films seems similar for the 100 and 500 μM solutions, although the DPPC monomers may be slightly more ordered on the 500 μM d_{34}-DTAB solution than on the 100 μM d_{34}-DTAB solution. Here, we again note that these admittedly simple interpretations overlook the possibility that vibrational bands can interfere with each other either constructively or destructively.

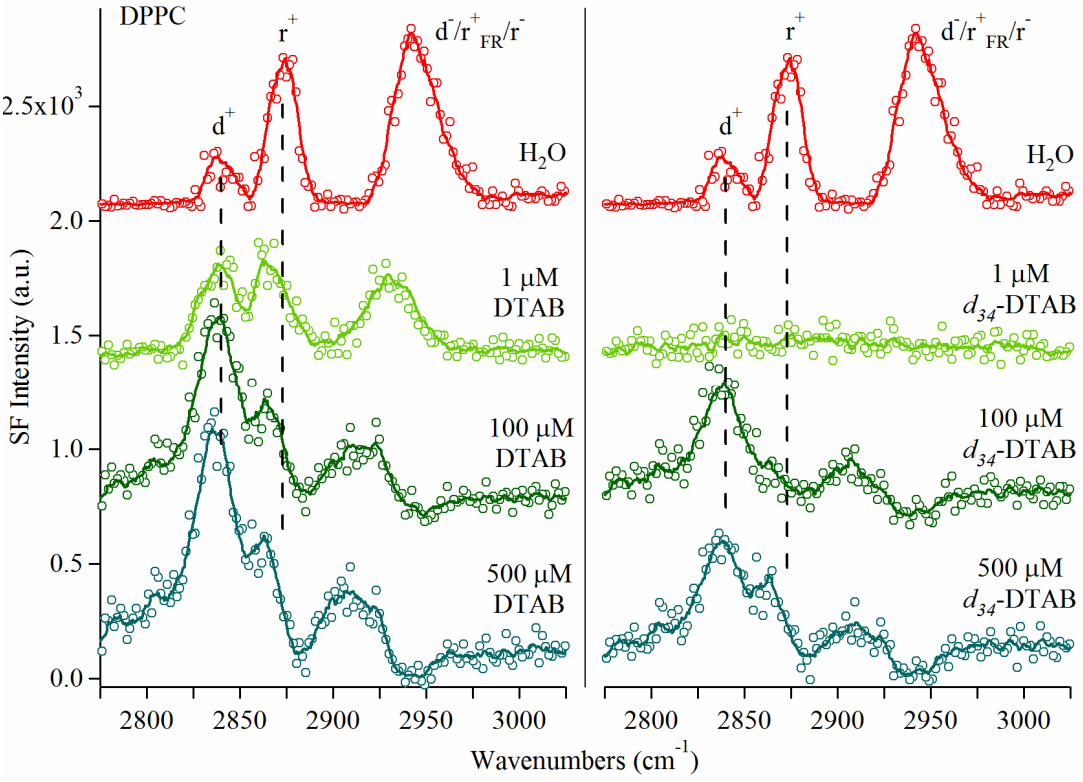

Figure 5.5. SFG spectra of DPPC on pure water and 1, 100 and 500 μM DTAB solutions. The circles appear in every 3rd data point for clarification. The lines are obtained by box averaging of 5 consecutive data points. The spectra are offset vertically for clarity.

To understand the differing effects of SDS and DTAB surfactants on DPPC monolayer formation, we begin by focusing on the Coulomb interactions that can occur between the zwitterionic phospholipid headgroup and the charged headgroups of the soluble surfactants. In particular, we consider first the results from solutions containing low surfactant concentrations. Previous studies showed that DPPC adopts an equilibrium structure at the air/water interface that points the alkyl chains along the surface normal and orients the zwitterionic headgroup mostly parallel to the surface with slight inclination into the water subphase.[19,139,141] This orientation of the phospholipid headgroup leaves the negatively charged phosphate group less accessible for direct interactions with other adsorbed species. In contrast, the positively charged quaternary ammonium group is much more exposed. With the help of these simple considerations, one predicts that the anionic surfactant, SDS, interacts easily with the phospholipid headgroup in such a way that the electrostatic attraction between the two oppositely charged sites helps promote surface organization by stabilizing lipid-surfactant interactions. However, the easy-to-access quaternary ammonium group interacts repulsively with the cationic DTAB surfactant molecule resulting in poor organization and more expanded structure in the mixed monolayer. These effects show up in the surface pressure isotherms that lift off at higher DPPC monomer areas on SDS containing solutions and effective equilibrium surface pressures ($\Pi_{surfctant}$) that are consistently higher on SDS solutions.

Note that these Coulomb interactions do not implicitly require any assumptions about the homo- or heterogeneity of the monolayer formed at the aqueous/vapor interface. When considering simple charged surfactants adsorbed to

the aqueous vapor interface, one generally assumes that the monolayer is homogeneous and that the surfactants do not aggregate due to repulsive coulomb interactions. Zwitterionic surfactants including phospholipids, however, can show complex 2-dimentional phase behavior with different thermo states coexisting at different surface pressures/coverages. Such coexistence raises the possibility that the monolayers probed in VSF experiments are heterogeneous and that the data reflect two distinctive contributions, one from well ordered DPPC monomers organized in islands and a second contribution from areas populated primarily with soluble surfactants. Mixed – or "patchwork" – interfacial film organization has very clear consequences for the properties of the aqueous/vapor interface and the resulting vibrational structure.

5.3.3. Interference Effects in VSF Spectra of Mixed Lipid-Surfactant Films

Complicating the simple interpretation of film organization based on r^+ and d^+ intensities presented above is the fact that VSF is a coherent process whereby each symmetry allowed vibrational transition can contribute to a VSF spectrum with both an amplitude and a phase. If two vibrations share spectral overlap and have the same phase, they can interfere constructively. If vibrations in the same spectral region differ in phase by π radians, then they interfere destructively. Such effects were discussed earlier in Chapter 2 and 3 in the context of interfering signals from methyl groups of branched alcohols. In the case of 2- and 3-position soluble alcohols, monomers adsorbed to aqueous/vapor interface adopted conformations where both

methyl groups were oriented in the same direction and thus shared the same phase. The result was intensity in the r^+ band that was larger than anticipated. In contrast, 2-C_{16}OH at its ESP was tightly packed with methyl groups in the C_1 and C_{16} positions oriented in opposite directions and leading to a phase difference of 180°. The resulting destructive interference diminished signal relative to what was expected based on surface coverage considerations. For both soluble and insoluble monomers, the frequency difference between the C_1 and C_n group r^+ bands is negligible meaning that the primary observed difference between the different phases of the two methyl groups is either a decrease or increase in measured r^+ intensity.

Features in VSF spectra of DPPC monolayers on surfactant solutions contain interference effects from a variety of sources. To understand these effects quantitatively would require extensive modeling and numerous assumptions about vibrational amplitudes, frequencies and phases. Such parameters are difficult to intuit simply based on the absence and presence of specific vibrational bands, or by making quantitative comparisons of band intensities. Thus, in this section we consider a systematic but qualitative approach to help identify trends that appear in mixed DPPC/surfactant monolayers, especially those formed on solutions having higher bulk surfactant concentrations.

As pointed out in Equation 5.1, the measured sum frequency response from a given system can contain nonresonant and resonant contributions. In many cases presented in Chapter 2 and Chapter 3 as well as DPPC monolayers on pure water, we neglected the nonresonant contribution to the observed signal. The assumption that $\chi^{(2)}_{NR} = 0$ was based on symmetric band shapes and a relatively flat baseline on the

high and low frequency sides of spectra. However, the spectra of DPPC monolayers on solutions containing charged surfactants often show strong asymmetry in –CH vibrational features and an inclined *background* usually on the high frequency side of the –CH stretching region. As noted in Section 5.2.2, this behavior represents a contribution from water molecules oriented by the electrical double layer at the interface. A number of studies have examined how this double layer affects the structure and VSF spectra of water, but few reports have considered explicitly how the electrical double layer will interfere with vibrations in the –CH stretching region.[130,142-149] In the next several pages, we explore several ways in which different elements of the second order susceptibility can affect vibrational band intensities in the spectra of mixed lipid-surfactant films adsorbed to the aqueous/vapor interface.

Since the widths of water stretching bands are much larger compared to the –CH stretching bands and the peak position of the water band is shifted several hundred cm^{-1} away from the –CH stretches, the effects of water oriented by the electrical double layer can be treated as a nonresonant contribution to the $\chi^{(2)}$ tensor. If we assume the presence of two vibrational bands, a and b, in addition to the nonresonant (water) signal, Equation 5.1 can be expressed as:

$$I_{sf} \propto \left|\chi^{(2)}_{NR} + \chi^{(2)}_{R_a} + \chi^{(2)}_{R_b}\right|^2 = \left|\chi^{(2)}_{NR} + \frac{A_a e^{i\phi_a}}{\omega_{ir} - \omega_a + i\Gamma_a} + \frac{A_b e^{i\phi_b}}{\omega_{ir} - \omega_b + i\Gamma_b}\right|^2 \qquad (5.3)$$

Here amplitude term of each vibration is expressed as a piece that depends explicitely on oscillator strength (A_{q_i}) and phase (ϕ_i). This expression is plotted below using representative parameters to obtain the estimated response functions plotted below. Due to the functional form of the water band, we approximate this contribution to the

susceptibility, $\left|\chi^{(2)}_{NR}\right|^2$, as a line with a slope m and an intercept b, $y = mx + b$. The parameters we used in this two state system are given in Table 5.2.

Table 5.2. Parameters used to fit the nonresonant response curves.

Number of data points		2000	
Equation for nonresonant term		$\left\|\chi^{(2)}_{NR}\right\|^2 = 1\text{x}10^{-4}\ \omega_{ir} - 0.2965$	
A_a	1	A_b	0.5
ω_a	3000 cm^{-1}	ω_b	2985 cm^{-1}
Γ_a	$2\sqrt{3}$ cm^{-1} *	Γ_b	$2\sqrt{3}$ cm^{-1} *

* FWHM = $\left|\Gamma^2\right| = 12$, measured amplitude at $\omega_i = \left|A_i\right|^2/\left|\Gamma_i\right|^2$

With this idealized model, we can begin to visualize the role played by interference effects in VSF spectral band shapes and band intensities. We consider two general cases: one where the nonresonant term of the nonlinear susceptibility does not contribute the spectrum leaving only the vibrational resonances themselves to interfere with each other and a second case where $\chi^{(2)}_{NR}$ makes nonzero contributions to the measured VSF spectrum. When $\chi^{(2)}_{NR} \neq 0$, this term will also have a well defined phase relative to the two vibrational resonances.

Case I: $\chi^{(2)}_{NR} = 0$ 1) $\phi_a = \phi_b$

2) $\phi_a = \phi_b + \pi$

In Case I, we assume that there is no nonresonant contribution to the observed intensity. This condition is relevant for uncharged monolayers as well as for DPPC

monolayers on pure water where the zwitterionic headgroup lies parallel to the water surface. A zero nonresonant contribution is also appropriate for solutions having low surfactant concentrations as evidenced by spectra from the 1 μM surfactant solutions shown in Figures 5.4 and 5.5.

Figure 5.6 shows the calculated intensities of a model VSF spectrum containing contributions from the two vibrational resonances described in Table 5.2. The top panel shows the two vibrational bands themselves. The bottom panel shows the resulting VSF spectra that result when these two vibrations have the same ($\phi_a = \phi_b$) and opposite phases ($\phi_a = \phi_b + \pi$). Also appearing on the panel is a simple sum of the two Lorentzian lineshapes to highlight the effects of constructive and destructive interference.

For both constructive and destructive interference conditions, the primary effects of interference on the VSF spectra involve intensity changes. Constructive interference leads to higher intensity than a simple sum of two vibrational bands and destructive interference reduces vibrational intensity of both bands. When two vibrations interfere destructively, one also observes a pronounced dip in intensity between the two bands. In the model above, this effect has a larger impact on the lower frequency, lower intensity band, b, as the ratio of intensities I_a/I_b increases from 1.5 for Case I.1 to 3.0 for Case I.2. (This same ratio for the simple sum of vibrations is 1.9.) More subtle consequences resulting from interferences include small changes in linewidth and apparent vibrational frequency. These effects, however, are typically less than 1 cm^{-1} and incapable of being resolved by our experimental assembly. Clearly, the impact of interference on VSF spectra under Case I conditions will

depend upon the characteristics of the vibrations themselves (A_i, Γ_i, ω_i). Nevertheless, this simple treatment allows us to conclude that in the absence of a contribution from $\chi^{(2)}_{NR}$, the intensities of different vibrational bands *relative to each other* lead to qualitatively similar interpretations regardless of the respective phases of the vibrational resonances.

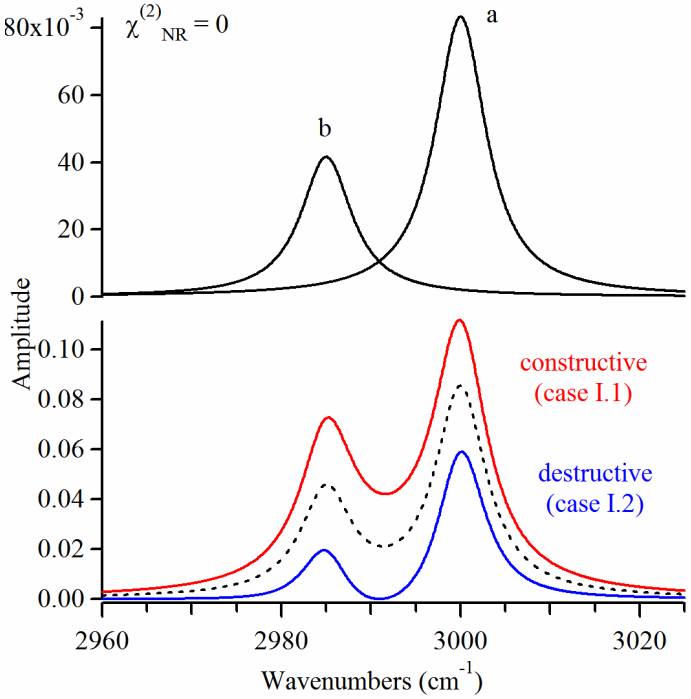

Figure 5.6. VSF spectra of imaginary vibrational bands, a and b, in the absence of any nonresonant contribution (Case I). The spectrum denoted by the dashed line in the lower panel represents a simple sum of vibrations a and b without allowing for any interference.

Case II: $\chi^{(2)}_{NR} \neq 0$ 1) $\phi_{NR} = \phi_a = \phi_b$

2) $\phi_{NR} = \phi_a + \pi = \phi_b + \pi$

3) $\phi_{NR} = \phi_a = \phi_b + \pi$

4) $\phi_{NR} = \phi_a + \pi = \phi_b$

Relative band intensities become more complicated to interpret in the presence of a nonresonant contribution to the spectral intensity (Case II). Here we consider the effects of $\chi^{(2)}_{NR}$ when all three terms (ϕ_{NR}, ϕ_a, ϕ_b) have the same phase (Case II.1), when the two vibrational resonances both have the opposite phase of $\chi^{(2)}_{NR}$ (Case II.2) and when one vibrational resonance is in phase with $\chi^{(2)}_{NR}$ and the other vibration has the opposite phase (Cases II.3 and II.4).

Figure 5.7 shows the effects of $\chi^{(2)}_{NR}$ on vibrational band intensities when the two vibrational resonances have the same phase (Cases II.1 and II.2) and are either in phase or 180˚ out of phase with $\chi^{(2)}_{NR}$. Spectra in the lower panel show that the primary effect of the interference is on the absolute band intensities. Relative intensities are not affected significantly. (I_a/I_b = 1.4 for Case II.1 and 1.9 for Case II.2.) This picture changes dramatically, however, when one vibration is in phase with $\chi^{(2)}_{NR}$ and the second resonance is 180˚ out of phase. (Figure 5.8) Under this condition, destructive interference virtually wipes out intensity from the out-of-phase vibration while modestly enhancing intensity of the in-phase vibration. Relative I_a/I_b intensity ratios vary between 130 (Case II.3) and 0.29 (Case II.4). Again, in the absence of any interference effects this ratio is 1.9 (Figure 5.6).

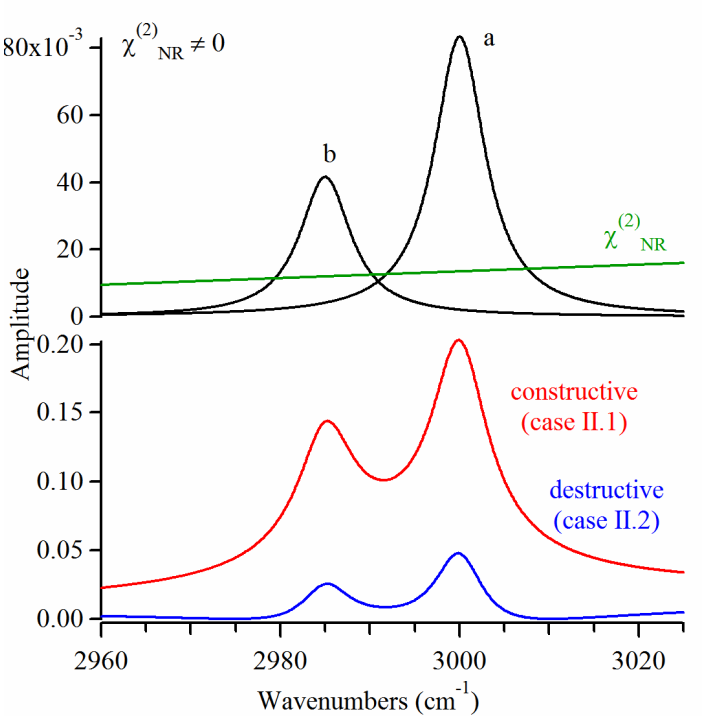

Figure 5.7. VSF spectra of imaginary vibrational bands, a and b, in the presence of a nonresonant contribution (Case II.1 and Case II.2).

Explicitly considering these situations allows us to revisit spectra from the mixed lipid-surfactant films with a goal of identifying whether specific systems can be categorized according to the cases defined above. Figure 5.9 presents side by side those spectra appearing in Figures 5.4 and 5.5.

Our analysis begins by noting that spectra from films of DPPC on pure water and dilute surfactant solutions show little evidence of interference from $\chi^{(2)}_{NR}$ meaning that all five spectra – four if the DPPC/1 μM d_{34}-DTAB system is excluded – fall into either the Case I.1 or Case I.2 limits. Of the three prominent features in each spectrum, d^+, r^+, and r^+_{FR}, only d^+ and r^+ are close enough in frequency to experience interference. The spectra do not show the characteristic "dip" between bands that indicates destructive interference. One might argue that the build-up of intensity

between the two features and the almost imperceptible shifts in frequency suggest limited constructive interference, but such claims test the limits of inherent experimental uncertainty. Thus, we conclude that this first collection of spectra show little evidence of interference of any type.

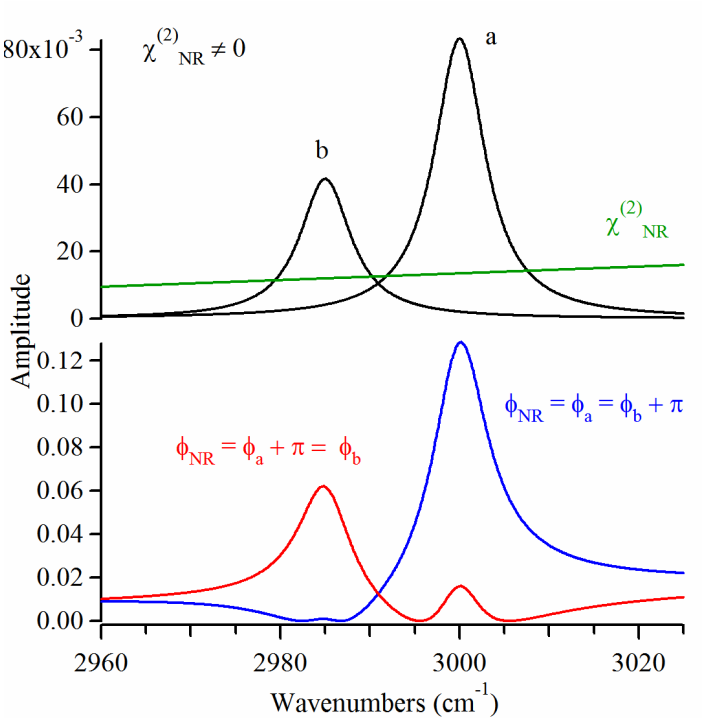

Figure 5.8. VSF spectra of imaginary vibrational bands, a and b, in the presence of a nonresonant contribution (Case II.3 and Case II.4).

The situation changes when the surfactant concentrations rise to 100 μM and 500 μM. Our analysis of these systems begins by noting that earlier studies by Gragson and Richmond demonstrated that solutions of SDS create electrical double layers that interfere constructively with r^+ (and r^+_{FR} at ~2945 cm^{-1}) whereas solutions of soluble cationic surfactants create electrical double layers at the aqueous/vapor interface that interfere destructively with r^+ and r^+_{FR}. Vibrational resonances that

show the most dramatic changes as a function of surfactant concentration are r^{+}_{FR}, and d^{+}.

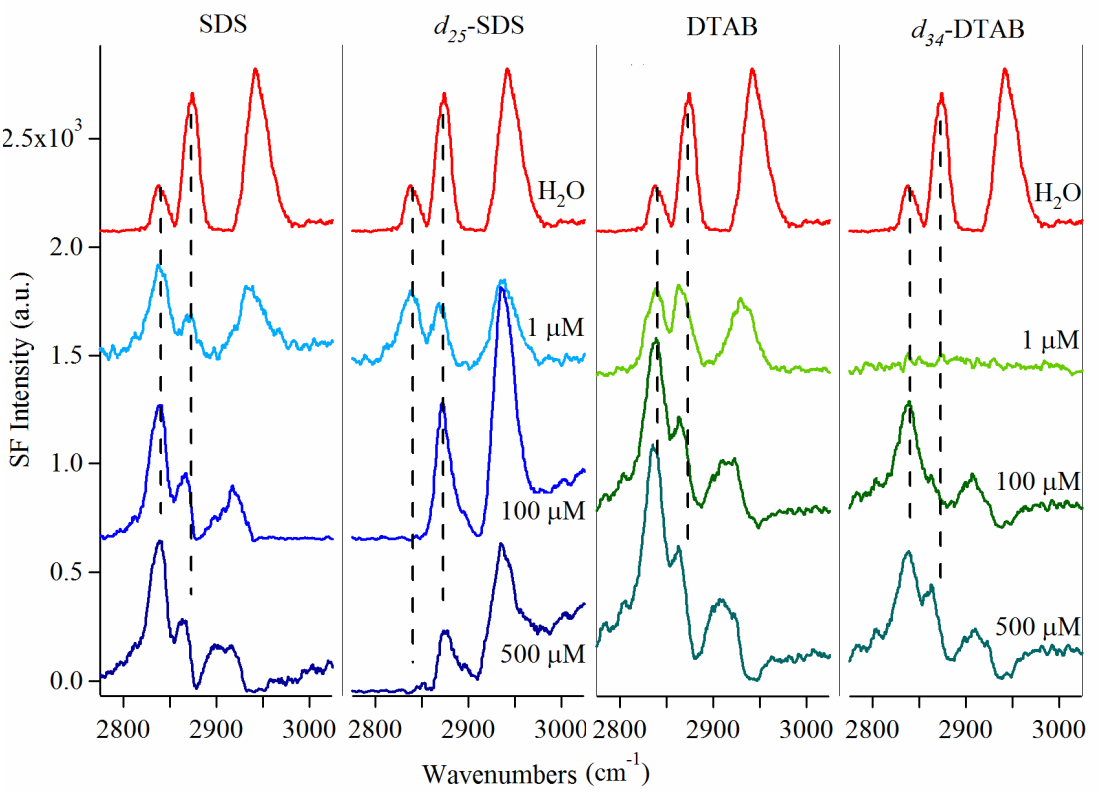

Figure 5.9. VSF spectra of DPPC on pure water and 1, 100 and 500 μM SDS and DTAB solutions. Presented spectra were obtained by box averaging 5 consecutive data points. Spectra of pure water and 1 and 100 μM subphases are vertically offset for clarity. Dashed lines correspond to positions of d^{+} (2840 cm^{-1}) and r^{+} (2873 cm^{-1}) bands.

Inspection of the spectra in Figure 5.9 shows that spectra from DPPC on 100 and 500 μM SDS solutions show the most pronounced effects of interference between $\chi^{(2)}_{NR}$ and –CH vibrational resonances. When both lipid and surfactant are hydrogenated, spectra show signs of destructive interference between r^{+}_{FR} and the nonresonant contribution of water coupled with constructive between d^{+} and $\chi^{(2)}_{NR}$.

Substituting d_{25}-SDS for h_{25}-SDS causes the interference to change sign with d^+ virtually disappearing from the spectrum and r^+_{FR} showing appreciable amplitude on top of the rising baseline due to water aligned by the electrical double layer. Using the notation developed above with d^+ corresponding to vibration b and either r^+ or r^+_{FR} corresponding to vibration a, the DPPC/h_{25}-SDS system appears to resemble Case II.4 (d^+ in phase with $\chi^{(2)}_{NR}$) while the DPPC/d_{25}-SDS system bears closer resemblance to Case II.3 (r^+ and r^+_{FR} in phase with $\chi^{(2)}_{NR}$).

Ironically, with constructive interference between r^+ and $\chi^{(2)}_{NR}$, the spectra from the d_{25}-SDS solutions more closely resemble those reported by Gragson and Richmond (for h_{25}-SDS on H_2O) than do spectra from the DPPC/h_{25}-SDS systems. Our data from the DPPC/h_{25}-SDS films have more similarities with spectra acquired from charged monolayers having a net *positive* charge. Thus, the difference between our data and studies of monolayers formed by simple charged surfactants must be related to the presence of DPPC monomers at the interface. The opposite effects observed between the two sets of data show that the adsorption of DPPC and presence of an anionic surfactant create a preferential water alignment, but h_{25}-SDS and d_{25}-SDS contribute to this equilibrium in opposite ways. In principle, one explanation for this trend might be related to a change in phase of $\chi^{(2)}_{NR}$. Such an effect would be equivalent to switching the orientation of the electrical double layer by 180°. Given the species that can create the mixed film – DPPC and SDS – this explanation seems unlikely. If $\chi^{(2)}_{NR}$ does not change sign, then the phases of the vibrations themselves must change sign. In the DPPC/h_{25}-SDS system, contributions to the –CH vibrational bands can come from both the lipid and the surfactant. When the surfactant is

deuterated, however, the phases of d^+, r^+ and r^+_{FR} are determined solely by the lipid. Consequently we assign all of the vibrational intensity in the DPPC/d_{25}-SDS spectra to DPPC noting the similarities between these data and those spectra resulting from simple SDS monolayers adsorbed to the aqueous/vapor interface. Furthermore, if the sign of r^+ and r^+_{FR} changes in moving from DPPC/h_{25}-SDS to DPPC/d_{25}-SDS, we conclude that the methyl groups of the SDS are in opposite phase with $\chi^{(2)}_{NR}$ and DPPC methyl groups. Such a structure clearly requires that the orientation of methyl groups from DPPC and SDS monomers are in opposite directions.

Spectra from the DPPC/DTAB are quite similar for both 100 and 500 μM concentrations. The strong d^+, weak r^+_{FR} and dip in intensity at 2950 cm^{-1} point to Case II.4 conditions. Unlike observations made with SDS, deuterating the cationic DTAB surfactant has very little effect on the resulting vibrational spectrum. Therefore, using reasoning similar to that applied to the SDS systems, the spectral features predicts a picture with water molecules having alignment where $\chi^{(2)}_{NR}$ has the opposite phase of the DPPC methyl groups. The $-CH_2$ and $-CH_3$ groups of h_{34}-DTAB do not qualitatively alter the relative phases observed for d^+ and r^+ compared to the d_{34}-DTAB/DPPC system. We therefore conclude that the alkyl groups of DTAB monomers adsorbed to the interface must have the opposite alignment as the corresponding functional groups of the DPPC monomers leading to Case II.4 rather than Case II.2 conditions.

In conclusion, both the anionic and cationic surfactants have opposite contributions with DPPC monomers into the VSF spectra. Because of the opposite sign of $\chi^{(2)}_{NR}$ electrical double layer created by oppositely charged surfactants,

interfacial water molecules are preferentially aligned in opposite directions. While the direction of water transition dipoles is in the same way as the DPPC monomers in SDS case, it is opposite to the DPPC methyl transition dipoles in DTAB case.

5.4. Conclusion

In conclusion, non-specific Coulomb interactions are responsible for surfactants inhibiting monolayer formation by DPPC at low concentrations. Distinctly opposite trends for both surfactants suggest that different domains probed simultaneously are responsible for the vibrational spectra measured at the aqueous/vapor interface. At higher concentrations, anionic and cationic surfactants have opposite effects on the DPPC monolayers. Interference contributions of water subphase to the spectra of monolayers at higher surfactant concentrations makes the study challenging from many points of view and requires careful analysis of observed effects.

Chapter 6: Conclusion

6.1. Projects and Achievements

For almost ten years, the Walker Research Group has studied how properties change across liquid surfaces. Previous work used second harmonic generation – a surface specific method for measuring a solute's electronic structure – to measure polarity at solid/liquid, liquid/liquid and liquid/vapor interfaces. The widths of different interfaces have been characterized by measuring SHG spectra of "molecular rulers", surface active organic molecules having varying chain lengths.[150-152] These experiments provided information about *how* properties changed at interfaces, but data could not be used to explain *why* properties changed the way they did. To understand why properties at interfaces are different, experiments need to probe the structure of the interfacial solvent itself. In this thesis research we began to answer these questions by investigating the structure and organization of molecules within organic monolayers at aqueous interfaces. Specifically, the first phase of our studies used alcohol monolayers to understand how chain length and chain structure affects the structure and organization of molecules adsorbed to the aqueous/vapor interface. Later, computer simulations of alcohol monolayers were employed to complement the experimental studies. In the last part of this work, we expanded the complexity of the systems studied to explore the structure of phospholipid monolayers at the air/water interface in the presence of charged, soluble surfactants.

In the first part of the study, the structure and organization of monolayers formed by hexadecanol isomers at the air/water interface were investigated. Experiments included surface tension measurements and VSFS. Comparing the sum frequency intensities of methyl symmetric stretch bands relative to molecular areas of isomers allowed us to infer equilibrium structures of each isomer. Data showed that the monolayers of 1- and 2-hexadecanol isomers pack together closely with all-*trans* conformations and have average molecular orientations along the surface normal. For 2-C_{16}OH monolayer, the intermolecular van der Waals interactions are strong enough to keep the chains in straight, all-*trans* conformations and the C_1 methyl group solvated within the water subphase. More asymmetric isomers, 3- and 4-C_{16}OH, cover significantly larger areas at their equilibrium spreading pressures where hydrophobic interactions of shorter alkyl segments with the water subphase play a large role in controlling monomer conformation and organization within the monolayer. Surface tension data and vibrational band intensities suggest that 3-C_{16}OH with a single gauche defect is the primary conformer in monolayers of this isomer at its ESP. On the other hand, for 4-C_{16}OH, a distribution of conformer structures is possible as the equilibrium conformation.

In Chapter 3 the structure and organization of soluble alcohols at the air/water interface were studied. Evaluation of the experimental results showed that linear alcohols form tightly packed monolayers with all-trans conformations aligned with the surface normal. However, unlike the 2-C_{16}OH monolayer, soluble 2-C_nOH monolayers did not pack efficiently and adopted gauche defects. For these monolayers, the cohesive chain-chain interactions were not strong enough to offset

the hydrophobic penalty of solvating the C_1 methyl group within the water phase. A conformation with two gauche defects directing both methyl groups away from the surface was proposed as the primary structure at the interface. 3-C_nOH monolayers were also found to adopt a two gauche defect conformation and formed monolayers with molecular areas twice as great as linear isomers. Surprising data were observed for monolayers formed from 5-C_nOH isomers ($n \geq 9$). Despite forming relatively expanded monolayers (having surface coverages equal to or less than those of 2- or 3-position isomers), vibrational spectra suggested that these monolayers were very well ordered with the alkyl segments having few gauche defects and both methyl groups of each monomer projected in the same direction along the surface normal.

Molecular dynamics simulations of soluble alcohol monolayers are helping to identify the microscopic causes responsible for the equilibrium conformer structures. Computational results allow us to isolate the individual, competing forces such as van der Waals attractions between long alkyl segments, hydrogen bonding with the subphase and hydrophobic repulsions between the short alkyl segments and the adjacent water. These studies are ongoing, but show great promise for developing models that allow us to predict *a priori* how amphiphiles having different shapes will organize spontaneously at different interfaces.

The final studies of this thesis research explored structure and organization in phospholipid monolayers to examine different the effects of soluble surfactants on the ability of lipids to self assemble at the aqueous/vapor interface. Dipalmitoyl phosphatidylcholine (DPPC) spontaneously forms ordered monolayer films on pure water/air interface. However, low concentrations of charged soluble surfactants, SDS

and DTAB, inhibit the spreading of DPPC at the interface. We believe that non-specific Coulomb interactions are responsible for surfactants inhibiting monolayer formation by DPPC. Also, DPPC appears to enhance the adsorbtion of surfactants onto the water surface. At higher surfactant concentrations, SDS and DTAB have opposite effects on the surface structure of DPPC. Use of deuterated surfactants showed that while SDS appears to enhance the organization of DPPC, DTAB introduces considerable disorder into the DPPC monolayers at the interface. Distinctly opposite trends for both surfactants suggest that different domains probed simultaneously are responsible for the vibrational spectra measured at the aqueous/vapor interface. Lipid-surfactant interactions are difficult to intuit but necessary to quantify if one is to understand structure and organization in biological films in the presence of charged surfactants. Interference contributions of water subphase to the spectra of monolayers at higher surfactant concentrations makes the study challenging from many points of view and requires careful analysis of observed effects.

6.2. Prominent Studies and Future Prospects

Results presented in Chapters 2 and 3 have appeared in the literature.[68,132] Data presented in Chapter 5 will also soon be submitted for publication. The molecular dynamics simulations have begun to yield valuable insight into the behavior of monolayer films and will allow us to use (calculated) quantitative data to understand why different amphiphilic isomers adopt specific conformations at aqueous interface.

Future studies will build upon the discoveries made during this thesis research. Our analyses of structure and organization within alcohol monolayers were based on terminal monolayer coverages and corresponding VSF spectra. Specifically, quantifying contributions from methyl symmetric stretch intensities played a key point in inferring the probable conformer structures that alcohol monolayers are likely to adopt. Data from MD simulations provide predictions about how monolayer structure evolves as a function of surface coverage and these predictions can now be tested. Predictions both from our experimental studies as well as simulation results can also be further tested by beginning to selectively deuterate individual functional groups (such as the C_1 **or** the C_n methyl groups). Finally, all of our interpretations are based on spectra and isotherms acquired from systems at equilibrium. These data contain no direct information about dynamics at the interface. Newly developed methods and planned studies will soon begin to examine motion within these films specifically looking for changes in dynamics that accompany 2-dimensional phase changes.

Studies on phospholipid monolayers included acquiring surface pressure isotherms and VSF spectra at ESP. The interpretations about spectra of mixed monolayer systems are limited to SSP polarized spectra. Acquiring the spectra under SPS polarization conditions may provide additional information about the orientation and order of monomers adsorbed to the interface. The VSF spectra were collected in the –CH stretching region for monolayer systems described in Chapter 5. For the systems including mixed monolayers of phospholipids and deuterated charged surfactants, VSF spectra at CD stretch region may provide complimentary data for the

current VSF spectra at CH region. These studies were postponed due to some technical difficulties, and are queued up for future studies.

Studies on phospholipid monolayers presented this dissertation focused specifically on DPPC monolayers. The experiments were performed for systems equilibrated under room temperature conditions which may be important and critical for spreading of phospholipid monomers at the interface. Temperature controlled experiments may be helpful for controlled spreading and the resulting monolayer structure especially in systems having mixed composition. For this purpose, use of phospholipids with varying chain length and different gel-liquid transition temperatures may also expand the studies to be more comprehensive and more representative of biologically relevant systems. Also, the interactions between the charged surfactants and the phospholipids were mostly controlled by electrostatic forces between the headgroups of both molecules. Therefore, these interactions and the resulting effects can be investigated using phospholipids with headgroups varying in size and charge. For example, the headgroup of dipalmitoyl phosphatidylethanolamine (DPPE) has the same charge structure as DPPC but a smaller cationic part. Consequently, the interaction between this phospholipid and SDS and DTAB may result in a different monolayer structure.

Appendices

Appendix A: VSF Spectra of 2-Octanol Enantiomers

The VSF spectra of monolayers formed by the 2-C_8OH racemic mixture and two enantiomers, (R)-(-)-2-C_8OH and (S)-(+)-2-C_8OH at aqueous/vapor interface are shown in Figure A.1. Racemic mixture was prepared by mixing the two enantiomer reagents in 1:1 volume ratio. The spectra, acquired at terminal monolayer coverage, are almost identical in positions and intensities of spectral features.

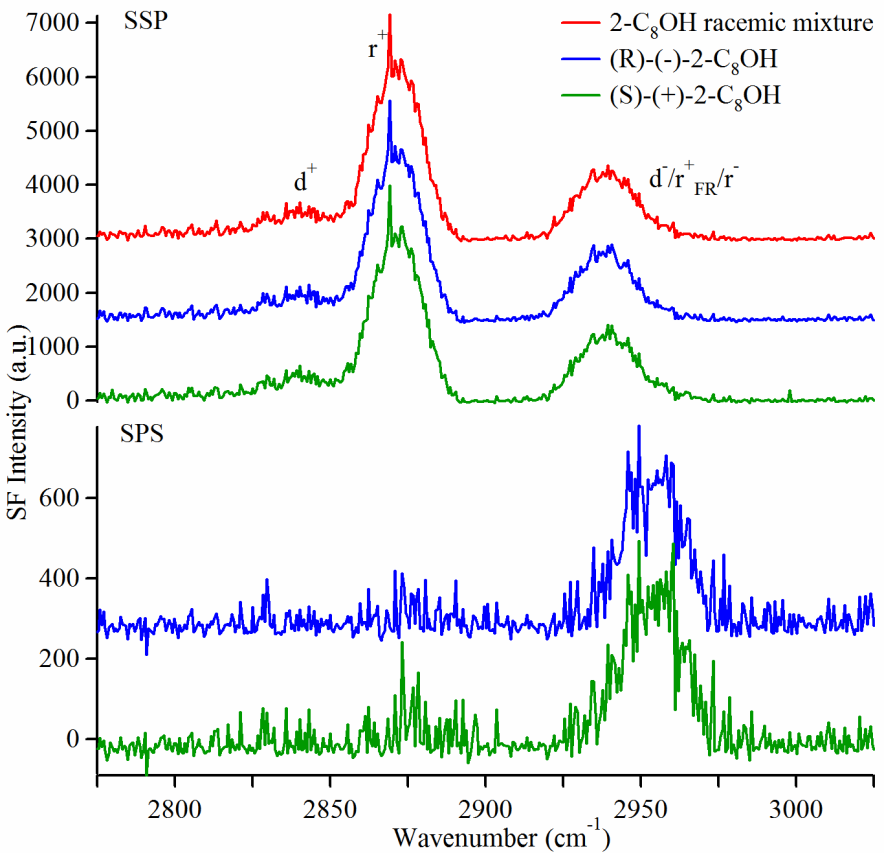

Figure A.1. VSF spectra of the monolayers formed by different 2-C_8OH enantiomers under SSP (top) and SPS (bottom) polarization conditions.

One question may arise from the fact that whether the tetrahedral geometry of the -OH carbon atom makes a difference in terms of surface organization. Our analysis of the data shown above indicates that the two 2-C_8OH enantiomers show organization that is indistinguishable to within the limits of experimental resolution.

Appendix B: Input and setup file formats used in MD simulations

MD simulation studies have been performed using the program code provided by Professor Ilan Benjamin. The file locations and the directory structure are as follows:

MD simulation directory
- *run* (MD code)
- *con_...* (configuration file)
- *setup.equ_...* (equilibration run setup file)
- *setup.run_...* (production run setup file)
- inpfiles
  - ....*asc* (created input file in ASCII format)
  - ....*min* (created input file that will be used in equilibration step)
  - ....*equ* (equilibrated input file that will be used in production step)
- data
  - ....*inf* (trajectory file having information about the trajectory)
  - ....*rsp* (input file printed for the last configuration in trajectory)
  - ....*xtr* (output file of a trajectory)

The data structures of some files (input, setup and configuration) are listed below with 1-decanol simulation as example. The parameters used or changed from one case to other are shaded and explained in each section.

1. Configuration File

File name: con_dec188

```
88 1 12 0                                   NCH, NCA
1.53 520.0 1.43 640.0 0.945 1106.0          R_CC, k_CC, R_CO, k_CO,
                                            R_OH, k_OH
112.0 126.0 108.0 100.0 108.5 110.0         t_CCC, k_CCC, t_CCO,
                                            k_CCO, t_COH, k_COH
0.7055      -0.1355     1.50725             Vt1, Vt2, Vt3
0.5         -0.1        1.0                 Vt1, Vt2, Vt3
0.417       -0.058      0.3735              Vt1, Vt2, Vt3
3.86  0.1811                                sigC[0],  epsC[0]
3.98  0.1142                                sigC[1],  epsC[1]
3.98  0.1142      0.285                     sigC[2],  epsC[2],  qC[2]
3.08  0.1748      -0.685                    sigC[3],  epsC[3],  qC[3]
2.0   0.1   0.4                           sigC[4],  epsC[4],  qC[4]
4.0   0.1   0.5                           sig14, eps14, factor14
```

88: 88 molecules are placed in simulation box.

1: OH group is attached to the first carbon atom.

12: There are 12 units to be tracked throughout the simulation: 10 unified carbon atoms, an oxygen and a hydrogen.

0: All potentials are set to normal. For the first equilibration step, the value is set to 1 in order to activate the repulsive interactions and turn off the torsional potentials.

2. Setup File for Equilibration Run

File Name: setup.equ_dec188

```
 .EQU.
1 1                     numIn       numTraj
188 188                 inVers      outVers
inpfiles/dec            inRoot
inpfiles/dec            outRoot
300                     kelvin
20 500                  numRand     numStep
0 1 1 0                 fixTQ prStatQ vScaleQ offsetQ
1.0                     ts
con_dec188              confile
no_constrain            constraints file
CUB
.ENDEQU.
```

188: OH position (1 for linear alcohols) and number of molecules (88 for full monolayer coverage) included in simulation.

dec: Prefix for the carbon chain length (dec: decanol). The input file will be read from subdirectory "inpfiles" and the equilibrated file will be written to the same directory.

300: Temperature in Kelvins that equilibration will be run.

20: Number of randomizations. (100 randomizations were performed for the branched alcohols)

500: Number of steps in each randomization. (500 randomizations are typical for the simulations presented in this study)

con_dec188: Name of the configuration file from which physical parameter will be read. The file should in the same directory as setup.equ file.

3. Setup File for Production Run

File Name: setup.run_dec188

```
.RUN.
1 20 0                  numIn   numTraj
188 000                 inVers  outVers
inpfiles/dec            inRoot
data/dec188             outRoot
300                     kelvin
1000 25                 numTs   dataRate
1.0                     ts
1 0 1 1                 rcmQ    fixTQ   prStatQ vScaleQ
0 0 0 0 10              datQ    posQ    velQ    frcQ    xtrQ
con_dec188              confile
no_constrain
CUB
.ENDRUN.
```

20: Number of trajectories printed

0: Normal potentials defined in configuration file will be used.

188: OH position (1 for linear alcohols) and number of molecules (88 for full monolayer coverage) that will be added to the data file name. (e.g. dec188 for 1-decanol will 88 molecules)

000: The trajectories will be named systematically starting from 0.

inpfiles/dec: Directory and prefix of the equilibrated input file that will be used in production run.

data/dec188: Directory and prefix for the trajectory files that will be created during the production run.

300: Temperature in Kelvins that production run will be performed.

con_dec188: Name of the configuration file from which physical parameter will be read. The file should in the same directory as setup.run file.

4. Input and Equilibrated File

File Name: dec188.asc (.equ and .rsp files have the same structure when converted to ASCII format)

```
Input File --     1
Filetype  --      .inp
Datestamp --      Mon Feb 19 00:40:14 2007
Status --   EQU
Number of atoms (natoms) --   3960
Number of solute atoms (nsolute) --       0
X box size (xwall) --   21.500000
Y box size (ywall) --   21.500000
Z box size (zwall) --   75.000000
Equilibration Temperature (EqTemp) --     300.000000
St. Dev. of Equil. Temp. (DEqTemp) --     0.000000
Equilibration Pressure (EqTemp) --  0.000000
St. Dev. of Equil. Press. (DEqPress) --   0.000000
Extra file flag (xtrInQ) --   0
  # type x position y position z position flags parent param1 param2
   0   0     4.58669     -9.48109    -0.43979   0026     0    2    3
   1   1     5.16122     -9.16020     0.35443   0004     0    0    0
   2   1     3.99441    -10.23946    -0.08725   0004     0    0    0
   3   0     8.80367      5.88716   -11.93580   0026     3    2    3
   4   1     9.48758      5.18996   -11.65940   0004     3    0    0
   5   1     8.29003      5.49029   -12.72113   0004     3    0    0
……
2904  86   -19.93756    -16.82663     4.10506   0026  2904   11   10
2905  20   -20.87077    -17.51156     5.11759   0024  2904    0    0
2906  20   -21.18395    -16.69556     6.43873   0024  2904    0    0
2907  20   -21.63713    -17.64322     7.55015   0024  2904    0    0
2908  20   -21.89539    -16.78727     8.80971   0024  2904    0    0
2909  20   -22.18481    -17.61168    10.16137   0024  2904    0    0
2910  20   -22.61312    -16.93659    11.47426   0024  2904    0    0
2911  20   -22.24946    -17.82056    12.60044   0024  2904    0    0
2912  20   -22.37735    -17.14242    14.00174   0024  2904    0    0
2913  10   -22.25306    -18.18042    15.17965   0024  2904    0    0
2914  46   -19.66885    -17.82652     3.13885   0024  2914    0    2
2915   7   -18.81302    -17.61226     2.78940   0004  2914    0    0
……
```

type: Type of the atom in simulation box that a specific potential parameter is assigned during the simulation.

0: Oxygen of water.

1: Hydrogen of water.

86: Methyl group at C_1 position.

20: Methylene groups.

10: Methyl group at C_n position.

46: Oxygen of alcohol.

7: Hydrogen of alcohol OH group.

x position, y position and z position: x, y and z coordinates of a specific atom in simulation box.

References

(1) Donaldson, D. J.; Vaida, V. *Chem. Rev.* **2006**, *106*, 1445.

(2) Gaines, G. L., JR. *Insoluble Monolayers at Liquid-Gas Interfaces*; Interscience Publishers: New York, 1966; Vol. 1.

(3) Bain, C. D. *J. Chem. Soc. Faraday T.* **1995**, *91*, 1281.

(4) Eisenthal, K. B. *Chem. Rev.* **1996**, *96*, 1343.

(5) Miranda, P. B.; Shen, Y. R. *J. Phys. Chem. B* **1999**, *103*, 3292.

(6) Richmond, G. L. *Annu. Rev. Phys. Chem.* **2001**, *52*, 357.

(7) Shultz, M. J.; Schnitzer, C.; Simonelli, D.; Baldelli, S. *Int. Rev. Phys. Chem.* **2000**, *19*, 123.

(8) Watry, M. R.; Brown, M. G.; Richmond, G. L. *Appl. Spectrosc.* **2001**, *55*, 321a.

(9) Ma, G.; Allen, H. C. *Langmuir* **2006**, *22*, 5341.

(10) Richter, L. J.; Petralli-Mallow, T. P.; Stephenson, J. C. *Opt. Lett.* **1998**, *23*, 1594.

(11) Esenturk, O.; Walker, R. A. *J. Phys. Chem. B* **2004**, *108*, 10631.

(12) Esenturk, O.; Walker, R. A. *J. Chem. Phys.* **2006**, *125*, 174701.

(13) Esenturk, O. Ph. D. Thesis, University of Maryland - College Park, 2004.

(14) Chanda, J.; Bandyopadhyay, S. *J. Chem. Theory Comput.* **2005**, *1*, 963.

(15) Dominguez, H.; Berkowitz, M. L. *J. Phys. Chem. B* **2000**, *104*, 5302.

(16) Rodriguez, J.; Clavero, E.; Laria, D. *J. Phys. Chem. B* **2005**, *109*, 24427.

(17) Schweighofer, K. J.; Essmann, U.; Berkowitz, M. *J. Phys. Chem. B* **1997**, *101*, 3793.

(18) Smondyrev, A. M.; Berkowitz, M. L. *J. Chem. Phys.* **1999**, *111*, 9864.

(19) Smondyrev, A. M.; Berkowitz, M. L. *J. Comput. Chem.* **1999**, *20*, 531.

(20) Takaoka, Y.; Miyagawa, H.; Kitamura, K. *Fluid Phase Equilib.* **1998**, *144*, 387.

(21) Dzikovskii, B. G.; Livshits, V. A. *Russ Chem B+* **1998**, *47*, 402.

(22) Kothekar, V. *Indian J. Biochem. Biophys.* **1996**, *33*, 431.

(23) Huang, P.; Perez, J. J.; Loew, G. H. *J. Biomol. Struct. Dyn.* **1994**, *11*, 927.

(24) Egberts, E.; Marrink, S. J.; Berendsen, H. J. C. *Eur Biophys J Biophy* **1994**, *22*, 423.

(25) Thompson, T. R.; Goldstein, D. A. *Biophys. J.* **1979**, *25*, A178.

(26) Dominguez, H.; Smondyrev, A. M.; Berkowitz, M. L. *J. Phys. Chem. B* **1999**, *103*, 9582.

(27) Raymond, E. A.; Tarbuck, T. L.; Brown, M. G.; Richmond, G. L. *J. Phys. Chem. B* **2003**, *107*, 546.

(28) Walker, D. S.; Moore, F. G.; Richmond, G. L. *J. Phys. Chem. C* **2007**, *111*, 6103.

(29) Walker, D. S.; Richmond, G. L. *J. Am. Chem. Soc.* **2007**, *129*, 9446.

(30) Walker, D. S.; Richmond, G. L. *J. Phys. Chem. C* **2007**, *111*, 8321.

(31) Michael, D.; Benjamin, I. *J. Chem. Phys.* **2001**, *114*, 2817.

(32) Squitieri, E.; Benjamin, I. *J. Phys. Chem. B* **2001**, *105*, 6412.

(33) Gopalakrishnan, S.; Jungwirth, P.; Tobias, D. J.; Allen, H. C. *J. Phys. Chem. B* **2005**, *109*, 8861.

(34) Gopalakrishnan, S.; Liu, D. F.; Allen, H. C.; Kuo, M.; Shultz, M. J. *Chem. Rev.* **2006**, *106*, 1155.

(35) Burkert, U.; Allinger, N. L. *Molecular mechanics*; American Chemical Society: Washington, D.C., 1982.

(36) Leach, A. R. *Molecular modelling : principles and applications*, 2nd ed.; Prentice Hall: Harlow, England ; New York, 2001.

(37) Besse, P.; Sokoltchik, T.; Veschambre, H. *Tetrahedron-Asymmetry* **1998**, *9*, 4441.

(38) Cammaerts, M. C.; Attygalle, A. B.; Evershed, R. P.; Morgan, E. D. *Physiological Entomology* **1985**, *10*, 33.

(39) Campbell, C.; Brink, G.; Glasser, L. *J. Phys. Chem.* **1976**, *80*, 686.

(40) Cho, B. T.; Kim, D. J. *Tetrahedron* **2003**, *59*, 2457.

(41) Kamezawa, M.; Raku, T.; Tachibana, H.; Ohtani, T.; Naoshima, Y. *Biosci., Biotechnol., Biochem.* **1994**, *58*, 598.

(42) Zada, A.; Ben-Yehuda, S.; Dunkelblum, E.; Harel, M.; Assael, F.; Mendel, Z. *J. Chem. Ecol.* **2004**, *30*, 631.

(43) Langmuir, I. *J. Am. Chem. Soc.* **1917**, *39*, 1848.

(44) Gaines, G. L. *Insoluble monolayers at liquid-gas interfaces*; Interscience Publishers: New York,, 1966.

(45) Hiemenz, P. C.; Rajagopalan, R. *Principles of colloid and surface chemistry*, 3rd ed.; Marcel Dekker: New York, 1997.

(46) Israelachvili, J. N. *Intermolecular and surface forces*, 2nd ed.; Academic Press: London ; San Diego, 1991.

(47) Penfold, J.; Richardson, R. M.; Zarbakhsh, A.; Webster, J. R. P.; Bucknall, D. G.; Rennie, A. R.; Jones, R. A. L.; Cosgrove, T.; Thomas, R. K.; Higgins, J. S.; Fletcher, P. D. I.; Dickinson, E.; Roser, S. J.; McLure, I. A.; Hillman, A. R.; Richards, R. W.; Staples, E. J.; Burgess, A. N.; Simister, E. A.; White, J. W. *J. Chem. Soc. Faraday T.* **1997**, *93*, 3899.

(48) Thoma, M.; Schwendler, M.; Baltes, H.; Helm, C. A.; Pfohl, T.; Riegler, H.; Mohwald, H. *Langmuir* **1996**, *12*, 1722.

(49) Alsnielsen, J.; Jacquemain, D.; Kjaer, K.; Leveiller, F.; Lahav, M.; Leiserowitz, L. *Phys. Rep.* **1994**, *246*, 252.

(50) Richmond, G. L. *Chem. Rev.* **2002**, *102*, 2693.

(51) Wolfrum, K.; Laubereau, A. *Chem. Phys. Lett.* **1994**, *228*, 83.

(52) Dluhy, R. A. *Appl. Spectrosc. Rev.* **2000**, *35*, 315.

(53) Widayati, S.; Stephens, S. M.; Dluhy, R. A. *Mikrochim. Acta* **1997**, 679.

(54) Perry, A.; Neipert, C.; Kasprzyk, C. R.; Green, T.; Space, B.; Moore, P. B. *J. Chem. Phys.* **2005**, *123*, 144705.

(55) Rodriguez, J.; Clavero, E.; Laria, D. *J. Phys. Chem. B* **2005**, *109*, 24427.

(56) Alonso, C.; Bringezu, F.; Brezesinski, G.; Waring, A. J.; Zasadzinski, J. A. *Langmuir* **2005**, *21*, 1028.

(57) Lawrie, G. A.; Gentle, I. R.; Barnes, G. T. *Colloid Surface A* **2000**, *171*, 217.

(58) Lee, K. Y. C.; Gopal, A.; von Nahmen, A.; Zasadzinski, J. A.; Majewski, J.; Smith, G. S.; Howes, P. B.; Kjaer, K. *J. Chem. Phys.* **2002**, *116*, 774.

(59) Park, S. Y.; Chang, C. H.; Ahn, D. J.; Franses, E. I. *Langmuir* **1993**, *9*, 3640.

(60) Park, S. Y.; Franses, E. *Langmuir* **1995**, *11*, 2187.

(61) Rhee, T. K.; Sosnowski, T. S.; Norris, T. B.; Arns, J. A.; Colburn, W. S. *Opt. Lett.* **1994**, *19*, 1550.

(62) Jyoti, A.; Prokop, R. M.; Neumann, A. W. *Colloids Surf., B* **1997**, *8*, 115.

(63) Brooks, J. H.; Pethica, B. A. *T. Faraday Soc.* **1964**, *60*, 208.

(64) Liu, W. T.; Zhang, L. N.; Shen, Y. R. *Chem. Phys. Lett.* **2005**, *412*, 206.

(65) Lu, R.; Gan, W.; Wu, B. H.; Zhang, Z.; Guo, Y.; Wang, H. F. *J. Phys. Chem. B* **2005**, *109*, 14118.

(66) Walker, R. A.; Gruetzmacher, J. A.; Richmond, G. L. *J. Am. Chem. Soc.* **1998**, *120*, 6991.

(67) Yildirim, A.; Cakir, A.; Mavi, A.; Yalcin, M.; Fauler, G.; Taskesenligil, Y. *Flavour Frag. J.* **2004**, *19*, 367.

(68) Can, S. Z.; Mago, D. D.; Walker, R. A. *Langmuir* **2006**, *22*, 8043.

(69) Watry, M. R.; Richmond, G. L. *Langmuir* **2002**, *18*, 8881.

(70) Chen, X. Y.; Wang, J.; Sniadecki, J. J.; Even, M. A.; Chen, Z. *Langmuir* **2005**, *21*, 2662.

(71) Wang, J.; Chen, X. Y.; Clarke, M. L.; Chen, Z. *Proc. Natl. Acad. Sci. U. S. A.* **2005**, *102*, 4978.

(72) Safran, S. A. *Statistical thermodynamics of surfaces, interfaces, and membranes*; Addison-Wesley Pub.: Reading, Mass., 1994.

(73) Kahan, T. F.; Kwamena, N. O. A.; Donaldson, D. J. *Atmos. Environ.* **2006**, *40*, 3448.

(74) Donaldson, D. J.; Mmereki, B. T.; Chaudhuri, S. R.; Handley, S.; Oh, M. *Faraday Discuss.* **2005**, *130*, 227.

(75) Eliason, T. L.; Gilman, J. B.; Vaida, V. *Atmos. Environ.* **2004**, *38*, 1367.

(76) Eliason, T. L.; Aloisio, S.; Donaldson, D. J.; Cziczo, D. J.; Vaida, V. *Atmos. Environ.* **2003**, *37*, 2207.

(77) Dobson, C. M.; Ellison, G. B.; Tuck, A. F.; Vaida, V. *Proc. Natl. Acad. Sci. U. S. A.* **2000**, *97*, 11864.

(78) Tervahattu, H.; Hartonen, K.; Kerminen, V. M.; Kupiainen, K.; Aarnio, P.; Koskentalo, T.; Tuck, A. F.; Vaida, V. *J. Geophys. Res.-Atmos.* **2002**, *107*.

(79) Mmereki, B. T.; Chaudhuri, S. R.; Donaldson, D. J. *J. Phys. Chem. A* **2003**, *107*, 2264.

(80) Donaldson, D. J.; Tervahattu, H.; Tuck, A. F.; Vaida, V. *Origins Of Life And Evolution Of The Biosphere* **2004**, *34*, 57.

(81) Voss, L. F.; Hadad, C. M.; Allen, H. C. *J. Phys. Chem. B* **2006**, *110*, 19487.

(82) Hommel, E. L.; Ma, G.; Allen, H. C. *Anal. Sci.* **2001**, *17*, 1325.

(83) Bell, G. R.; Bain, C. D.; Ward, R. N. *J. Chem. Soc. Faraday T.* **1996**, *92*, 515.

(84) Sefler, G. A.; Du, Q.; Miranda, P. B.; Shen, Y. R. *Chem. Phys. Lett.* **1995**, *235*, 347.

(85) Macphail, R. A.; Strauss, H. L.; Snyder, R. G.; Elliger, C. A. *J. Phys. Chem.* **1984**, *88*, 334.

(86) Snyder, R. G.; Strauss, H. L.; Elliger, C. A. *J. Phys. Chem.* **1982**, *86*, 5145.

(87) Lee, S. H.; Wang, J.; Krimm, S.; Chen, Z. *J. Phys. Chem. A* **2006**, *110*, 7035.

(88) Himmelhaus, M.; Eisert, F.; Buck, M.; Grunze, M. *J. Phys. Chem. B* **2000**, *104*, 576.

(89) Nishi, N.; Hobara, D.; Yamamoto, M.; Kakiuchi, T. *J. Chem. Phys.* **2003**, *118*, 1904.

(90) Casson, B. D.; Bain, C. D. *J. Phys. Chem. B* **1999**, *103*, 4678.

(91) Casson, B. D.; Braun, R.; Bain, C. D. *Faraday Discuss.* **1996**, 209.

(92) Gurau, M. C.; Castellana, E. T.; Albertorio, F.; Kataoka, S.; Lim, S. M.; Yang, R. D.; Cremer, P. S. *Journal of the American Chemical Society* **2003**, *125*, 11166.

(93) Braun, R.; Casson, B. D.; Bain, C. D. *Chem. Phys. Lett.* **1995**, *245*, 326.

(94) Rieu, J. P.; Legrand, J. F.; Renault, A.; Berge, B.; Ocko, B. M.; Wu, X. Z.; Deutsch, M. *Journal De Physique Ii* **1995**, *5*, 607.

(95) Fourkas, J. T.; Walker, R. A.; Can, S. Z.; Gershgoren, E. *J. Phys. Chem. C* **2007**, *111*, 8902.

(96) Bandyopadhyay, S.; Shelley, J. C.; Klein, M. L. *J. Phys. Chem. B* **2001**, *105*, 5979.

(97) Bruce, C. D.; Berkowitz, M. L.; Perera, L.; Forbes, M. D. E. *J. Phys. Chem. B* **2002**, *106*, 3788.

(98) Pohorille, A.; Benjamin, I. *J. Chem. Phys.* **1991**, *94*, 5599.

(99) Pohorille, A.; Benjamin, I. *J. Phys. Chem.* **1993**, *97*, 2664.

(100) Yuan, S. L.; Ma, L. X.; Zhang, X. Q.; Zheng, L. Q. *Colloid Surface A* **2006**, *289*, 1.

(101) Benjamin, I. *Annu. Rev. Phys. Chem.* **1997**, *48*, 407.

(102) Bruce, C. D.; Senapati, S.; Berkowitz, M. L.; Perera, L.; Forbes, M. D. E. *J. Phys. Chem. B* **2002**, *106*, 10902.

(103) Yuan, S. L.; Chen, Y. J.; Xu, G. Y. *Colloid Surface A* **2006**, *280*, 108.

(104) Napoleon, R. L.; Moore, P. B. *J. Phys. Chem. B* **2006**, *110*, 3666.

(105) Vieceli, J.; Benjamin, I. *J. Phys. Chem. B* **2003**, *107*, 4801.

(106) Rudich, Y.; Benjamin, I.; Naaman, R.; Thomas, E.; Trakhtenberg, S.; Ussyshkin, R. *J. Phys. Chem. A* **2000**, *104*, 5238.

(107) Jorgensen, W. L. *J. Phys. Chem.* **1986**, *90*, 1276.

(108) Berendsen, H. J. C.; Postma, J. P. M.; van Gunsteren, W. F.; Hermans, J. In *Intermolecular Forces*; Pullman, B., Ed.; Reidel, Dordrecht, 1981; pp 331.

(109) Chorny, I.; Benjamin, I. *J. Mol. Liq.* **2004**, *110*, 133.

(110) Chorny, I.; Vieceli, J.; Benjamin, I. *J. Chem. Phys.* **2002**, *116*, 8930.

(111) Kuchitsu, K.; Morino, Y. *Bull. Chem. Soc. Jpn.* **1965**, *38*, 814.

(112) Ma, G.; Allen, H. C. *Langmuir* **2007**, *23*, 589.

(113) Wenk, M. R. *Nat. Rev. Drug Discovery* **2005**, *4*, 594.

(114) van Meer, G. *EMBO J.* **2005**, *24*, 3159.

(115) Lockwood, A. P. M.; Lee, A. G. *The membranes of animal cells*, 3rd ed.; E. Arnold: London ; Baltimore, Md., U.S.A., 1984.

(116) Vance, D. E.; Vance, J. E. *Biochemistry of lipids and membranes*; Benjamin/Cummings Pub. Co.: Menlo Park, Calif., 1985.

(117) Csermely, P.; Vígh, L. *Molecular aspects of the stress response : chaperones, membranes and networks*; Springer Science and Business Media: New York, N.Y., 2007; Vol. 594.

(118) Silvius, J. R. Thermotropic Phase Transitions of Pure Lipids in Model Membranes and their Modification by Membrane Proteins. In *Lipid-protein interactions*; Jost, P. C., Griffith, O. H., Eds.; Wiley: New York, 1982; Vol. 2; pp 239.

(119) Veatch, S. L.; Keller, S. L. *Phys. Rev. Lett.* **2002**, *89*, 268101.

(120) Keller, S.; Heerklotz, H.; Jahnke, N.; Blume, A. *Biophys. J.* **2006**, *90*, 4509.

(121) Keller, S.; Tsamaloukas, A.; Heerklotz, H. *Biophys. J.* **2005**, *88*, 17a.

(122) Keller, S.; Tsamaloukas, A.; Heerklotz, H. *J. Am. Chem. Soc.* **2005**, *127*, 11469.

(123) de Lange, M. J. L.; Bonn, M.; Muller, M. *Chem. Phys. Lipids* **2007**, *146*, 76.

(124) Gaines, G. L. *Insoluble monolayers at liquid-gas interfaces*, 1 ed.; Interscience Publishers: New York, 1966.

(125) Kozak, M.; Domka, L.; Jurga, S. *J. Therm. Anal. Calorim.* **2007**, *88*, 395.

(126) Chen, X. Y.; Wang, J.; Boughton, A. P.; Kristalyn, C. B.; Chen, Z. *J. Am. Chem. Soc.* **2007**, *129*, 1420.

(127) Diociaiuti, M.; Ruspantini, I.; Giordani, C.; Bordi, F.; Chistolini, P. *Biophys. J.* **2004**, *86*, 321.

(128) Liu, J.; Conboy, J. C. *J. Phys. Chem. C* **2007**, *111*, 8988.

(129) Rinia, H. A.; Bonn, M.; Muller, M.; Vartiainen, E. M. *ChemPhysChem* **2007**, *8*, 279.

(130) Harper, K. L.; Allen, H. C. *Langmuir* **2007**, *23*, 8925.

(131) Pastrana, B.; Mautone, A. J.; Mendelsohn, R. *Biochemistry* **1991**, *30*, 10058.

(132) Can, S. Z.; Mago, D. D.; Esenturk, M.; Walker, R. A. *J. Phys. Chem. C* **2007**, *111*, 8739.

(133) Vontscharner, V.; Mcconnell, H. M. *Biophys. J.* **1981**, *36*, 409.

(134) McConlogue, C. W.; Malamud, D.; Vanderlick, T. K. *Biochimica Et Biophysica Acta-Biomembranes* **1998**, *1372*, 124.

(135) Pallas, N. R.; Pethica, B. A. *Langmuir* **1985**, *1*, 509.

(136) Mansour, H. M.; Zografi, G. *Langmuir* **2007**, *23*, 3809.

(137) Liu, J.; Conboy, J. C. *Langmuir* **2005**, *21*, 9091.

(138) Brun, A.; Brezesinski, G.; Mohwald, H.; Blanzat, M.; Perez, E.; Rico-Lattes, I. *Colloid Surface A* **2003**, *228*, 3.

(139) Minones, J.; Patino, J. M. R.; Conde, O.; Carrera, C.; Seoane, R. *Colloid Surface A* **2002**, *203*, 273.

(140) Rosen, M. J.; John Wiley & Sons. Surfactants and interfacial phenomena; 3rd ed.; Wiley-Interscience: Hoboken, N.J., 2004.

(141) Mohwald, H. *Annu. Rev. Phys. Chem.* **1990**, *41*, 441.

(142) Petersen, P. B.; Johnson, J. C.; Knutsen, K. P.; Saykally, R. J. *Chem. Phys. Lett.* **2004**, *397*, 46.

(143) Petersen, P. B.; Saykally, R. J. *Chem. Phys. Lett.* **2004**, *397*, 51.

(144) Baldelli, S.; Schnitzer, C.; Shultz, M. J.; Campbell, D. J. *J. Phys. Chem. B* **1997**, *101*, 10435.

(145) Gragson, D. E.; McCarty, B. M.; Richmond, G. L. *J. Am. Chem. Soc.* **1997**, *119*, 6144.

(146) Gragson, D. E.; Richmond, G. L. *Langmuir* **1997**, *13*, 4804.

(147) Gragson, D. E.; Richmond, G. L. *J. Chem. Phys.* **1997**, *107*, 9687.

(148) Bain, C. D.; Manning-Benson, S.; Darton, R. C. *J. Colloid Interface Sci.* **2000**, *229*, 247.

(149) Baldelli, S.; Schnitzer, C.; Campbell, D. J.; Shultz, M. J. *J. Phys. Chem. B* **1999**, *103*, 2789.

(150) Beildeck, C. L.; Steel, W. H.; Walker, R. A. *Langmuir* **2003**, *19*, 4933.

(151) Steel, W. H.; Walker, R. A. *Nature* **2003**, *424*, 296.

(152) Zhang, X.; Steel, W. H.; Walker, R. A. *J. Phys. Chem. B* **2003**, *107*, 3829.